


1-1-2017

Comparison Of The Scavenging Intensity, Remineralization And Residence Time Of ^{210}Po And ^{210}Pb At Key Interfaces (biotic, Sediment- Water And Hydrothermal) Along The Geotraces East Pacific Zonal Transect

John Niedermiller
Wayne State University,

Follow this and additional works at: https://digitalcommons.wayne.edu/oa_theses

 Part of the [Geochemistry Commons](#), and the [Other Oceanography and Atmospheric Sciences and Meteorology Commons](#)

Recommended Citation

Niedermiller, John, "Comparison Of The Scavenging Intensity, Remineralization And Residence Time Of ^{210}Po And ^{210}Pb At Key Interfaces (biotic, Sediment-Water And Hydrothermal) Along The Geotraces East Pacific Zonal Transect" (2017). *Wayne State University Theses*. 580.

https://digitalcommons.wayne.edu/oa_theses/580

This Open Access Thesis is brought to you for free and open access by DigitalCommons@WayneState. It has been accepted for inclusion in Wayne State University Theses by an authorized administrator of DigitalCommons@WayneState.

**COMPARISON OF THE SCAVENGING INTENSITY, REMINERALIZATION
AND RESIDENCE TIME OF ^{210}Po AND ^{210}Pb AT KEY INTERFACES
(BIOTIC, SEDIMENT-WATER AND HYDROTHERMAL)
ALONG THE GEOTRACES EAST PACIFIC ZONAL TRANSECT**

by

JOHN NIEDERMILLER

THESIS

Submitted to the Graduate School

of Wayne State University,

Detroit, Michigan

in partial fulfillment of the requirements

for the degree of

MASTER OF SCIENCE

2017

MAJOR: GEOLOGY

Approved by:

Advisor

Date

ACKNOWLEDGEMENTS

I want to express my sincere gratitude to my advisor and mentor, Professor Mark Baskaran for his support. He encouraged and challenged me throughout this academic journey and he inspired me to do my best. I would also like to thank my thesis committee members, Professor Sarah Brownlee and Professor Jeffrey Howard for their guidance and support during this endeavor. In particular, I would like to thank Professor Brownlee for the use of her laboratory so I could process my water samples.

I would like to thank the captain, crew and chief scientists (Jim Moffett, Chris German and G. Cutter) of the R/V Thomson and the science team who helped collect the samples in both the Niskin bottles and the in situ pumps at sea. The work presented in this thesis was supported National Science Foundation (OCE-1237059; PI: Mark Baskaran).

I also want to thank several people who have collaborated and helped with this thesis project. First, Professor Gillian Stewart and her graduate student Yi Tang, both from Queens College, NY who shared their particulate ^{210}Po and ^{210}Pb data. Secondly, a special thank you to Professor Joseph Resing for shipboard data and preliminary Total Dissolvable Fe data and Hydrothermal Plume figures, and to the Radium group led by Professor Matthew Charette from Woods Hole Oceanographic Institution for sharing his unpublished ^{226}Ra data. Thank you also to Professor Willard S. Moore from University of South Carolina for sharing the ^{226}Ra data and to Phoebe Lam for sharing particulate Fe, Mn and Al data.

Furthermore, I would like to thank WSU students Ken Nash, Rojer Babu, Pranesh Kumar and Chelsea Walsh for their help during the initial first week of processing my water samples. Finally, I want to thank my beautiful wife Dawn, for recognizing my academic potential and for her continued encouragement and faith in me as I pursued my research. And, I express my gratitude to my father for showing me the value of hard work and to my Mother who instilled in me the desire to learn. Inspiring a child to learn is the greatest gift that can be given.

TABLE OF CONTENTS

ACKNOWLEDGEMENTS	ii
LIST OF TABLES	vi
LIST OF FIGURES	vii
CHAPTER	
1. INTRODUCTION	1
1.1 Background.....	1
1.2 Historical Perspective of GEOTRACES Study.....	5
1.3 Rationale for GEOTRACES Study.....	6
1.4 Background and Review of Earlier Studies of Oceanic ^{210}Pb and $^{210}\text{Pb} / ^{226}\text{Ra}$ Ratio.....	7
1.5 Background and Review of Earlier Studies of Oceanic ^{210}Po and $^{210}\text{Po} / ^{210}\text{Pb}$ Ratio.....	9
1.6 Rationale for this Present Study.....	14
1.7 Hypotheses of this Study.....	14
2. MATERIALS AND METHODS	16
2.1 Sampling Locations.....	16
2.2 Water Sampling.....	18
2.3 Laboratory Analysis.....	21
2.4 Digestion of Particulate and Aerosol Filters.....	33
2.5 Quantification of the Sorbed ^{210}Po and ^{210}Pb onto Walls of Cubitainers.....	35
2.6 Quality Assurance and Quality Control (QA/QC).....	36
2.6.1 <i>Blanks</i>	36
2.6.2 <i>Accuracy of Measurements</i>	36

2.6.3	<i>Comparison to Historical Data</i>	36
2.7	Model Calculations for Final Activities of ^{210}Po and ^{210}Pb in Samples.....	37
2.7.1	Calculation of In situ ^{210}Po Activity.....	37
2.7.2	Calculation of In situ ^{210}Pb Activity.....	39
3.	RESULTS	42
3.1	Introduction.....	42
3.2	Quality Assurance and Quality Control (QA/QC).....	42
3.2.1	<i>Blanks</i>	42
3.2.2	<i>Accuracy of the Measurements</i>	43
3.2.3	<i>Comparison of Recent GEOTRACES EPTZ Data with the Historical Data</i>	44
3.2.4	<i>Quantification of the Sorbed ^{210}Po and ^{210}Pb on to Cubitainer Walls</i>	46
3.3	Distribution of ^{210}Po and ^{210}Pb	47
3.3.1	<i>Activity Ratios of $^{210}\text{Po}/^{210}\text{Pb}$ and $^{210}\text{Pb}/^{226}\text{Ra}$ in the Upper 60 m and Mixed Layers</i>	49
3.4	Variations in Activities and Inventories of ^{210}Po and ^{210}Pb , Activity Ratios of $^{210}\text{Po}/^{210}\text{Pb}$ and $^{210}\text{Pb}/^{226}\text{Ra}$	55
3.4.1	<i>Full Water Column</i>	55
3.4.2	<i>Upper 60 m and Mixed layer</i>	64
3.4.3	<i>Biotic, Sediment-water and Hydrothermal (Upper and Bottom 300 m) Interfaces</i>	69
3.4.4	<i>Activity Ratios of $(^{210}\text{Po}/^{210}\text{Pb})_T$ and $(^{210}\text{Pb}_T/^{226}\text{Ra})$ Based on the Integrated Activities of $^{210}\text{Po}_T$, $^{210}\text{Pb}_T$ and ^{226}Ra in the Whole Water Column</i>	70
3.4.5	<i>Inventories of ^{210}Po, ^{210}Pb, and Inventories of Al, Mn, Fe and Other Major Nutrients in the Mixed Layer</i>	71

4. DISCUSSION.....	73
4.1 Introduction.....	73
4.2 Atmospheric Depositional Flux Estimation using ^{210}Pb in Aerosols and the Upper 500 m Water	74
4.3 Variations of Fraction of Particulate ^{210}Po and ^{210}Pb Activities at Key Interfaces	80
4.4 Residence Time of ^{210}Po and ^{210}Pb at Key Interfaces and Relationship between Inventories of ^{210}Po , ^{210}Pb , Nutrients and Trace Elements.....	82
4.4.1 <i>Upper 60 m and Mixed Layer</i>	82
4.4.2 <i>Residence Time of ^{210}Po and ^{210}Pb in the Biotic, Sediment-water and Hydrothermal Interfaces (Upper and Bottom 300 m)</i>	88
4.4.3 <i>Vertical Variations in $^{210}\text{Po}_T/^{210}\text{Pb}_T$ Activity Ratios, Depth-normalized Inventories of ^{210}Po and ^{210}Pb and Residence Time of ^{210}Pb in the Whole Water and Implications of Deep-water Remineralization of Particulate ^{210}Po.....</i>	90
4.5 $^{210}\text{Po} / ^{210}\text{Pb}$ Activity Ratios in 500 m Thick Layers in Deeper Waters to Evaluate Extent of Remineralization and Preferential Removal of ^{210}Po by Particulate Matter.....	93
4.6 Vertical Variations of Fractionation Factor for ^{210}Po and ^{210}Pb	96
4.7 Export Fluxes Macro- and Micro-nutrient Elements.....	99
5. CONCLUSIONS.....	103
References.....	107
Abstract.....	118
Autobiographical Statement.....	120

LIST OF TABLES

Table	Page
2.1 Sampling location, total water depth and mixed-layer depth of six super stations of the US GEOTRACES GP16 East Pacific Zonal Transect (EPZT).....	18
2.2 Alpha detector efficiency and background counts per hour (cph).....	29
3.1 Reagent blank activities (range and median) of ^{210}Po and ^{210}Pb in 13 batches of samples and percentage subtracted* from samples for blanks.....	43
3.2 Comparison of dissolved ^{210}Po and ^{210}Pb on samples collected from the same station and time collected at different time in the Atlantic Ocean.....	44
3.3 Inter-comparison of measured total ^{210}Po and ^{210}Pb activities of GEOTRACES to those of GEOSECS in the Eastern South Pacific.....	45
3.4 Amount of ^{210}Po and ^{210}Pb lost during storage of acidified (pH~ 2.0) water samples for at least 3 months in storage cubitainers.....	47
3.5 Activities of particulate and dissolved and total ^{210}Po , ^{210}Pb and activity ratios of $^{210}\text{Po}/^{210}\text{Pb}$ and $^{210}\text{Pb}/^{226}\text{Ra}$	50
3.6 EPZT ^{210}Po , ^{210}Pb (Small, Large & Dissolved) %.....	62
3.7 Inventories in the upper 60 m of $^{210}\text{Po}_T$, $^{210}\text{Pb}_T$ and ^{226}Ra , DO, SiO_4^{2-} , NO_3^- , PO_4^{3-} , Particulate Al, Mn and Fe and $(^{210}\text{Po}/^{210}\text{Pb})_T$ AR and $(^{210}\text{Pb}_T/^{226}\text{Ra})$ AR EPZT.....	67
3.8 Inventories and activity ratios of ^{210}Po , ^{210}Pb , ^{226}Ra , particulate Al, Mn, Fe and the residence times at the top and bottom 300 m of all six super stations of the EPZT.....	70
3.9 Whole column inventory of total ^{210}Po , ^{210}Pb , and ^{226}Ra inventories and residence times.....	71
4.1 Activity of ^{210}Pb in aerosols and calculated flux for the six super stations of the EPZT.....	78
4.2 Inventories of particulate and dissolved ^{210}Po , ^{210}Pb and ^{226}Ra , Al, Mn and Fe at the top 60 m of all six super stations in the EPZT.....	82
4.3 Dissolved and total Residence time.....	90
4.4 $^{210}\text{Po}_T/^{210}\text{Pb}_T$ activity ratios of inventories in 500 m intervals at EPZT.....	95
4.5 $^{210}\text{Pb}_T/^{226}\text{Ra}$ activity ratios of inventories and residence times of ^{210}Pb in 500 m intervals of the GEOTRACES EPZT.....	95
4.6 Export fluxes at 100 and 500 meters for all 6 EPZT stations.....	101

LIST OF FIGURES

Figure	Page
1.1 ^{238}U decay series isotopes and their half-lives.....	2
1.2 Radionuclides tracers for particle transport.....	3
2.1 Sample locations of six super stations in US GEOTRACES GP16 East Pacific Zonal Transect (EPZT; RV Thomson; October to December 2013).....	17
2.2 Research Vessel Thomas G. Thompson.....	19
2.3 Rosette of Niskin bottle used for sample collection.....	19
2.4 EPZT Water Filterization, Group I (Dissolved) and Group II (Particulates).....	20
2.5 Sample collection preparation of cubitainers, milk crates and pallet shipping containers.....	21
2.6 Flow chart of chemical processing for dissolved ^{210}Po and ^{210}Pb	22
2.7 Fossil Pb dissolved to make stable Pb carrier.....	23
2.8 Addition of sodium chromate to enhance Pb yield.....	24
2.9 $\text{Fe}(\text{OH})_3$ precipitate containing ^{210}Po , ^{209}Po , ^{210}Pb , and stable Pb.....	25
2.10 Decanting and filtration of solution.....	26
2.11 Filtered precipitate collecting on filter paper.....	26
2.12 Solution after adding ascorbic acid prior to electroplating.....	27
2.13 Plated 15.9 mm Polished silver planchet.....	27
2.14 Taping of 15.9 mm planchet.....	28
2.15 Electroplating of ^{210}Po on to polished silver planchets.....	28
2.16 Octete PC 8-input alpha spectrometers.....	29
2.17 Po plated planchet with thick coating of iron compounds (left) compared to planchet without iron compounds (right).....	30
2.18 Residual solution dried before taking to 9M HCL for anion exchange column.....	31

2.19	Separation of residual Po from Pb using anion-exchange columns.....	31
2.20	Analyzing samples for Stable Pb concentrations using ICP-MS.....	32
2.21	McLane Pump from RV/ Thomson, EPZT cruise.....	33
2.22	High-Volume Tisch Environmental TSP TE5170V aerosol sampler.....	34
3.1	Vertical profile of total ^{210}Po activity, Ocean Data View.....	48
3.2	Vertical profile of total ^{210}Pb activity, Ocean Data View.....	48
3.3	Activities of dissolved and particulate ^{210}Po and ^{210}Pb for all six stations.....	54
3.4	Vertical profile of total $^{210}\text{Po}/^{210}\text{Pb}$ activity ratio in full water column.....	56
3.5	Vertical profiles of dissolved and particulate $^{210}\text{Po}/^{210}\text{Pb}$ activity ratio in full water column	57
3.6	Vertical profile of $^{210}\text{Pb}_T/^{226}\text{Ra}$ activity ratio (ST 4, 11, 18, 26 at depths 110, 110, 115, 45 and AR 3.96, 3.22, 5.26, 3.30 respectively were removed).....	58
3.7	Vertical profiles of $^{210}\text{Pb}_T/^{226}\text{Ra}$ activity ratio in full water column for all six stations.....	59
3.8	Vertical profiles of $^{210}\text{Pb}_T/^{226}\text{Ra}$ activity ratio to 400 m depth for all six stations.....	65
3.9	Vertical section of $^{210}\text{Pb}_T/^{226}\text{Ra}$ activity ratio down to 500 m, Ocean Data View	66
3.10	Bar diagram of total ^{210}Po and ^{210}Pb inventories in the upper 60 m of 6 super stations in U.S. GEOTRACES GP16 EPZT.....	67
3.11	Comparison of aerosol and upper 60 m for all six stations.....	68
4.1	Equatorial trade winds and the South Pacific Gyre.....	75
4.2	Specific activity of ^{210}Pb (dpm/ 100m ³) in aerosols and calculated ^{210}Pb atmospheric depositional flux.....	76
4.3	Model-derived ^{210}Pb atmospheric depositional flux using equation (4.3) for various residence times (1 to 50 y) of ^{210}Pb in the upper 500 m.....	79
4.4	Vertical profiles particulate ($\geq 1 \mu\text{m}$) ($^{210}\text{Po}/^{210}\text{Pb}$) _P activity ratio.....	81
4.5	Inventory of ^{210}Po vs. inventory of nutrients (SiO_4^{2-} , NO_3^- , PO_4^{3-}) in the upper 60 m (mixed layer).....	85

4.6	Inventory of ^{210}Po or ^{210}Pb vs. total nutrients ($\text{SiO}_4^{2-} + \text{NO}_3^- + \text{PO}_4^{3-}$) in the upper 60 m. (^{210}Po inventory for ST-4 is excluded).....	86
4.7	Inventory of ^{210}Po or ^{210}Pb vs. particulate Al inventory in the upper 60 m (mixed layer).....	87
4.8	Bar diagram of total ^{210}Po and ^{210}Pb inventories in 1,000 m-normalized depths of six super stations in US GEOTRACES GP16 EPZT.....	91
4.9	Fractionation factor for all 6 Stations to Depth.....	98

CHAPTER 1

INTRODUCTION

1. Introduction

One of the least understood biogeochemical processes in the marine environment is the contribution of key macro- and micro nutrient elements to the deep ocean water column from remineralization of sinking particles. The observed disequilibrium between ^{210}Po (Polonium-210) and ^{210}Pb (Lead-210) denoted as $^{210}\text{Po}/^{210}\text{Pb}$ activity ratio as well as ^{210}Pb and ^{226}Ra (Radium-226) denoted as $^{210}\text{Pb}/^{226}\text{Ra}$ activity ratio in marine systems has been exploited to investigate several biogeochemical processes that include deep ocean scavenging of Pb, settling velocity of sinking particles, adsorption-desorption rate constants between particles and solution, export fluxes of particulate organic carbon, biogenic silica, and remineralization of sinking particulate matter (Craig et al., 1973; Bacon et al., 1976; Somayajulu and Craig, 1976; Nozaki et al., 1990, 1997; Friedrich and Rutgers van der Loeff, 2002; Henderson and Maier-Reimer, 2002; Cochran and Masque, 2003; Murray et al., 2005; Verdeny et al., 2009; Rigaud et al., 2015). The activity ratios (AR) of $^{210}\text{Po}/^{210}\text{Pb}$ and $^{210}\text{Pb}/^{226}\text{Ra}$ in the water column that differ widely at different interfaces (near sediment-water and air-sea) can be utilized to quantify the processes that cause such disequilibria. Furthermore, ^{210}Po , ^{210}Pb and ^{226}Ra also serve as geochemical analogs for several other elements in the oceanic water column.

1.1 Background

Many of the naturally-occurring particle-reactive radionuclides in the ^{238}U -series, as seen in Figure 1.1, have been widely utilized as tracers to investigate POC/PON (Particulate Organic Carbon / Particulate Organic Nitrogen) export fluxes, particle cycling, remineralization and residence time and scavenging intensity of particulate matter.

The Uranium-238 Decay Chain

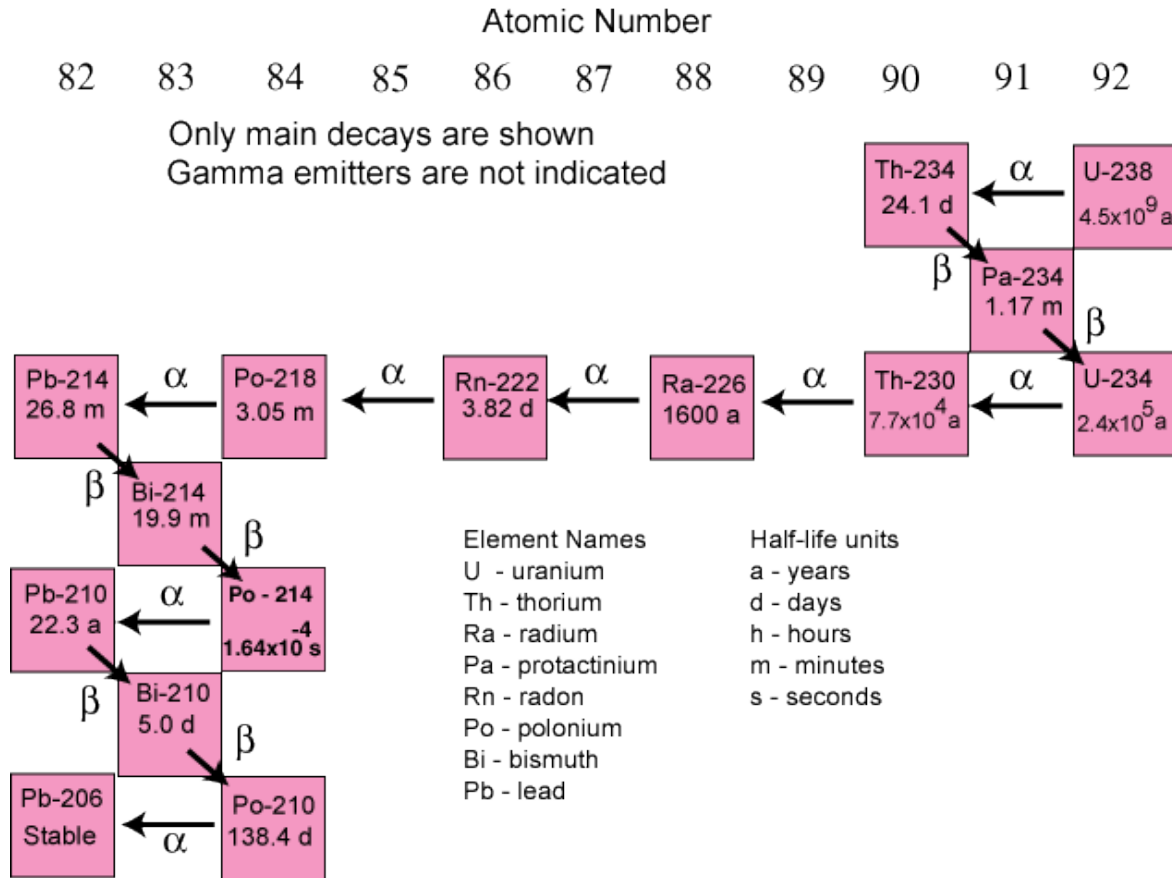


Figure 1.1. ^{238}U decay series isotopes and their half-lives. Source: [U.S. Geological Survey \(USGS\)](https://pubs.usgs.gov/of/2004/1050/U-238-Decay-Chain.gif)
<https://pubs.usgs.gov/of/2004/1050/U-238-Decay-Chain.gif>

In particular, two of the longest-lived daughter products of ^{222}Rn , namely ^{210}Pb (half-life, $t_{1/2} = 22.3$ years) and ^{210}Po (half-life, $t_{1/2} = 138.4$ d) have been used in quantifying particulate scavenging, carbon flux from the surface ocean, and to infer the importance of oceanic boundaries in scavenging particle-reactive nuclides (Bacon et al., 1976; Nozaki et al., 1976; Thomson and Turekian, 1976; Cochran, 1992; Rutgers van der Loeff and Geibert, 2008). An overview of radionuclides and tracers for particle transport can be seen in Figure 1.2 below.

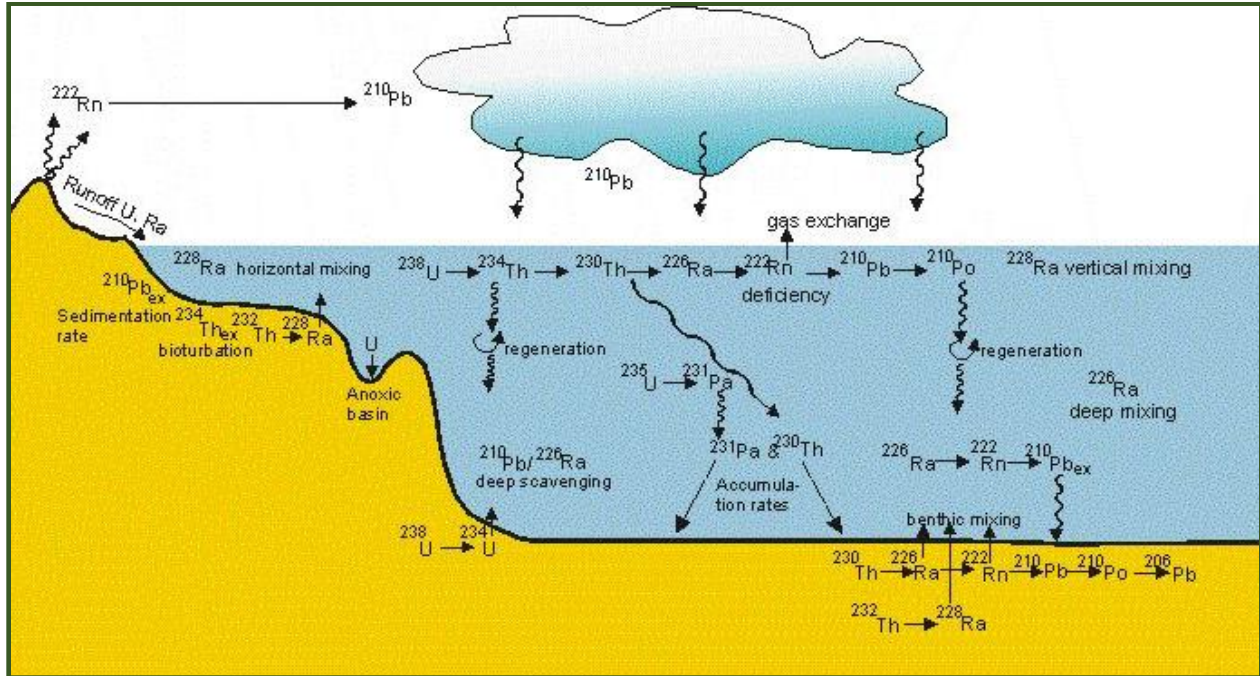


Figure 1.2. Radionuclides/Tracers for Particle Transport

http://www.awi.de/fileadmin/user_upload/Research/Research_Divisions/Geosciences/Marine_Geochemistry/natural-radionuclides/tracers_for_particle_transport/processes.jpg

The sources of ^{226}Ra , ^{210}Pb and ^{210}Po isotopes in the water column are strikingly different. Most of the ^{226}Ra in the open ocean is ultimately derived from pore-water diffusion at the sediment-water interface, with $\sim 1.1\%$ of the ^{226}Ra in the near-surface Atlantic and $< 1\%$ in the Pacific contributed by rivers (Key et al., 1985, Cochran, 1992). In surface waters, most of the ^{210}Pb is derived from atmospheric deposition (e.g., at Bermuda, in the upper 500 m). For example, ^{210}Pb supply from atmospheric deposition in Bermuda is $\sim 87\%$ compared to $\sim 13\%$ from ^{226}Ra decay, assuming the atmospheric depositional flux of $0.69 \text{ dpm cm}^{-2} \text{ y}^{-1}$ (Turekian et al., 1983) and ^{226}Ra concentration of $7 \text{ dpm } 100 \text{ L}^{-1}$, Cochran, 1992), and the penetration depth of the atmospheric ^{210}Pb input in the deep-ocean is up to $\sim 500 \text{ m}$ (Bacon et al., 1976). Most of the oceanic ^{210}Po is derived from the decay of dissolved ^{210}Pb , as expected.

Radium-226 is utilized as a water mass tracer, implying that it is conservative in marine systems whereas ^{210}Pb and ^{210}Po trace the particulate matter. Po-210 is also accumulated within

organic tissues (Heyraud and Cherry, 1979, Stewart and Fisher, 2003). The differences in the activities of ^{210}Pb and ^{226}Ra in the water column as well as ^{210}Po and ^{210}Pb in the particulate and dissolved phases are utilized to quantitatively assess the dissolved-particulate partitioning and export fluxes of sinking particulate matter in time scale of months (^{210}Po) and decades (^{210}Pb). The residence times of particulate and dissolved ^{210}Po and ^{210}Pb are useful in the investigations of biogeochemical cycles of other trace elements that display similar biogeochemical behavior.

The first disequilibrium study between ^{210}Pb and ^{226}Ra in the deep ocean was reported by Craig et al. (1973) in the Pacific and Atlantic oceans. Craig et al. (1973) estimated the mean residence time of ^{210}Pb to be 54 years using a vertical advection-diffusion model in which ^{210}Pb was scavenged by settling particles. In addition to the scavenging by the vertical particulate flux, Bacon et al. (1976) suggested that ^{210}Pb scavenging at oceanic boundaries (including continental shelf and slope, mid-ocean ridges, and the deep-sea floor), could also be important removal sites. The deficiency of ^{210}Pb relative to its ancestor ^{226}Ra has been reported to increase from mid-ocean interior towards the continental edges and bottom seafloor where it is more intensely scavenged. Bacon et al. (1976), from the measurements of particulate and dissolved ^{210}Po and ^{210}Pb from 10 vertical profiles in eastern North Atlantic and Pacific Oceans, reported the residence time of ^{210}Po to be 0.6 years and 2.5 years for ^{210}Pb , indicating faster removal of ^{210}Po . These residence times are much longer than the particle turnover time of about a month.

A number of vertical profiles of ^{210}Po , ^{210}Pb , ^{226}Ra and their activity ratios from the world oceans have been published during 1970s and 1980s from the GEOSECS cruises, showing disequilibrium between ^{210}Pb and ^{226}Ra (Nozaki et al., 1976, 1980; Cochran et al., 1983, 1990; Chung, 1981). However, there was disagreement on whether there is disequilibrium between ^{210}Po and ^{210}Pb in the deep waters of the open ocean (e.g., Bacon et al., 1976; Thomson and

Turekian, 1976; Turekian and Nozaki, 1980). Most studies have reported disequilibrium at discrete depths, even in deep waters >500 m, but no rigorous analyses on how the $^{210}\text{Po}/^{210}\text{Pb}$ activity ratios vary over a depth interval as well as for the overall water column were conducted. This was partially due to analytical uncertainties associated with the methodology employed. Thorough intercalibration efforts performed during the first phase of the GEOTRACES program, from both the Atlantic and Pacific cruises, significant improvements on the precision of measurements of these two radionuclides were attained, and hence we are able to do an in-depth analysis of the disequilibria between ^{210}Po and ^{210}Pb activity. In contrast to previous studies where disequilibrium between ^{210}Po and ^{210}Pb as well as ^{210}Pb and ^{226}Ra have been widely reported, this thesis presents a new approach to address the differences in the scavenging intensities and residence times by integrating these activities (decays per minute per 100L, $\text{dpm } 100\text{L}^{-1}$) at key interfaces and as well as in the whole column.

The GEOTRACES program involved simultaneous analysis of a large number of parameters including particulate organic carbon, dissolved oxygen, nutrients (nitrate/nitrite, ammonia), and key trace metals (Al, Fe, Mn, Co, Cu, Zn, Ti, ^{232}Th , etc.), which will provide insight on the partitioning of ^{210}Po , and ^{210}Pb under different conditions. The unique advantage of the ^{210}Po - ^{210}Pb pair is that it yields a time-scale of intense scavenging of ^{210}Po or remineralization of biogenic particulate matter at different layers of the vertical column.

1.2 Historical Perspective of GEOTRACES Study

Much of the mapping of ^{210}Po and ^{210}Pb along with ^{226}Ra distributions was carried out as part of the GEOSECS program in the Atlantic Ocean (July 1972 – May 1973), the Pacific Ocean (August 1973 – June 1974) and in the Indian Ocean (December 1977 – March 1978). The GEOTRACES program was started with the Intercalibration cruise in the Atlantic (July

2008) and Pacific (May 2009) Oceans. One of the overarching goals of the GEOTRACES program has been to study the distribution of trace elements and isotopes (TEIs), to assess their sources, sinks and internal cycling and to characterize the physical, chemical and biological processes that regulate their distribution, in particular across major ocean boundaries. As a part of the GEOTRACES-Pacific, ^{210}Pb parent ($t_{1/2} = 22.3\text{y}$) and ^{210}Po grand-daughter ($t_{1/2} = 138\text{d}$) radionuclide pair was included into the GEOTRACES Eastern South Pacific Zonal, EPZT section as unique radiometric TEIs that are both geochemically and biochemically active. These isotopes are expected to complement the other particle-reactive nuclides operating on shorter and longer time scales (e.g. ^{234}Th , ^{228}Th) that were also measured in the EPZT as well as the water-soluble tracers (e.g. ^{226}Ra) to evaluate the lateral transport of ^{210}Pb from the $^{210}\text{Pb}/^{226}\text{Ra}$ activity ratio in one of the most productive (Peruvian coast) and least productive waters of the ultra-oligotrophic South Pacific subtropical gyre.

http://www.usgeotraces.org/documents/pacificDOC/Pacific_Report_Jun09_000.pdf

http://www.usgeotraces.org/html/WS_Pacific2011.html

1.3 Rationale for GEOTRACES Study

GEOTRACES is an internationally-approved science program by International Geosphere-Biosphere Programmes/Scientific Committee on Oceanic Research or IGBP/SCOR. Some background information is provided about the GEOSECS program in accord with their Principles and Priorities, including the three goals of the project beginning with an intercalibration project. The guiding mission of the GEOTRACES Science Plan (www.geotraces.org) is: *“To identify processes and quantify fluxes that control the distributions of key trace elements and isotopes in the ocean, and to establish the sensitivity of these*

distributions to changing environmental conditions.” The three overriding goals that support this mission are:

- 1) *To determine global ocean distributions of selected trace elements and isotopes – including their concentration, chemical speciation and physical form – and to evaluate the sources, sinks, and internal cycling of these species to characterize more completely the physical, chemical, and biological processes regulating their distributions.*
- 2) *To understand the processes involved in oceanic trace-element cycles sufficiently well that the response of these cycles to global change can be predicted, and their impact on the carbon cycle and climate understood.*
- 3) *To understand the processes that control the concentrations of geochemical species used for proxies of the past environment, both in the water column and in the substrates that reflect the water column.*

1.4 Background and Review of Earlier Studies of Oceanic ^{210}Pb and $^{210}\text{Pb}/^{226}\text{Ra}$ Ratio

Lead-210 has its primary source from the decay of ^{222}Rn in the atmosphere released primarily from continental sources. The amount of ^{210}Pb in atmospheric air is a function of distance from the land source and the length and breadth of the upwind continental land mass. It is primarily delivered by wet precipitation (e.g. Baskaran, 2011). Once delivered to the surface ocean, most of the ^{210}Pb is removed by sorption onto particulate matter in the upper ocean and driven by the flux of biogenic material from surface productivity (Fisher et al., 1988; Moore and Dymond, 1988) and lithogenic material. The atmospherically-delivered ^{210}Pb is reported to penetrate the mixed layer into thermocline at depths of ~500 m (Bacon et al., 1976). It is rapidly removed by particle scavenging, such that unsupported activities are maintained down to several hundred meters. Box model calculations have yielded scavenging residence times of Pb in open

ocean surface waters of 2-3 years, but less than a year in inland and coastal waters (Rama et al., 1961; Bacon et al., 1976; Nozaki et al., 1991; Cochran, 1992; Baskaran and Santschi, 1993). The gradient of ^{210}Pb with depth allows estimation of settling velocities of particles ranging from several hundred meters per year in the Pacific up to a thousand in the Atlantic (Somayajulu and Craig, 1976; Bacon et al., 1976). The relative horizontal gradient of $^{210}\text{Pb}/^{226}\text{Ra}$ is a function of the removal rate of ^{210}Pb by particles generated either from lithogenic sources or biogenic *in situ* productivity (Cochran et al., 1983). According to Cochran et al., 1990, the residence time of ^{210}Pb in the N. Pacific deep waters (140 ± 60 years) is longer than that in the N. Atlantic (35 ± 15 years), and thus, ^{210}Pb can be transported from areas of low particle concentrations to areas of high particle concentrations such as ocean margins where upwelling is occurring, and removal of ^{210}Pb can take place by boundary scavenging. Areas in the Eastern Pacific off of California, Washington shelf, and off of Panama Basin have been reported to be sinks for water column ^{210}Pb (Carpenter et al., 1981; Moore et al., 1981). Higher ^{210}Pb inventories in sediment cores from different marine systems compared to the atmospheric deposition. Furthermore, water column production is attributed to boundary scavenging (Carpenter et al., 1981; Baskaran and Santschi, 2002). In southern basins such as the Indian Ocean, the ratio signifies eddy diffusion toward a boundary sink together with the scavenging by sinking particles. The enhanced scavenging at ocean margins is related to both increase in particle fluxes and Fe or Mn redox cycling at eastern versus western boundaries (Bacon et al., 1980). Specific ocean boundaries where such cycles are active include anoxic basins (Todd et al., 1986) and hydrothermal vents (Kadko et al., 1987; Wei and Murray, 1994).

Excesses of ^{210}Pb are reflected in areas with increased atmospheric deposition (Nozaki et al., 1980; Murray et al., 2005), and less so in areas with lower deposition (Chung and Craig,

1983). In particular, the atmospheric deposition of ^{210}Pb in the eastern South Pacific is significantly lower than that in the western North Pacific, $\sim 2 \text{ dpm cm}^{-2} \text{ y}^{-1}$ (Turekian et al., 1977). As a result, surface distributions of ^{210}Pb show maxima in mid-ocean and subtropical rain zones such as the Inter Tropical Convergence Zone, ITCZ near the equator (Nozaki et al., 1976). Data on atmospheric deposition over open ocean regions represents a major uncertainty in the use of ^{210}Pb and $^{210}\text{Pb}/^{226}\text{Ra}$ ratio for scavenging studies. Compared to its parent ^{226}Ra , ^{210}Pb shows disequilibrium in bottom waters, allowing estimates of bottom scavenging ranging from decades in the Atlantic to over a century in the Pacific. This is in agreement with bottom water circulation and horizontal contrasts in scavenging efficiencies (Cochran et al., 1983). Further, ^{210}Pb measurements allow calculations of vertical diffusion coefficients of several cm s^{-1} across the main thermocline in the water column. Horizontal model residence times in the center of the North Pacific gyre decrease from about four to one century landward (Nozaki et al., 1980). Bacon et al. (1976) did not find any significant vertical gradient in particulate ^{210}Pb and it is not known if there is any gradient in the specific activity of ^{210}Pb (dpm gram^{-1} of suspended particulate matter) and how it varies across a gradient in productivity, from highly productive waters such as off of Peru and the most oligotrophic waters such as the western part of the sampling station in the Pacific gyre.

1.5 Background and Review of Earlier Studies of Oceanic ^{210}Po and $^{210}\text{Po}/^{210}\text{Pb}$ Ratio

The source of the majority of the dissolved ^{210}Po in the upper waters is the decay of ^{210}Pb , but it is also supplied from atmospheric fallout with a $^{210}\text{Po}/^{210}\text{Pb}$ activity ratio generally < 0.1 (Hussain et al., 1998, reviewed in Baskaran, 2011). The particulate matter in surface waters is enriched in ^{210}Po , with $^{210}\text{Po}/^{210}\text{Pb}$ activity ratios > 1.0 . At depths 100-300 m, ^{210}Po maxima occur resulting in the common occurrence of excess ^{210}Po ; or unsupported with ^{210}Po activity $>$

^{210}Pb activity (Bacon et al., 1976, Rigaud et al., 2015). Bacon et al. (1976) also have shown that $\geq 50\%$ of the ^{210}Po removed from the mixed layer is recycled within the thermocline while for ^{210}Pb the recycling efficiencies are much lower. The recycling efficiency of ^{210}Po is much higher in the mixed layer. Thus the $^{210}\text{Po}/^{210}\text{Pb}$ activity ratio in surface waters of the world ocean is approximately 0.5, and increases somewhat greater than 1.0 within a few hundred meters depth. In the deep ocean water, ^{210}Po rapidly associates with particulate matter and its residence time in solution is on the order of ~ 4 years (Bacon et al., 1976). In filtered seawater in the Atlantic and Pacific, Bacon et al. (1976) reported the ^{210}Po to be deficient by $\sim 10\%$ relative to ^{210}Pb , and it is not known how this varies across a spectrum of particle concentrations and composition.

Polonium-210, granddaughter of ^{210}Pb , an O-S Group VI element, is readily assimilated into ocean biota and can be used in conjunction with ^{210}Pb to track the removal flux of particulate organic carbon (POC) and other particle-reactive TEIs from the surface ocean on sub-annual time scales (Murray et al., 2005; Verdeny et al., 2008; Hong et al., 2013). The stronger affinity of ^{210}Po for biotic marine particulate matter compared to ^{210}Pb in most ocean basins, combined with contrastingly different primary productivity of the waters in the two extreme environments (most productive waters off of Peru and most-oligotrophic subtropical South Pacific Gyre), will result in ^{210}Po having a strikingly different residence time than ^{210}Pb , which is removed by lithogenic particles and boundary scavenging across the sampling transect. Earlier data show both a deficiency ^{210}Po in the water column with $^{210}\text{Po}/^{210}\text{Pb} < 1.0$ at the East Pacific Rise near $8^{\circ}45'\text{N}$ (Kadko et al., 1987) as well as equilibrium values at deeper depths (Turekian and Nozaki, 1980).

Besides tracking POC export, the $^{210}\text{Po} - ^{210}\text{Pb}$ pair in the ^{222}Rn daughter series has seen wide application over the past several decades for quantifying rates of diverse oceanic processes

at ocean boundaries. This nuclide pair can track both vertical and horizontal scavenging at ocean margins and intermediate nepheloid layers (INL) or benthic nepheloid layers (BNL) on similar time scales. Identification and quantification of the processes that control the distribution of these nuclides in the ocean, and their sensitivity to and relationships with other TEIs and nutrients are core missions of the GEOTRACES program, including the south Eastern Pacific Zonal Transect (EPZT). This includes an attempt to trace these radionuclides in both nepheloid layers and precipitates in hydrothermal plumes.

From the extensive work during GEOSECS, the concentrations of ^{210}Po and ^{210}Pb in the upper water profiles are similar in the Pacific (Nozaki et al., 1976; Cochran et al., 1983), the Atlantic (Bacon et al., 1976) and Indian Oceans (Cochran et al., 1983; Chung and Finkel, 1988). The general consensus is that the ^{210}Po deficiency yields scavenging residence times of months, shorter than ^{210}Pb (years), both of which are related to higher particle fluxes. The shorter residence times of dissolved ^{210}Po in the upper waters is attributed to recycling within the ocean surface. The observed regeneration gradient was used to estimate new production from the upwelling of nitrate in the Arabian Sea (Sarin et al., 1992). However, this ratio has been reported to vary in deep waters and with geography.

It has been shown that the dissolved ^{210}Po and ^{210}Pb can be in equilibrium in upwelling areas, in spite of high production (Thompson and Turekian, 1976; Turekian and Nozaki, 1980). Upwelling refers to the how deeper cold, nutrient-rich water “wells up” from below to displace surface waters. It was suggested that $^{210}\text{Po}/^{210}\text{Pb}$ scavenging is driven by different affinities of the nuclides during active biological uptake, versus passive adsorption (Nozaki et al., 1998). However, in oligotrophic waters (low nutrient concentrations and low plant growth; thus low biological uptake), deficiency is observed down to 4000 meters (Kim and Church, 2001). Deep

water deficiencies were also suggested in the north eastern Indian basin (Chung and Finkel, 1988) and cited earlier by Bacon et al. (1976) in the deep Atlantic, yet the isotopes were close to equilibrium within the total uncertainties of the $^{210}\text{Pb} - ^{210}\text{Po}$ pair beyond just counting statistics during GEOSECS profiles. Increasing $^{210}\text{Pb}/^{210}\text{Po}$ deficiency profiles in oligotrophic areas that exceed either subducted or trapped fluxes suggests ^{210}Po assimilation by bacteria and subsequent larger transfer to higher (nekton) trophic levels (Kim, 2001). The ^{210}Po deficiency remains a paradox in that deep water deficiency of short lived ^{210}Po would require deep scavenging residence times on the order of years to a decade (as reviewed in Rutgers van der Loeff and Geibert, 2008). This could reflect an important food chain sink in deep (benthic) waters, a result of not sampling benthic nekton, or an analytical result. However, the overall equilibrium in the water column will indicate the key role that remineralization plays. It was reported that the total (dissolved + particulate) inventories of ^{210}Po and ^{210}Pb for the whole water column did not show any departure from equilibrium (Bacon et al., 1976). However, it is not clear if there is any disequilibrium between the most productive and most oligotrophic waters.

The disequilibrium of ^{210}Po to ^{210}Pb often observed in the upper ocean should also depend on both the flux and cycling of organic versus inorganic particles, and provide the basis for tracing carbon flux (Verdeny et al., 2009). The distribution of ^{210}Po has direct relevance to global biogeochemical cycling of other oxygen Group VI elements (S, Se and Te) as well as other particle-reactive elements. Not only is ^{210}Po accumulated in phytoplankton, but it has the potential to bioaccumulate in marine food chains due to its slow loss rate from organic material and to it being biologically recycled (similar to POC), whereas ^{210}Pb is not accumulated in organisms and therefore displays shorter residence times in the surface waters. In fact, ^{210}Po is the only U-Th natural radionuclide (as a Group VI element) that is fundamentally bioactive and

therefore mechanistically applicable as a tracer for oceanic carbon flux (Cochran and Masque, 2003; Murray et al., 2005; Stewart et al., 2007; Verdeny et al., 2009). Furthermore, ^{210}Pb has strong affinity for lithogenic material while ^{210}Po has strong affinity for biogenic particulate material (Kharkar et al., 1976). While both Po and Pb can be sorbed onto particle surfaces (both lithogenic and biogenic), Po is also assimilated into phytoplankton cells by entering the biological cycle of the living organisms similar to other sulfur group elements. As a result, Po becomes enriched in organic soft tissue, in particular proteins, and can bioaccumulate within the food web (Fisher et al., 1983, Cherrier et al., 1995; Stewart and Fisher, 2003).

Similar to the $^{234}\text{Th} - ^{238}\text{U}$ pair, the disequilibrium between ^{210}Po and ^{210}Pb has been used to determine particulate organic carbon (POC) export fluxes from surface waters (from the mixed layer or from euphotic zone). The ‘biological pump’ (mechanism in which biologically driven sequestration of carbon from the atmosphere to the deep water via particulate organic carbon) enables the surface water POC to be transferred to the deep oceanic water column. Similar to POC export fluxes, from the concentrations of elements (or metals, M), ^{210}Po (for biogenic elements) or ^{210}Pb (for lithogenic elements) in particulate matter and export fluxes of ^{210}Po or ^{210}Pb , one can determine the export fluxes from various depths of the water column as follows:

Export flux of metal ‘M’ = (concentration of M / concentration of ^{210}Po or ^{210}Pb)_{particulate} X net export fluxes of ^{210}Po or ^{210}Pb via sinking particulate matter. This approach has not been attempted before but will be presented as part of this thesis. Furthermore, partitioning of Po and Pb between phases of particulate matter has not previously been attempted. Recent studies have shown the importance of five major phases of particulate matter (lithogenic, CaCO_3 , opal, organic matter (POM), $\text{Fe}(\text{OH})_3$ and MnO_2) in the scavenging of ^{230}Th and ^{231}Pa . This method

involves the determination of bulk K_d , and the fractional amount of these five phases (from the measured concentrations of Al or Ti for lithogenic material, biogenic silica for opal, organic carbon for POC, iron and Mn in the particulate matter). These five fractional amounts are $f(\text{lith})$, $f(\text{CaCO}_3)$, $f(\text{opal})$, $f(\text{POM})$, $f(\text{Fe}(\text{OH})_3)$ and $f(\text{MnO}_2)$, respectively (Hayes et al., 2015; Lam et al., 2015). Using a non-negative least-square regression, the pure-end member K_d s for each phase can be determined.

1.6 Rationale for this Present Study

The only three $^{210}\text{Po}/^{210}\text{Pb}$ vertical profiles in this region were obtained > 30 years ago off the coast of Peru as part of GEOSECS (Thomson and Turekian, 1976; Turekian and Nozaki, 1980). These profiles were taken at stations within the continental margin with a very strong influence of upwelling. A comparison of the GEOSECS ^{210}Po and ^{210}Pb profiles with GEOTRACES profiles will be made to assess environmental change that could have caused the changes, if any, during the past ~35-40 years in this region. Comparison of the $^{210}\text{Pb}/^{226}\text{Ra}$ ratios in the oligotrophic South Pacific subtropical gyre to those in the most productive waters off of Peru associated with the Peru current will provide information on the boundary scavenging of ^{210}Pb and will complement information obtained from $^{231}\text{Pa}/^{230}\text{Th}$ ratios and stable Pb, conducted by other GEOTRACES teams for this regional study. The massive gradient in productivity and export from the coast of Peru to the center of the oligotrophic subtropical gyre along this GEOTRACES transect will aid in testing the hypotheses listed below. As a part of this thesis, the following hypotheses will be tested:

1.7 Hypotheses of this Study

This study involved collecting, processing and analyzing 135 water samples from the GEOTRACES EPZT cruise to determine the scavenging intensity, remineralization and

residence time of ^{210}Po and ^{210}Pb at key interfaces (biotic, sediment-water and hydrothermal). The analysis included dissolved ($< 0.45 \mu\text{m}$) and particulate ($1 - 51 \mu\text{m}$, small particulate and $> 51 \mu\text{m}$, large particulate) phases. Based on the data presented in this thesis, the following hypotheses were tested:

1) Due to trade wind direction in the southern Hemisphere (southeast Pacific Ocean), there is a decreasing ^{210}Pb flux (from mixed layer inventories) from east to west in the transect;

2) There is a difference in scavenging intensity of ^{210}Po and ^{210}Pb at key interfaces including the biotic interface (mixed-layer and upper 300), the sediment-water interface (bottom 300 m), the hydrothermal interface (bottom 300 m at the East Pacific Rise, ST 18), and 'least-biological activity' interface (upper and bottom 300 m of an oligotrophic site, ST 36);

3) In the EPR plume, differential scavenging rates of ^{210}Po (as a sulfide congener, e.g., elements in the same group of the periodic table) and ^{210}Pb by Fe/Mn-oxyhydroxides can be quantified from stable $\text{Pb}/^{210}\text{Pb}$ and stable $\text{Pb}/^{210}\text{Po}$ relationships;

4) The $^{210}\text{Po}/^{210}\text{Pb}$ and $^{210}\text{Pb}/^{226}\text{Ra}$ activity ratios vary at different depth intervals and there is disequilibria between ^{210}Po and ^{210}Pb in the water column; and

5) The residence time of ^{210}Pb varies at different layers in the vertical profile.

To test these hypotheses, 135 water samples were analyzed along with 135 particulate material ($>51 \mu\text{m}$ and $1-51 \mu\text{m}$; analysis conducted at our collaborating institution). The results are presented and discussed in this thesis.

CHAPTER 2

MATERIALS AND METHODS

2.1 Sampling Locations

Water samples were collected during the US GEOTRACES GP16 East Pacific Zonal Transect (EPZT) on the Research Vessel, RV Thomson during October to December 2013 from Manta, Ecuador on October 25 to Tahiti on December 22, 2013 for the analysis of dissolved ($< 0.45 \mu\text{m}$) and particulate ($1 - 51 \mu\text{m}$, small particulate and $> 51 \mu\text{m}$, large particulate) phases. Samples at six super stations (ST) were collected on this zonal transect that began offshore from Peru near 12° S latitude, 78° W longitude (ST 4) and ended with the last station, ST 36 near 11° S latitude and 152° W longitude with water depths ranging from 755 to 5533 m (Figure 2.1, Table 2.1). This transect included an area characterized by high rates of primary production and particle export in the eastern boundary (ST 1 and 4, Figure 2.1) as well as extremely oligotrophic conditions farther west (ST 36, Figure 2.1). Samples were also collected from the large Oxygen Minimum Zone (OMZ) off Peru, namely ST 11, during the first half of this transect. Furthermore, ST 18 is located at a major hydrothermal vent that disperses west away from the East Pacific Rise, EPR (Figure 2.1) and was sampled to assess how redox-cycling will affect the removal of ^{210}Po and ^{210}Pb . The sampling locations of the six super stations are given in Figure 2.1.

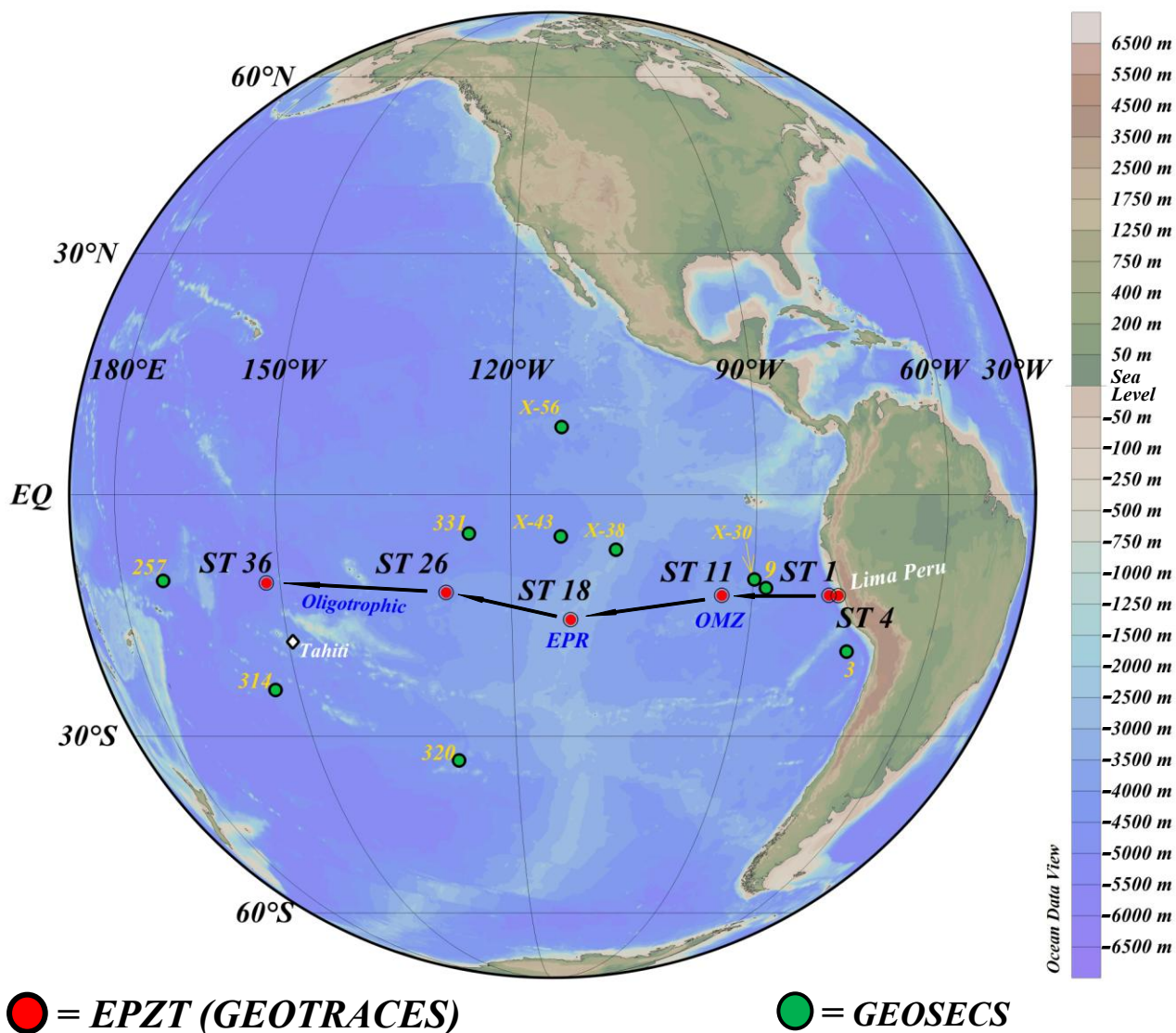


Figure 2.1. Sample location of six super stations in US GEOTRACES GP16 East Pacific Zonal Transect (EPZT) on the ship RV Thomson during October to December 2013. ST 3 and 9 of the Navoceanoo cruise (U.S.S. "Bartlett") to supplement the GEOSECS track (Thompson and Turekian, 1976). ST X-30, X-38, X-43 and X-56 Radium sampling, (Chung and Craig, 1973). ST 257, 314, 320, 331 Geosecs, (Chung and Craig, 1983).

Following the successful intercalibration for both ^{210}Po and ^{210}Pb efforts conducted as a part of the GEOTRACES Intercalibration program, samples were collected and highly accurate and precise radiochemical measurements of these nuclides were ascertained (Church et al., 2012; Baskaran et al., 2013). Details on the sample size, storage, pretreatment, and processing for

particulate and dissolved samples are given in earlier publications (Church et al., 2012; Baskaran et al., 2013) and in the *Cruise and Methods Manual*. This manual, the ‘Cook Book’, can be referenced at <http://www.geotraces.org/images/stories/documents/intercalibration/Cookbook.pdf>.

Sampling location information including the station number, location, and the bottom and mixed layer depths are shown in Table 2.1 below.

Table 2.1
Sampling location, total water depth and mixed-layer depth of six super stations of the US GEOTRACES GP16 East Pacific Zonal Transect (EPZT).

Station #	GEOTRACES #	Location	Latitude (°S)	Longitude (°W)	Sample Collection Date	Bottom Depth (m)	Mixed Layer Depth * (m)
EPZT-4	2300	Peru Shelf	12.0448	77.8181	11/2/2013	755	16
EPZT-1	2100	Peru Margin	12.0054	79.1955	10/29/2013	5533	46
EPZT-11	3600	Galapagos Rise (OMZ)	11.9999	94.0001	11/11/2013	3663	51
EPZT-18	8400	East Pacific Rise	14.9835	112.7504	11/20/2013	2972	36
EPZT-26	9400	South of Marquesas Fracture Zone	11.6706	127.9998	12/3/2013	4008	57
EPZT-36	10300	South of Vostok Island	10.5002	152.0004	12/17/2013	5162	60

* Mixed layer depth was taken from Ohnemus et al. (2016).

2.2 Water Sampling

A total of 135 water samples from six stations that were collected aboard the R/V Thomas G. Thompson (Figure 2.2) at various depths were analyzed. It has been established

during GEOTRACES inter-calibration cruises that Niskin bottles (Figure 2.3) with Teflon coated springs are suitable in the collection of seawater for ^{210}Po and ^{210}Pb (Church, et al., 2012).



Figure 2.2a (left photo) R/V Thomas G. Thompson.

http://www.interactiveoceans.washington.edu/file/The_Research_Vessel_the_Thompson_in_Nootka_Sound

Figure 2.2b (right photo) Rear view of RV Thompson.

https://www.ocean.washington.edu/files/tgtstarboardquarterportagebay-20150903035458_large@2x.jpg

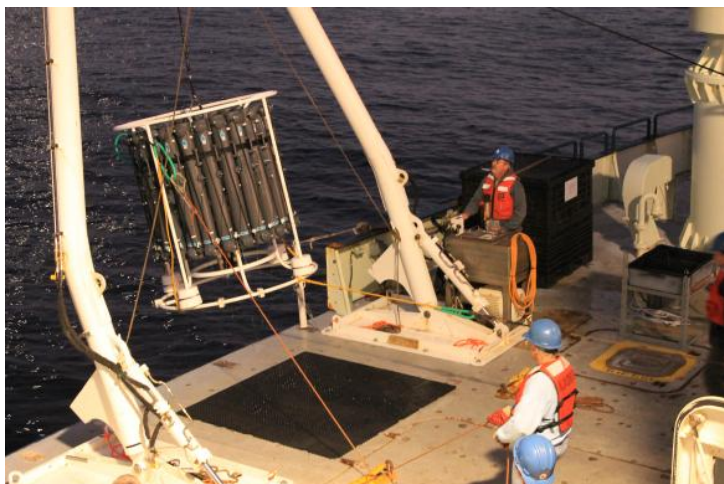
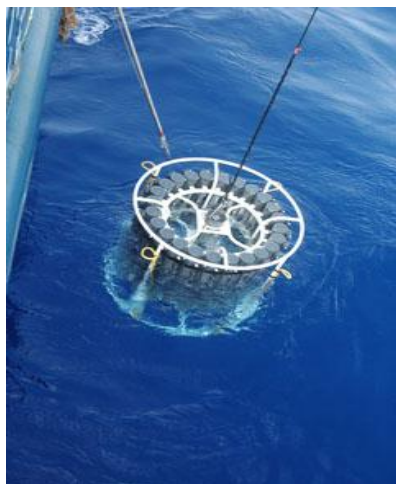


Figure 2.3a (left photo) Rosette of niskin bottles used for dissolved sample collection.

<https://websites.pmc.ucsc.edu/~kbruland/Photos/compPhotos/comp08GeotracesRosette.jpg>

Figure 2.3b (right photo) GEOTRACES rosette collecting seawater samples at different depths.

<https://hginthesea.wordpress.com/category/north-atlantic/page/9/>

As seen in Figure 2.4, for operationally defined dissolved particles of Po and Pb, the water samples collected in Niskin bottles that were analyzed for this thesis were filtered through the Supor cartridge filters with a pore size of $0.45\ \mu\text{m}$ by Group I (WSU). Particulates, both large

and small, were filtered through a McLane Pump and then analyzed by Group II (Queens College).

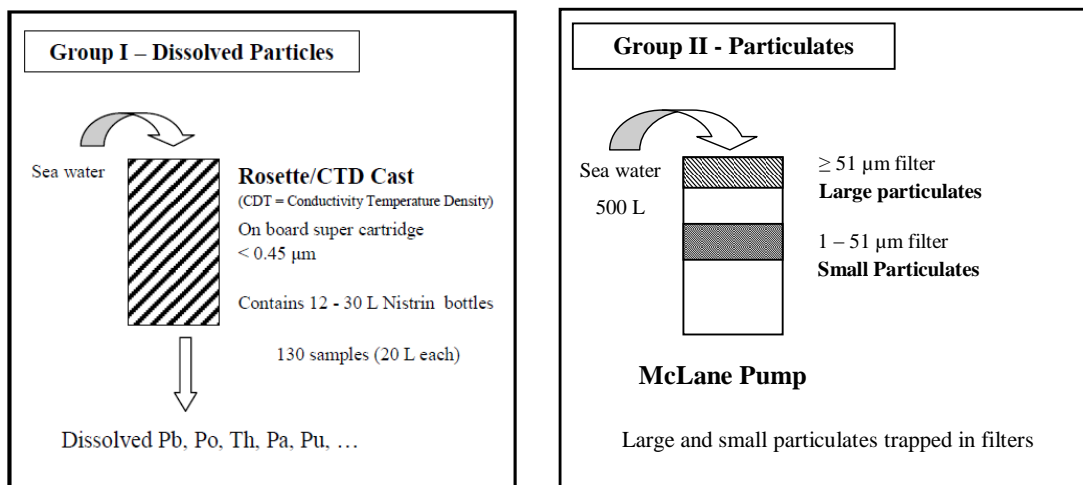


Figure 2.4. GEOTRACES Water Filterization, Group I (Dissolved) and Group II (Particulates).

Since both Po and Pb are particle-reactive, the samples were filtered (details given in Figure 2.6) within 1-2 hours after collection. The filtered seawater sample, with volumes ranging between 12 to 22 liters, were collected in acid-cleaned polyethylene (LDPE) cubitainers, and acidified with trace-metal grade 6M HCl to a pH of ~ 2 (60 mL of 6M HCl for each ~ 20 L sample). The cubitainer cap was sealed with plastic wrap (e.g., Parafilm) and stored double bagged in plastic bags. The samples were appropriately labeled with the GEOTRACES specific number ID according to sample station, date and depth. The date is essential in the radionuclide decay and in-growth corrections. Sample collection preparation of cubitainers, milk crates and pallet shipping containers are shown in Figure 2.5. The dissolved data was combined with particulate ($>1 \mu\text{m}$) ^{210}Po and ^{210}Pb data (provided by Yi Tang and Gillian Stewart; details on particulate matter sampling are given in Rigaud et al., 2015). The dissolved ^{226}Ra data was provided by Matt Charette (Woods Hole Oceanographic Institution) for the interpretation of ^{210}Pb data.



Figure 2.5. Sample collection preparation of cubitainers, milk crates and pallet shipping containers.

2.3 Laboratory Analysis

The determination of ^{210}Po and ^{210}Pb in dissolved water samples (and analyses of ^{210}Po and ^{210}Pb on particulate matter that were conducted at Queens College, NY) is routinely conducted on the same sample, first by measuring ‘in situ’ ^{210}Po and then keeping the sample for a period of 6 months to 1 year for the in-growth of ^{210}Po from ^{210}Pb . The second ^{210}Po (called ‘parent-supported’) measurement provides the data on the concentration of ^{210}Pb . There is a number of important decay and in-growth corrections that need to be applied in the calculation of the final activities of in situ ^{210}Po and ^{210}Pb activities. Reference can be made to Baskaran et al. (2013) for evaluation of these corrections and basis for their calculations.

Prior to the beginning of the analysis of the water samples to be analyzed in the laboratory at Wayne State University using the procedure listed below in Figure 2.6 the total weight of the sample was measured on a balance to a precision ± 1 g. Each batch analyzed is comprised of ten water samples along with a reagent blank.

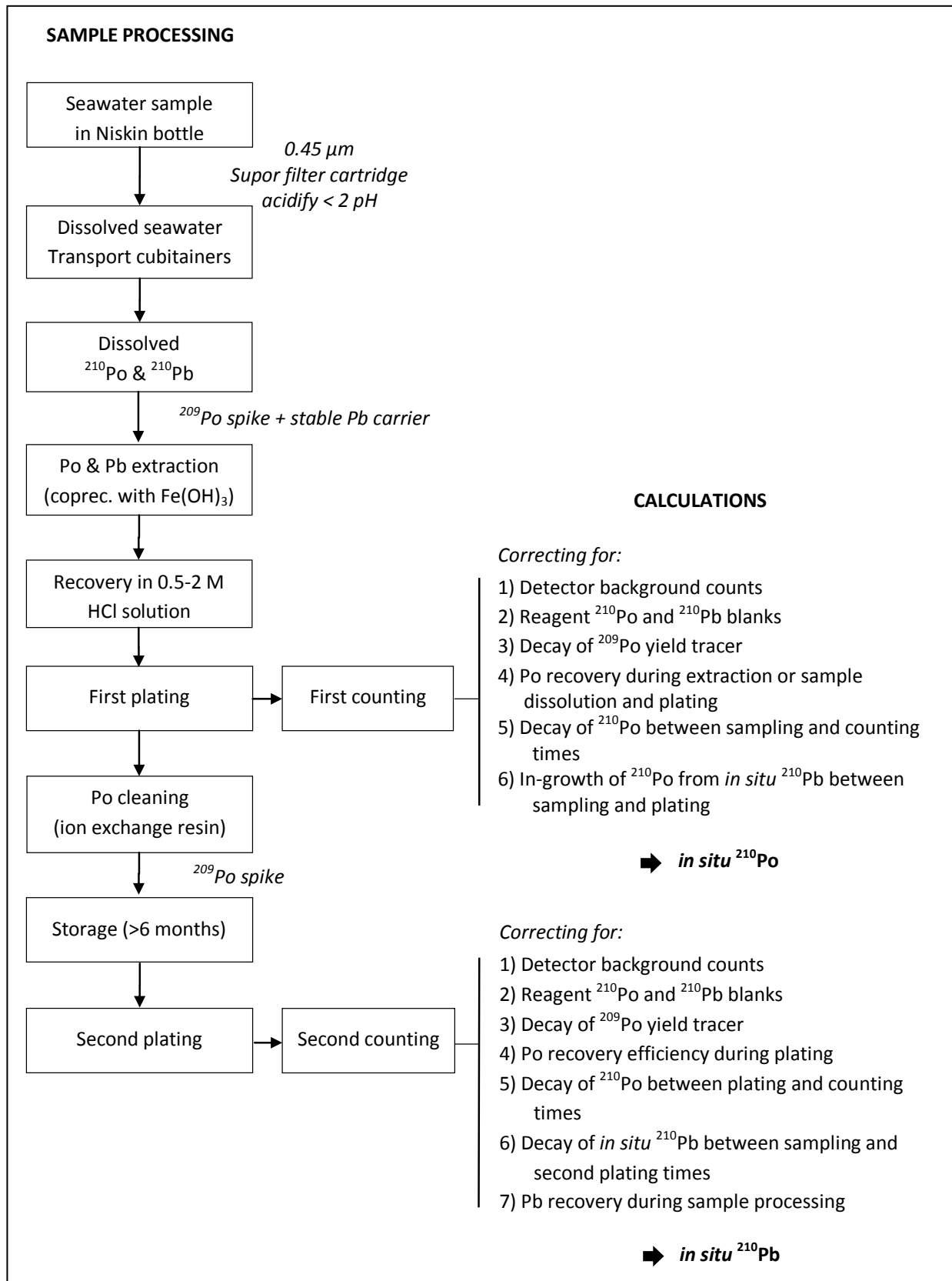


Figure 2.6. Flow chart of chemical processing for dissolved ²¹⁰Po and ²¹⁰Pb.

Each batch of samples were transferred in to pre-acid-cleaned 20-L buckets. To each of the water samples, a pre-weighed amount of NIST (National Institute of Standards and Technology) Standard Reference Material ^{209}Po (spike) with $t_{1/2} = 125.2$ years, corresponding to an activity of $\sim 1\text{-}2$ dpm for 20-L water sample was added. It is assumed that there is no loss of ^{210}Po and ^{210}Pb to walls of the container during the storage period (from collection onboard the ship till beginning of sample processing offshore laboratory). To ensure that there is very little or no ^{210}Po and/or ^{210}Pb are sorbed on to the container walls, some of the water sample stored cubitainers were leached for adsorbed ^{210}Po and ^{210}Pb (details given later).

In addition to the ^{209}Po spike, 20 mg of stable Pb carrier, prepared from a fossil lead (figure 2.7) was added as PbCl_2 , (it was found to have very low ^{210}Pb and ^{210}Po blanks) and ~ 100 mg of iron carrier (5 mg Fe/L of water) in the form of FeCl_3 was also added to the water sample (Church et al., 2012).

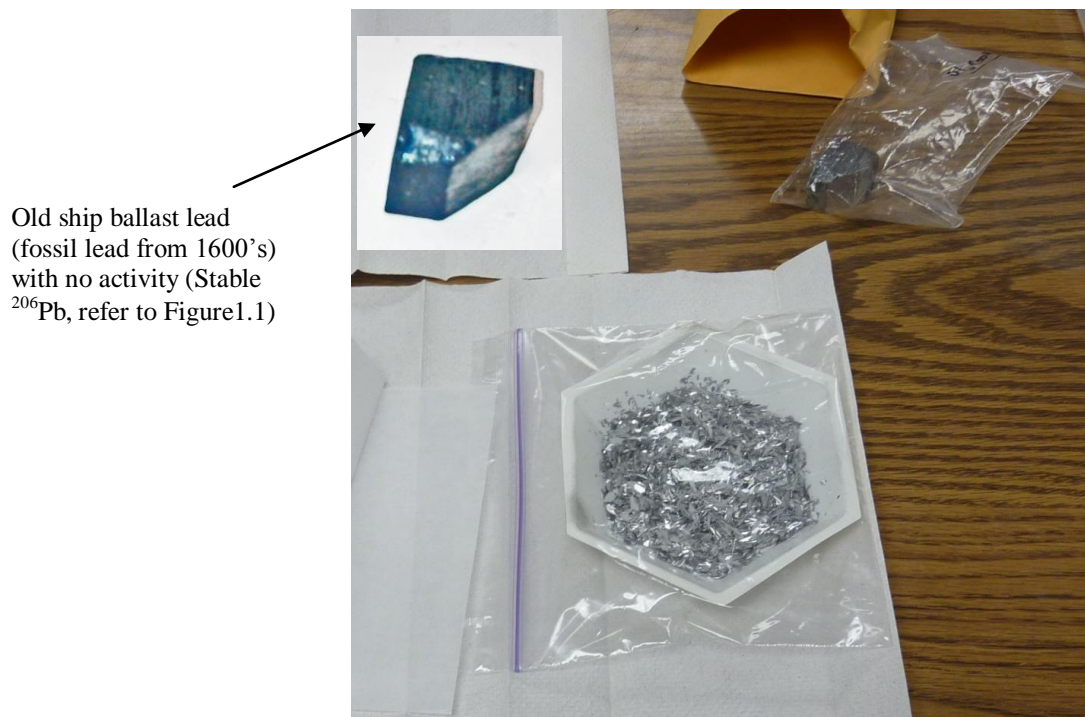


Figure 2.7. Fossil lead shaved then dissolved to make stable Pb carrier.

The acidified and spiked sample with stable Pb, ^{209}Po and Fe carriers was allowed to equilibrate for about 24 hours. After equilibration, Pb and Po were simultaneously co-precipitated with $\text{Fe}(\text{OH})_3$ by adding ammonium hydroxide (NH_3OH) to bring the solution to a pH to 4. Then 1 ml of 10% sodium chromate was added to enhance the Pb yields by co-precipitation of lead chromate (Figure 2.8). Next, the solution pH was increased to ~ 8 by adding additional NH_3OH for complete precipitation of ^{210}Po and ^{210}Pb . This was all done while continuous stirring; the solution was then allowed to settle overnight (Figures 2.9).

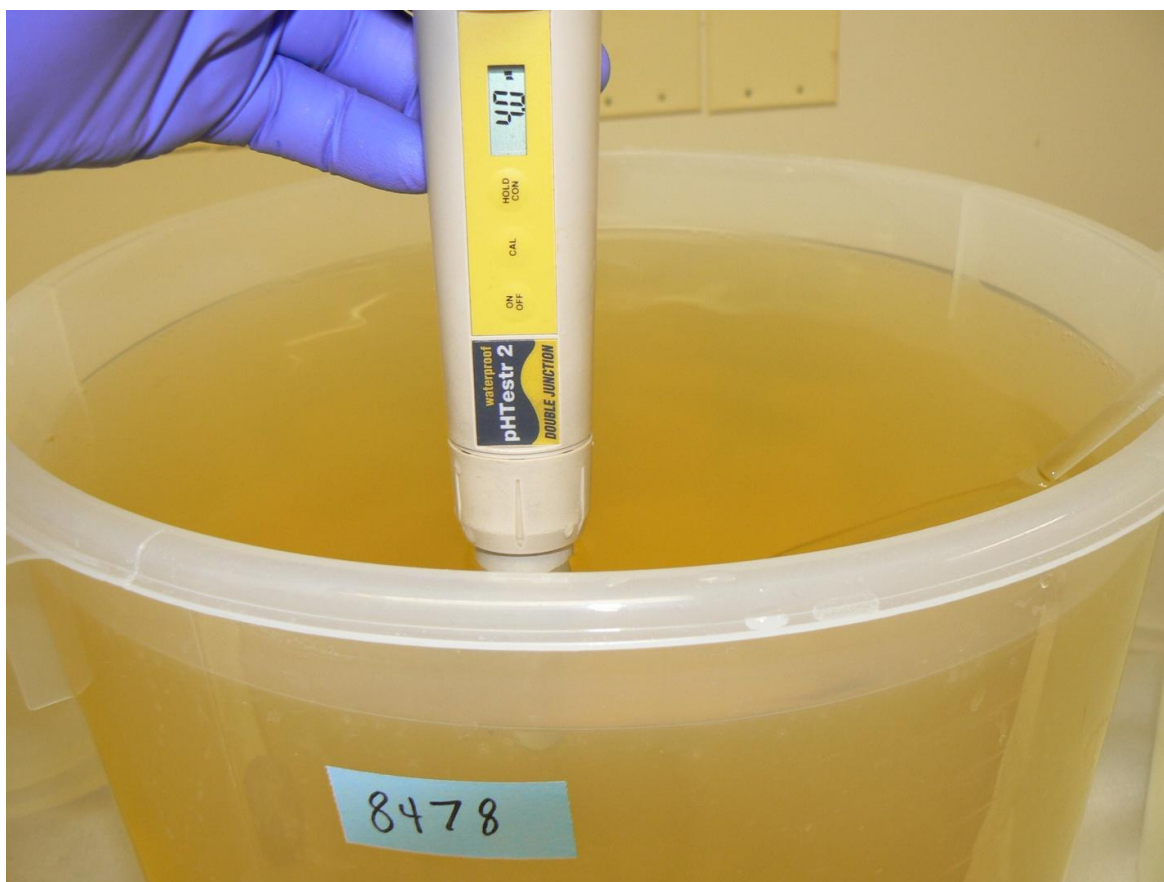


Figure 2.8. At pH 4, 10% sodium chromate added to water sample to co-precipitate lead chromate.

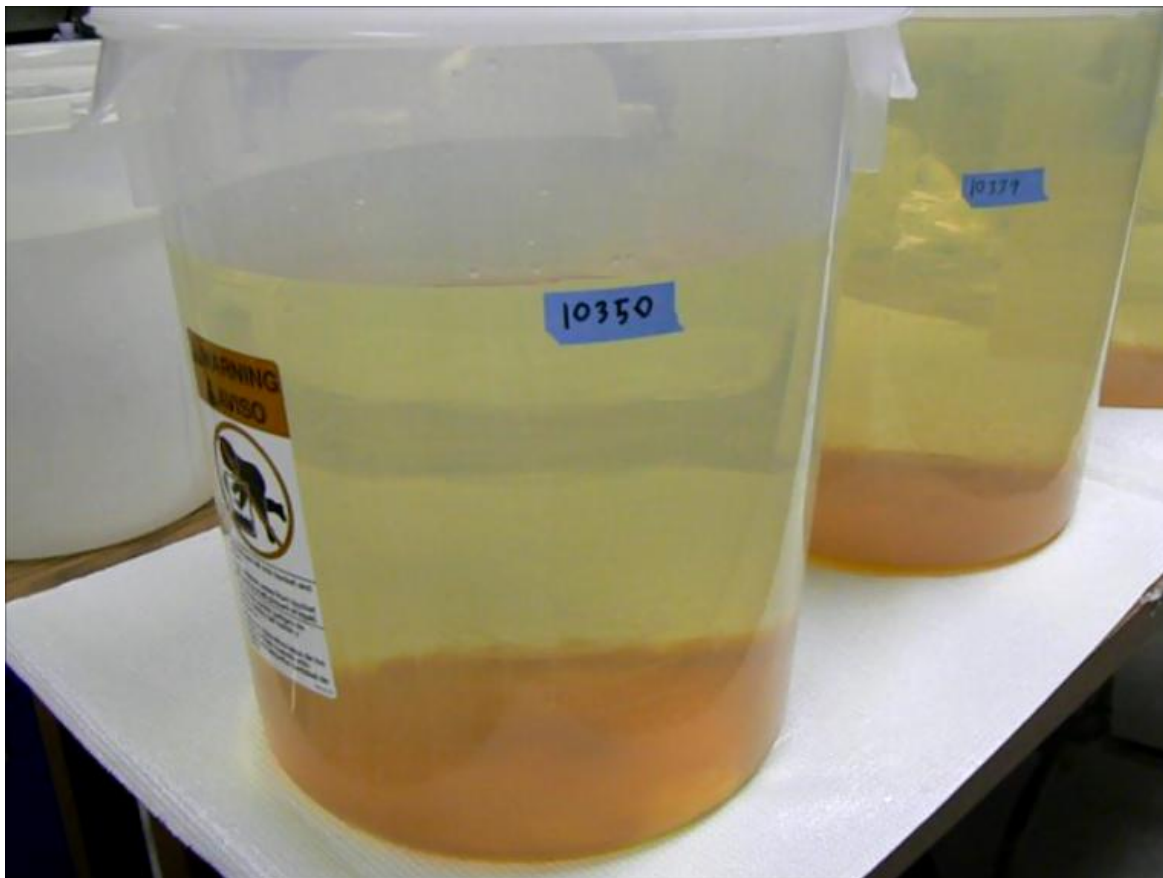


Figure 2.9. $\text{Fe}(\text{OH})_3$ precipitate containing ^{210}Po , ^{209}Po , ^{210}Pb , and stable Pb settled overnight.

The precipitate and the solution were separated by successive decanting, followed by filtration (Figure 2.10 and 2.11). The precipitate was dissolved by adding ~5 milliliters of 6M HCl to the filter paper followed by washing of the filter paper with deionized water to bring the volume to 50 ml for plating in 0.2-0.5 N HCl solution. To this solution, 200 mg of ascorbic acid was added to reduce Fe^{3+} to Fe^{2+} yielding a colorless solution and adjusted to pH ~2 (Figure 2.12).

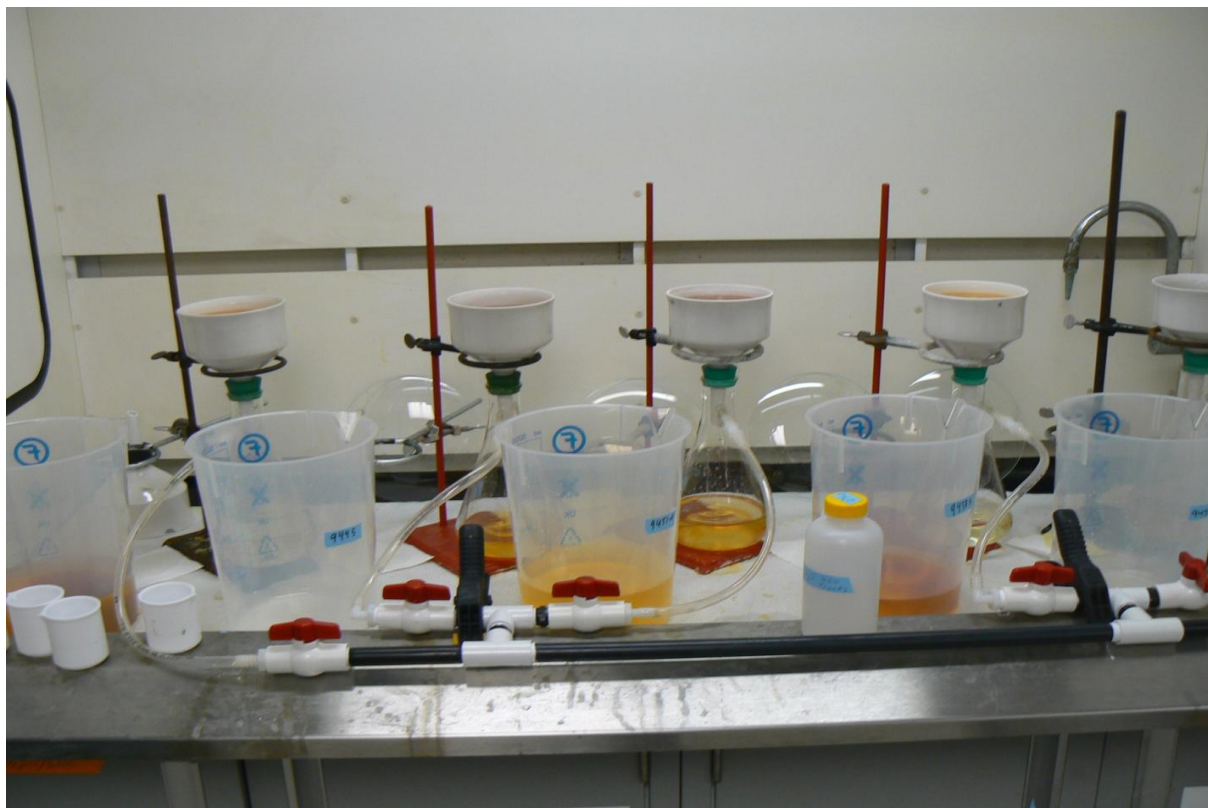


Figure 2.10. Decanting and filtration.



Figure 2.11. Filtered precipitate collecting on filter paper.



Figure 2.12. Solution after adding ascorbic acid prior to electroplating.

The Po isotopes in solution were deposited on a 15.9 mm polished silver (Ag) disc or planchet (Figure 2.13) and the reverse side of each planchet is covered by a transparent tape to block plating (Figure 2.14). As seen in Figure 2.15, the solution was heated to just below 90°C for ~ 4 hours under continuous stirring using a magnetic stirrer and Po was plated by spontaneous electroplating (Flynn, 1968; Church et al., 1994; Lee et al., 2014).

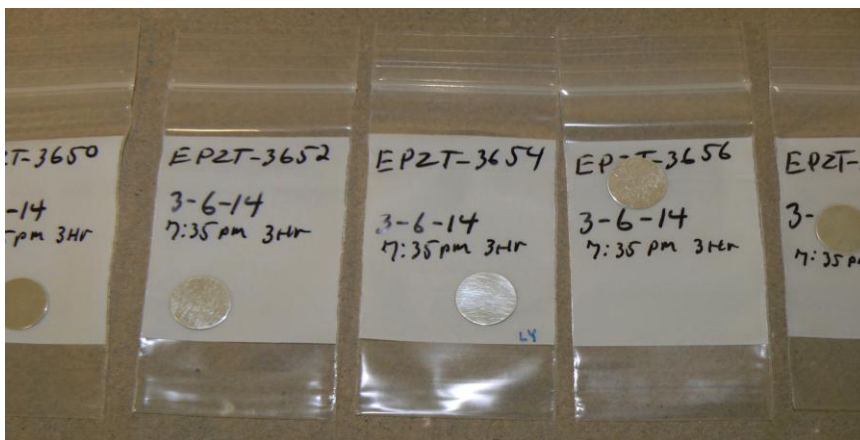


Figure 2.13. 15.9 mm Polished silver planchet on sample bags.



Figure 2.14. Taped 15.9 mm planchets.



Figure 2.15. Electroplating of ^{210}Po on to polished silver planchets.

The most widely used instrument for analyzing dissolved ^{210}Po and ^{210}Pb in seawater is isotope dilution method using alpha spectroscopy (Sarin et al., 1992; Radakovitch et al., 1998; Hong et al., 1999; Kim et al., 1999; Rutgers van der Loeff and Moore, 1999; Baskaran et al., 2009). All ^{210}Po -plated silver discs for this study were assayed in one of the two Octete PC 8-input alpha spectrometers (Figure 2.16).



Figure 2.16. Silver planchet analyzed in (16) Octete PC 8-input alpha spectrometers.

The background of each of the detectors used for the measurements of ^{210}Po was monitored periodically. The background of each detector is < 0.1 count per hour (cph) and the appropriate background was subtracted from each of the samples and blanks (Table 2.2).

Table 2.2.

Alpha Detector Efficiency and Background Counts per hour (cph)

Detector #	^{209}Po Bkg cph	^{210}Po Bkg cph	Am-based detector efficiency (%)	Pu-based detector efficiency (%)
D-1	0.06 ± 0.01	0.05 ± 0.01	27.4	30.9
D-2	0.08 ± 0.01	0.01 ± 0.01	16.7	18.6
D-3	0.09 ± 0.02	0.01 ± 0.01	17.7	19.8
D-4	0.04 ± 0.01	0.02 ± 0.01	28.7	31.9
D-5	0.06 ± 0.01	0.02 ± 0.01	27.0	30.2
D-6	0.06 ± 0.02	0.03 ± 0.01	26.7	29.6
D-7	0.07 ± 0.02	0.04 ± 0.01	26.6	29.6
D-8	0.04 ± 0.01	0.03 ± 0.01	27.6	30.5
D-9	0.06 ± 0.01	0.03 ± 0.01	27.2	30.0
D-10	0.04 ± 0.01	0.02 ± 0.01	27.4	30.8
D-11	0.03 ± 0.01	0.02 ± 0.01	27.1	30.2
D-12	0.06 ± 0.01	0.02 ± 0.01	26.6	29.7
D-13	0.05 ± 0.01	0.03 ± 0.01	28.0	31.2
D-14	0.07 ± 0.01	0.04 ± 0.01	27.9	31.0
D-15	0.06 ± 0.01	0.04 ± 0.01	26.9	30.2
D-16	0.06 ± 0.01	0.03 ± 0.01	26.9	30.0

The efficiency of each alpha detector was determined using standard Am (Americium) and Pu (Plutonium) sources. Note that the alpha detector efficiency is not required in the calculation of the ^{210}Po activities, as ^{209}Po is an internal tracer and the $^{210}\text{Po}/^{209}\text{Po}$ ratio and the activity of ^{209}Po are only involved in the calculation of ^{210}Po activity.

In a couple of Po plated planchets (out of a total of 135 samples + 13 reagent blanks), the thickness of the plating was found to be thick, likely from the plating of iron compounds (Figure 2.17). The Ag planchets were leached for one hour with concentrated (~12 M) HCl. After a major portion of the impurities plated on the Ag disk were removed, the same cleaned planchet was recounted without much loss of Po and with improved resolution. The procedure is detailed in Benoit and Hemond (1988).

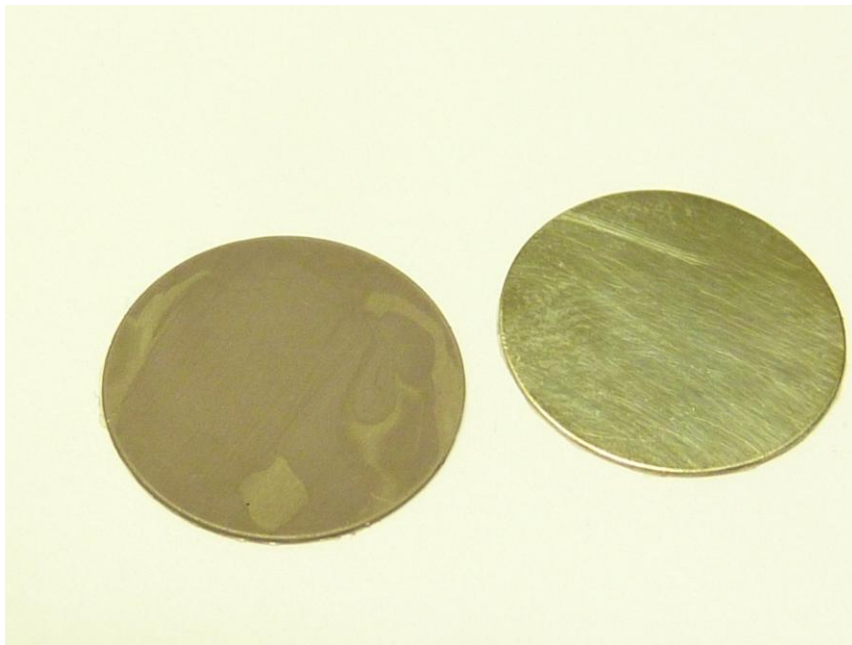


Figure 2.17. Po plated planchet with thick coating of iron compounds (left) compared to planchet without iron compounds (right).

The residual solution (Figure 2.18) was dried completely and the residue was taken in 5 ml of 9M HCl for the separation of residual Po from the Pb using an anion-exchange (AG1-X8) column as seen in Figure 2.19 (Baskaran et al., 2013).



Figure 2.18. Residual solution dried before taking to 9M HCl for anion exchange column.

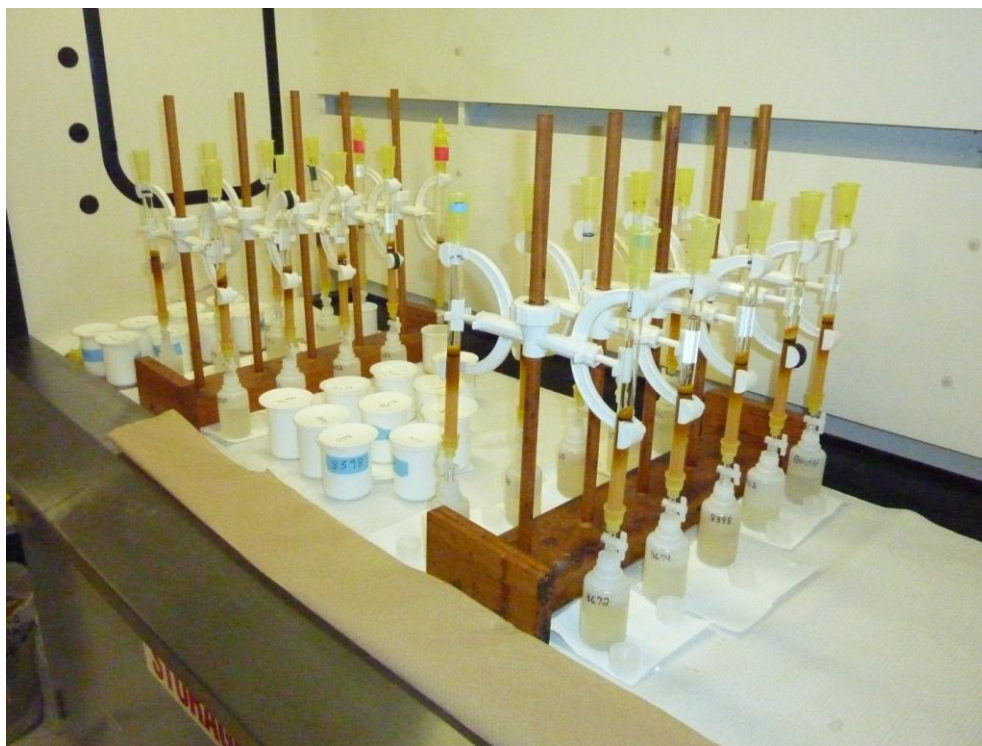


Figure 2.19. Separation of residual Po from Pb using anion-exchange columns.

The purified Pb fraction was spiked again with ^{209}Po and stored in a clean plastic bottle for at least 6 - 12 months after which the ^{210}Pb activity was measured by the ingrown activity of its granddaughter ^{210}Po . The second ^{210}Po activity (called ‘parent-supported’) measurement provides the data on the activity of ^{210}Pb . A number of important decay and in-growth corrections were applied in the calculation of the final activities of in situ ^{210}Po and ^{210}Pb activities (Baskaran et al., 2013). For the determination of ^{210}Pb yield, a precise volume of the aliquot of the stored solution (5%) was taken after column separation (and ^{209}Po spike addition) in an acid-cleaned polyethylene bottle for stable Pb determination. The concentrations of stable Pb were determined using an inductively coupled plasma mass spectrometry, ICP-MS (Figure 2.20). The remaining solution was utilized for the electroplating of ingrown ^{210}Po as described above. The final activity of ^{210}Pb calculation involves the in-growth factor for ^{210}Po , decay of ^{210}Pb from collection to the second ^{210}Po plating, and chemical recovery of Pb (Baskaran et al., 2013).

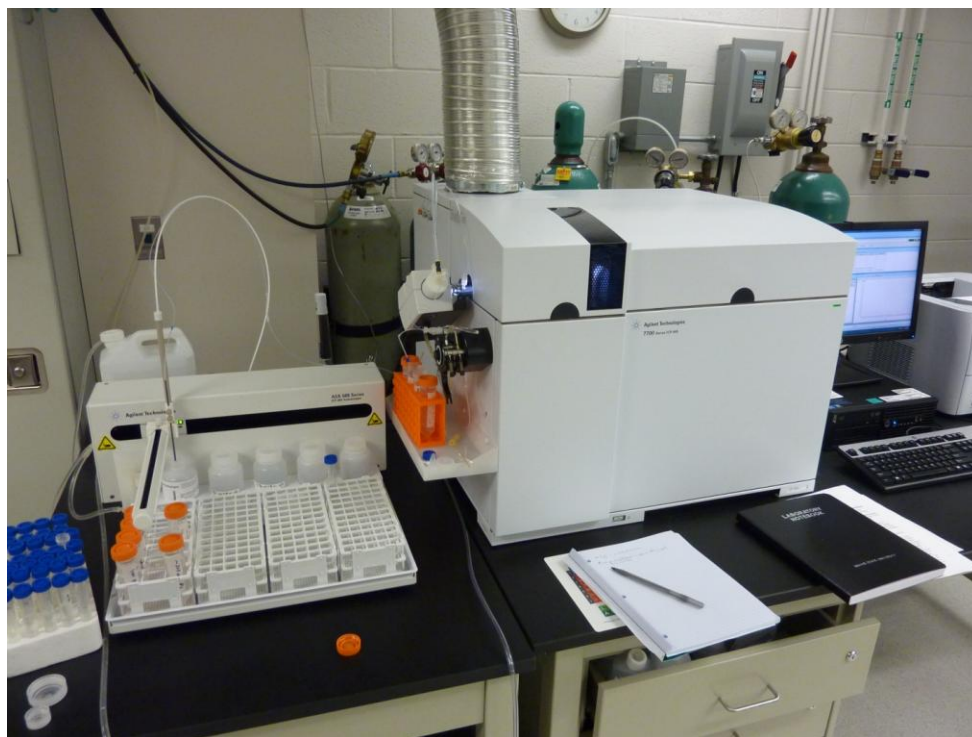


Figure 2.20. Agilent Technologies, 7700 Series, ICP-MS used for Stable Pb determination.

2.4 Digestion of Particulate and Aerosol Filters

A number of procedures have been followed in the digestion of the particulate water and aerosol filter material. Particulate samples were collected using a McLane in situ pump (Figure 2.21) at approximately the same depths as the dissolved samples along the transect. Approximately 600-700 liters of seawater were filtered through a 51 μm pre-filter screen followed by 1 μm QMA quartz filter to obtain the small particulates samples. Approximately one half of the polyester pre-filter (>51 μm , large particles) and 16% of the QMA filter (1-51 μm , small particles) were used for ^{210}Po and ^{210}Pb analysis. Details on the digestion of particulate matter and subsequent analysis are given in Baskaran et al. (2013) and Rigaud et al. (2015). All particulate ^{210}Po and ^{210}Pb activity values were corrected for decay and in-growth, similar to dissolved water samples.

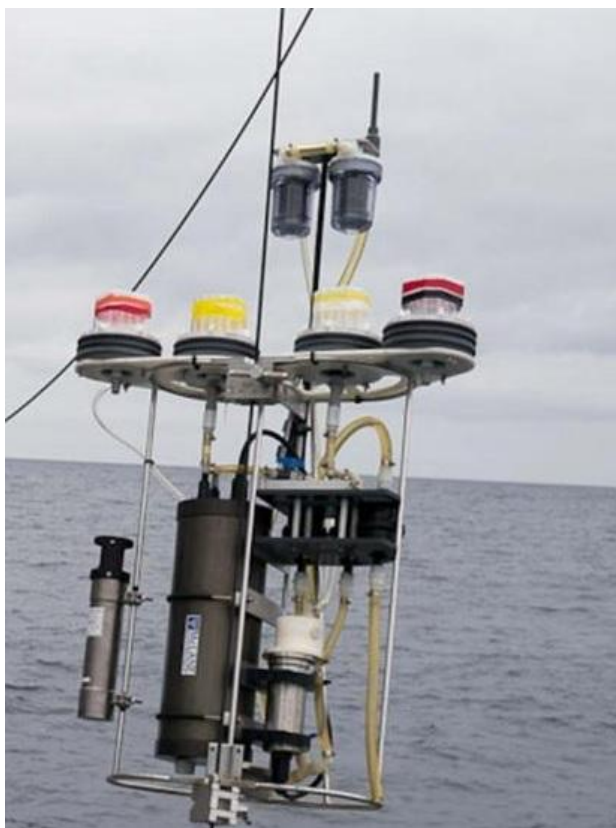


Figure 2.21. McLane Pump from RV/Thomson, EPZT cruise.
Photo credit Brett Longworth/Woods Hole Oceanographic Institution.

Since the aerosol particulate matter (collected with a Tisch Environmental TSP TE5170V aerosol sampler, Figure 2.22) is adsorbed on the QFA filter paper, digestion with a combination of hydrofluoric acid, HF (to break the Si matrix), nitric acid, HNO₃ (to break the organic matrix) and hydrochloric acid, HCl (to convert to chloride medium) was found to be sufficient. An aliquot (equivalent to 342 to 506 m³ air) of the filter (GFA) was obtained from the GEOTRACES aerosol group (William Landing).



Figure 2.22. High-Volume Tisch Environmental TSP TE5170V aerosol sampler.

The aerosol filter was placed in a digestion vessel and 5 ml of concentrated HCl, concentrated HNO₃ and HF was added. To the mixture, precisely weighed ²⁰⁹Po equivalent to 1 dpm was also added. The mixture was digested at 100°C for about 24 hours in a furnace. After the

digestion is complete, the solution was transferred into a 100 ml pre-cleaned Teflon beaker and evaporated. To the residue, 5 ml of concentrated HCl was added and dried. This was repeated one more time and finally 5 ml 6M HCl was added to the residue. To this, 45 ml of distilled water was added and the solution was quantitatively transferred into a 100 ml low density polyethylene bottle and stored for ~ 1 year. After the time elapsed, Po plating was conducted as described above. The planchet was assayed in an alpha spectrometer. Appropriate decay corrections, including the decay of ^{210}Pb from the time of sample collection to plating, were applied and the final activity of ^{210}Pb was calculated.

2.5 Quantification of the Sorbed ^{210}Po and ^{210}Pb onto Walls of Cubitainers

During the EPZT cruise seawater samples collected from Niskin bottles (Figure 2.3) were filtered using 0.8 μm cartridge filters and subsequently stored in 20-L cubitainers after acidification. The samples were stored for future analysis in the months of October – December 2013 for future shore-based laboratory analysis. The analysis for dissolved ^{210}Po and ^{210}Pb were conducted during the months of March - April 2014 (storage time of 2.7 to 3.8 months due to longer transit route). During this period, it is assumed that there was no loss of ^{210}Po and ^{210}Pb (note that no ^{209}Po spike or stable Pb carrier was added until the beginning of sample analysis) on to the walls of the storage containers. To assess if there is any loss by sorption onto the walls of the containers some of the cubitainers in which samples had been stored were leached for adsorbed ^{210}Po and ^{210}Pb . One water sample from the North Atlantic (UNDS 46-AW) was collected and stored on November 20, 2011 and was analyzed in February 2014. Five empty cubitainers (4 from the 2013 batch and 1 from the 2011 batch) were leached with 50 ml 6M HCl (trace metal grade) by shaking the cubitainer for 15 minutes. At the end of shaking, the cubitainer with this acid was immersed in hot tap water bath at 50°C for about 10 minutes and

then the cubitainer was again shaken vigorously. This procedure was repeated two more times. The three leached solutions were combined into one solution and then transferred into a 250 ml Teflon beaker. This solution was reduced to ~5 ml and then added 35 ml of distilled water to bring the solution to ~40 ml. Polonium from this solution was electroplated as described in Baskaran et al. (2013) for about 3 hours. The planchet was assayed using an Octete-PC (ORTEC Company) alpha spectrometer described above. Appropriate background and blank corrections were applied (Baskaran et al., 2013).

2.6 Quality Assurance and Quality Control

2.6.1 Blanks

A total of 13 complete reagent blanks, with one blank for each batch of samples were analyzed. The blanks included all the spikes and reagents, and followed all the procedures as the samples. The blank values (in dpm, with propagated error arising from counting statistics, error associated with the spike) for ^{210}Po and ^{210}Pb were calculated and the average blank value was subtracted from the samples (Table 3.1).

2.6.2 Accuracy of Measurements

A sample that was collected during 2011 North Atlantic GEOTRACES cruise was processed to compare with water samples collected during the GEOTRACES EPZT cruise data.

2.6.3 Comparison to Historical Data

Samples that were collected during the GEOTRACES EPZT cruise were compared with water samples taken close to corresponding locations and depths during the GEOSECS 1973 and 1976 cruise in the South Pacific.

2.7 Model Calculations for Final Activities of ^{210}Po and ^{210}Pb in Seawater Samples

2.7.1 Calculation of In situ ^{210}Po Activity

Generally, it is important to correct the in situ ^{210}Po for both its decay and in-growth from in situ ^{210}Pb via ^{210}Bi . This correction is for the time elapsed between sampling and that of first initial separation by plating.

Calculation of the in situ ^{210}Po activity (Baskaran et al., 2013) involves the following specific corrections:

- A) Background subtraction of the alpha spectrum for each detector for each ^{208}Po , ^{209}Po and ^{210}Po regions being used;
- B) Decay of ^{210}Po from the time of plating on Ag planchets to mid-counting time of the sample;
- C) Decay of ^{209}Po (or ^{208}Po) spike from the time of last calibration (or from the time certification for Standard Reference Materials, SRMs) to first plating; note that the half-life of ^{209}Po is 102 years first determined in 1956 has now changed to 125.2 years (Colle et al., 2014);
- D) In-growth correction from the decay of assayed in situ ^{210}Pb via ^{210}Bi ; and
- E) Decay of ^{210}Po from the time of collection to first plating on Ag planchets.

In principle, a correction factor to the measured ^{210}Po activity from the decay of in situ ^{210}Bi also needs to be applied. Since we did not measure the in situ ^{210}Bi , no correction for this was applied.

A detailed outline of these steps is presented. A set of model equations are offered that shows the step-by-step calculation. For this thesis project an extensive EXCEL spreadsheet was constructed with these equations to calculate decay/in-growth corrections, blank/background subtractions and error propagation. Furthermore, these calculations can be confirmed in consultation as presented here (Baskaran et al., 2013).

The alpha spectrometer background was obtained for every detector and its chamber geometry being used for a particular sample. The Ag planchets were made from a pure reliable source, and checked for blank/background in each batch. The background was conducted by analyzing an unused cleaned Ag planchet, and subtracting the counting rate from the Po isotope regions of interest. The detector chamber backgrounds without the Ag planchet were also checked to inspect for any spurious Po contamination, and the two backgrounds were the same within the counting uncertainty.

The ^{210}Po activity at the time of plating ($^{210}\text{A}'_{\text{Po-210}}$) is given by:

$$^{210}\text{A}'_{\text{Po-210}} \text{ (dpm)} = (^{210}\text{N}_n / ^{209}\text{N}_n) e^{\lambda_{\text{Po210}} t_1} e^{-\lambda_{\text{Pos}} t_2} \text{A}_{\text{spike}} \quad (1)$$

where $^{210}\text{N}_n$ and $^{209}\text{N}_n$ are the background-subtracted net counts of ^{210}Po and ^{209}Po , respectively; t_1 is the time elapsed between the first plating and mid-counting; t_2 is time elapsed between spike polonium (either ^{208}Po or ^{209}Po) assayed and mid-counting; A_{spike} is the amount of Po spike added (dpm); and λ_{Po210} and λ_{Pos} are decay constants of ^{210}Po and ^{209}Po , respectively.

The two sources of ^{210}Po that contribute to the $^{210}\text{A}'_{\text{Po-210}}$ activity are: i) *in situ* ^{210}Po present in the sample that had decayed from sample collection until plating; and ii) in-growth from ^{210}Pb , between the time of sampling to the time of first plating. While *in situ* ^{210}Po activity decreases with time from the time of collection, the amount of ^{210}Po derived from the in-growth of ^{210}Po via ^{210}Bi from the decay of *in situ* ^{210}Pb increases with time. Thus the in-growth of ^{210}Po from the *in situ* ^{210}Pb activity ($^{210}\text{A}_{\text{in-growth}}$) should be calculated using the Bateman's equation:

$$^{210}\text{A}_{\text{in-growth}} = ^{210}\text{A}_{\text{Pb-in situ}} \left[\lambda_{\text{Bi}} \lambda_{\text{Po}} e^{-\lambda_{\text{Pb}} T} / (\lambda_{\text{Bi}} - \lambda_{\text{Pb}}) (\lambda_{\text{Po}} - \lambda_{\text{Pb}}) + \lambda_{\text{Bi}} \lambda_{\text{Po}} e^{-\lambda_{\text{Bi}} T} / (\lambda_{\text{Pb}} - \lambda_{\text{Bi}}) (\lambda_{\text{Po}} - \lambda_{\text{Bi}}) + \lambda_{\text{Bi}} \lambda_{\text{Po}} e^{-\lambda_{\text{Po}} T} / (\lambda_{\text{Pb}} - \lambda_{\text{Po}}) (\lambda_{\text{Bi}} - \lambda_{\text{Po}}) \right] \quad (2)$$

where:

λ_{Pb} , λ_{Bi} and λ_{Po} are decay constants of ^{210}Pb , ^{210}Bi and ^{210}Po , respectively and T is the time elapsed between collection and first plating;

$^{210}A_{Pb-in\ situ}$ ($= N_1^0 \lambda_{Pb}$) denotes *in situ* ^{210}Pb activity.

The amount of in-growth correction for ^{210}Po depends on the concentration of *in situ* ^{210}Pb and the time elapsed between collection and *in situ* ^{210}Po plating, as described in Section 2.7.2. Thus, the final correction will be for the decay of *in situ* ^{210}Po from the time of collection to first plating.

The equation to calculate the *in situ* ^{210}Po activity is given by:

$$A_{in\ situ}^{Po-210} (dpm) = [^{210}A_{Po-210} (dpm) - ^{210}A_{in-growth}] e^{\lambda_{Po}T} \quad (3)$$

2.7.2 Calculation of *In situ* ^{210}Pb Activity

The *in situ* ^{210}Pb activity calculation (Baskaran et al., 2013) involves the following corrections:

- F) Background subtraction of the alpha spectrum for each detector and chamber geometry for each ^{209}Po ($^{209}N_{n2}$) (or ^{208}Po) and ^{210}Po ($^{210}N_{n2}$) regions being used;
- G) Decay of ^{210}Po from the time of second plating to mid-counting (t_3);
- H) Decay of ^{209}Po (or ^{208}Po) spike from the time of last calibration (or from the time of certification for SRM) to second plating (t_4);
- I) In-growth factor for ^{210}Po from the decay of ^{210}Pb for the time elapsed between Po-Pb separation (after first plating) and second Po plating (t_5);
- J) Chemical yield for ^{210}Pb ; and

K) Correction factor for the decay of ^{210}Pb from the time of collection to the second plating (t_6).

The activity of ^{210}Po (in-grown, from the decay of ^{210}Pb) at the time of second plating, corrected for the decay of ^{210}Po from plating to mid-counting (term G above) and for the decay of spike due to time elapsed between the last assay of spike ^{209}Po (or ^{208}Po) and the time of second plating (term H above) is given by:

$$^{210}\text{A}_{\text{Po-210}}^{\text{m}} (\text{dpm}) = \left(\frac{^{210}\text{N}_n}{^{209}\text{N}_n} \right) e^{\lambda_{\text{Po}} t_3} e^{-\lambda_{\text{Po}} t_4} A_{\text{spike}} \quad (4)$$

The in-growth of ^{210}Po from the decay of ^{210}Pb during the time elapsed between Po and Pb separation after the first plating to second plating (term J above) is given by:

$$^{210}\text{A}_{\text{Pb-210}} = ^{210}\text{A}_{\text{Po-210}}^{\text{m}} / [1 - e^{-\lambda_{\text{Po}} t_5}] \quad (5)$$

The chemical yield of $^{210}\text{A}_{\text{Pb-210}}$ is corrected by (term J above):

$$^{210}\text{A}_{\text{Pb}}' = ^{210}\text{A}_{\text{Pb-210}} / \text{chemical yield} \quad (6)$$

where:

the chemical yield (η_c) = amount of stable Pb carrier assayed/amount of stable Pb carrier added.

The *in situ* ^{210}Pb activity is corrected for the decay of ^{210}Pb from collection to plating is given

by:

$$^{210}\text{A}_{\text{Pb in situ}} = ^{210}\text{A}_{\text{Pb-210}}' e^{\lambda_{\text{Pb}} t_6} \quad (7)$$

where t_6 is the time elapsed between collection and 2nd plating and λ_{Pb} is the decay constant of ^{210}Pb .

Thus, the equation to calculate the *in situ* ^{210}Pb activity is given by:

$$^{210}\text{A}_{\text{Pb}} \textit{in situ} = (^{210}\text{A}_{\text{Po-210}}^{\text{m}}) e^{\lambda_{\text{Pb}} t_6} / \eta_c [1 - e^{-\lambda_{\text{Po-210}} t_5}] \quad (8)$$

where $^{210}\text{A}_{\text{Po-210}}^{\text{m}}$ is calculated using equation (4).

The results obtained from 135 analyzed samples along with a suite of blanks are given in Chapter 3 and the discussion of the results is presented in Chapter 4.

CHAPTER 3

RESULTS

3.1 Introduction

A total of 135 samples were analyzed for dissolved ^{210}Po and ^{210}Pb from six superstations along with thirteen reagent blanks. One water sample from North Atlantic collected in 2011 was also analyzed to assess if $^{210}\text{Po}/^{210}\text{Pb}$ activity is 1.0. For the sake of interpretation, the particulate (large particulate: $>51\ \mu\text{m}$ and small particulate: $1\text{-}51\ \mu\text{m}$) were also combined with the dissolved results. The particulate data were provided by the collaborating group from CUNY, New York (Dr. Gillian Stewart, PI). The dissolved ^{226}Ra data were provided by Matt Charette (Woods Hole Oceanographic Institution) for the interpretation of our ^{210}Pb data.

3.2 Quality Assurance and Quality Control

3.2.1 Blanks

As mentioned in the Materials and Methods section, a total of 13 complete reagent blanks, with one blank for each batch of samples were analyzed. The blanks include all the spikes, reagents added and followed all the procedures as that for the samples. The blank values (in dpm, with propagated error arising from counting statistics, error associated with the spike) for ^{210}Po and ^{210}Pb are given in Table 3.1. The blank activities are compared to the activities of ^{210}Po and ^{210}Pb in the samples. The activity of ^{210}Po in 13 blanks ranged between 2.0 and 10.3% ($= 100 \times \text{activity of } ^{210}\text{Po} \text{ in the blank}/\text{median activity of } ^{210}\text{Po} \text{ in that batch}$) while the corresponding values for ^{210}Pb ranged between 2.7 and 7.5% (Table 3.1). The average blank values for ^{210}Po and ^{210}Pb in the 13 blanks that were analyzed are 0.091 ± 0.018 dpm, (range 0.061 to 0.117 dpm); and 0.097 ± 0.011 dpm (range: 0.077 to 0.113 dpm), respectively (Table 3.1). This variable % of blank subtraction for ^{210}Po and ^{210}Pb is mainly due to the variable volume of water

samples available for analyses and the variations in the activities of the samples are also is a factor. The ^{210}Po and ^{210}Pb blank values are comparable to the blank value reported by the Yale group during the GEOSECS Indian Ocean expedition of 0.089 ± 0.049 dpm for ^{210}Pb (Cochran et al., 1983).

Table 3.1
Reagent blank activities (range and median) of ^{210}Po and ^{210}Pb in 13 batches of samples and percentage subtracted* from samples for blanks

Blk #	Date run	^{210}Po in blank			^{210}Pb in blank		
		dpm	% subtracted	Range (%)	dpm	% subtracted	Range (%)
1	2/27/2014	0.109 ± 0.020	9.8	5.5 - 20.1	-	-	-
2	2/28/2014	0.061 ± 0.016	4.6	3.4 - 6.6	0.092 ± 0.015	7.4	4.5 - 8.6
3	3/1/2014	0.117 ± 0.013	4.8	2.9 - 7.6	-	-	-
4	3/3/2014	0.088 ± 0.012	3.1	2.3 - 6.5	-	-	-
5	3/3/2014	0.095 ± 0.015	3.5	2.2 - 5.8	0.097 ± 0.014	4.7	2.3 - 7.1
6	3/5/2014	0.099 ± 0.016	10.3	4.5 - 56.6	0.104 ± 0.009	7.5	2.3 - 29.7
7	3/6/2014	0.064 ± 0.013	2.0	1.5 - 12.6	0.105 ± 0.008	4.0	2.6 - 17.3
8	3/6/2014	0.095 ± 0.014	4.6	2.5 - 9.3	0.082 ± 0.009	4.4	1.0 - 6.0
9	3/7/2014	0.076 ± 0.016	6.5	1.8 - 16.0	0.077 ± 0.009	5.2	2.2 - 9.7
10	3/8/2014	-	-	-	0.108 ± 0.009	4.0	2.7 - 6.1
11	3/8/2014	0.081 ± 0.015	3.5	1.8 - 11.3	0.113 ± 0.011	3.4	2.4 - 5.8
12	3/9/2014	0.088 ± 0.017	2.9	2.6 - 6.7	0.098 ± 0.009	2.7	2.3 - 3.3
13	3/11/2014	0.112 ± 0.019	4.9	3.3 - 9.3	0.094 ± 0.060	3.4	2.7 - 4.4
		Average	Std. dev.			Average	Std. dev.
		$0.091 \pm$	0.018			$0.097 \pm$	0.011

*: median value was used for subtraction

3.2.2 Accuracy of Measurements

As outlined in the Materials and Methods section, one dissolved water sample that was collected on November 20, 2011 North Atlantic GEOTRACES cruise was analyzed on February 21, 2014 for ^{210}Po and ^{210}Pb (time elapsed from collection to processing was 2.252 years). The final activities of ^{210}Po and ^{210}Pb were corrected for decay/ in-growth, as outlined in Baskaran et al. (2013). The final activity of ^{210}Po at 2090 m in ST 10 (USGT11-10) at the time of collection was found to be 8.56 ± 0.28 dpm 100 L^{-1} with the corresponding activity of ^{210}Pb to be 8.48 ± 0.29

dpm 100 L^{-1} and $^{210}\text{Po}/^{210}\text{Pb}$ activity ratio of 1.01 ± 0.05 (Table 3.2). Another sample from the same cruise at the same site and depth processed within 2 months after collection yielded the following values: $^{210}\text{Po} = 7.07 \pm 0.71 \text{ dpm } 100 \text{ L}^{-1}$; $^{210}\text{Pb} = 7.12 \pm 0.66 \text{ dpm } 100 \text{ L}^{-1}$; $^{210}\text{Po}/^{210}\text{Pb}$ AR = 0.99 ± 0.14 as seen in Table 3.2 (Rigaud et al., 2015). The values agree within 2σ , although the absolute activity values of ^{210}Po and ^{210}Pb of Rigaud et al. (2015) are lower by 17.4% and 16.0%, respectively, compared to the standard deviation calculated values obtained from analysis of all samples in 2014.

Table 3.2
Comparison of dissolved ^{210}Po and ^{210}Pb on samples collected from the same station and time and collected at different time in the Atlantic Ocean

Station	Location (latitude, longitude)	Depth (m)	Final ^{210}Po dpm 100L^{-1}	^{210}Pb in-situ dpm 100L^{-1}	$^{210}\text{Po}/^{210}\text{Pb}$ AR	Reference
ST-10 UDNA-46	31.7378 N; 64.1902 W	2099	8.56 ± 0.28	8.48 ± 0.29	1.01 ± 0.05	This study
USGT11-10	31.7378 N; 64.1902 W	2096	7.07 ± 0.71	7.12 ± 0.66	0.99 ± 0.14	Rigaud et al., 2015
Nares Abyssal Plain	23.20 N; 63.9817 W	2550	-	9.20 ± 2.20	-	Cochran et al., 1990**

*: ST-10 UDNA-46 and UST11-10 samples were collected in the same cruise

** : total ^{210}Pb (particulate ^{210}Pb in NAZT-GEOTRACES was reported to be $0.41 \pm 0.03 \text{ dpm } 100 \text{ L}^{-1}$) (Rigaud et al., 2015).

3.2.3 Comparison of Recent GEOTRACES EPZT Data with the Historical Data

In order to assess the extent of similarity between the data from this GEOTRACES study and the earlier GEOSECS published data from March 1973, a comparison was made of two stations in close proximity to each other. From this current study, as seen in Table 3.3, GEOTRACES EPZT ST 1, located at 12.0054°S , 79.1955°W with depth of 5,533 m was

compared to the GEOSECS ST 9, located at 11.145°S, 88.248°W (Thomson and Turekian, 1976). Since the ^{210}Po and ^{210}Pb activities in surface waters could vary seasonally, three deep water samples at ~500, 800 and 1,200 m were chosen from that one station (ST 1) for which there is data for comparison. Since Thomson and Turekian (1976) data is on unfiltered water, comparisons were made to the total ^{210}Po ($^{210}\text{Po}_T$) and total ^{210}Pb ($^{210}\text{Pb}_T$) activities. This study measured GEOTRACES EPZT ST 1 $^{210}\text{Po}_T$ and $^{210}\text{Pb}_T$ activities at 450, 550, 800 and 1200 m with results of 11.3 ± 0.9 , 11.3 ± 0.9 , 13.5 ± 1.0 , 16.1 ± 1.1 dpm 100L^{-1} and 10.4 ± 0.4 , 11.4 ± 0.5 , 14.6 ± 0.5 , 15.4 ± 0.5 , respectively and the corresponding earlier published values for the GEOSECS ST 9 are given in Table 3.3.

Table 3.3.

Inter-comparison of measured total ^{210}Po and ^{210}Pb activities of GEOTRACES⁺ (GTRACE, ST 1, 12.0054°S, 79.1955°W, 5,533 m, October 2013) to those of GEOSECS (GSECS, ST 9, 11.145°S, 88.248°W, 18 March 1973)^{*} in Eastern South Pacific

Depth (m)	$^{210}\text{Po}_T$	$^{210}\text{Po}_T$	$^{210}\text{Pb}_T$	$^{210}\text{Pb}_T$	$(^{210}\text{Po}_T/^{210}\text{Pb})_T$	$(^{210}\text{Po}_T/^{210}\text{Pb})_T$
	dpm/100L	dpm/100L	dpm/100L	dpm/100L	AR	AR
	GTRACE	GSECS	GTRACE	GSECS	GTRACE	GSECS
550 (498)**	11.3 ± 0.9	10.7 ± 1.4	11.4 ± 0.5	10.6 ± 1.0	1.00 ± 0.09	1.01 ± 0.17
450 (498)	11.3 ± 0.9	10.7 ± 1.4	10.4 ± 0.4	10.6 ± 1.0	1.08 ± 0.09	1.01 ± 0.17
800 (791)	13.5 ± 1.0	9.2 ± 1.2	14.6 ± 0.5	13.8 ± 1.1	$.93\pm 0.07$	0.67 ± 0.10
1200 (1237)	16.1 ± 1.1	20.1 ± 1.7	15.4 ± 0.5	15.4 ± 0.9	1.05 ± 0.08	1.31 ± 0.14

⁺: The GEOTRACES data for particulate ^{210}Po and ^{210}Pb were analyzed at Gillian Stewart's laboratory and the dissolved ^{210}Po and ^{210}Pb were analyzed at Wayne State University.

^{*}: Data taken from Thomson and Turekian (1976); the specific activity is converted from dpm 100 kg^{-1} to dpm 100 L^{-1} , assuming a density of 1027 kg m^{-3} .

^{**}: Numbers in parenthesis denote depths in GEOSECS

The agreement for total ^{210}Pb ($^{210}\text{Pb}_T$) activity between the GEOTRACES and GEOSECS data in all three depths as seen in Table 3.3 was excellent (agreement within $\pm 1\sigma$). However, the

total ^{210}Po ($^{210}\text{Po}_T$) activity in two of three samples agreed within 2σ , but in one (800 m), there was disagreement. The difference in ^{210}Po can be attributed to variable extents of remineralization of biogenic particulate matter through the water column which preferentially affects the ^{210}Po profile (since $^{210}\text{Po}/^{210}\text{Pb}$ AR in particulate phase is >1.0 , remineralization is expected to affect ^{210}Po much more than ^{210}Pb). Furthermore, ^{210}Po may not be a suitable candidate for comparison of current EPZT data with previously published data. This implies that $(^{210}\text{Po}/^{210}\text{Pb})_T$ activity ratio in deeper waters could depend on the extent of remineralization of biogenic particulate matter.

3.2.4 Quantification of the Sorbed ^{210}Po and ^{210}Pb on to Cubitainers Walls

To quantify the amount of ^{210}Po lost from the sample to the walls of the container due to long-term storage, the cubitainers were leached with 6M HCl as outlined in the Materials and Methods section. The blank-subtracted in situ ^{210}Po activities in the leachate of the containers in which the samples were stored for ~ 4 months varied between 0.017 and 0.054 dpm in Table 3.4. The average of two reagents blanks is 0.049 ± 0.007 dpm and the average blank-subtracted Pacific ^{210}Po activity is 0.034 ± 0.004 dpm (69% of the blank value). This corresponds to 3.13 ± 0.01 % of the total ^{210}Po stored in the container and this value falls generally within the 1σ error associated with the ^{210}Po data in the samples and therefore no subtraction for the wall-absorbed ^{210}Po was made. It was noted that the blank-subtracted ^{210}Po in one sample, UDNA 46-AW that was stored for 27 months is 0.064 ± 0.007 dpm, which corresponds to 3.47 ± 0.004 % of the total ^{210}Po in the sample indicating there is not much difference in the amount of sorption loss between 3 to 4 months and 27 months storage of water samples, although the data is limited to make firm conclusion. Thus, long-term storage of acidified samples at a pH of ~ 2 results in measurable loss of Po by sorption on to the container walls. Adding ^{209}Po spike and stable Pb carrier at the time

of storage of the acidified sample will aid in minimizing the loss by sorption and thereby improving the quality of in situ ^{210}Po and ^{210}Pb determination. Cochran et al. (1983) reported ~ 0.9 dpm/100 kg for ^{210}Po and 1.4 dpm/100 kg for ^{210}Pb from the leachate of the PVC containers when filtered, unspiked and unacidified samples were stored for a few days from collection to analysis during the Indian Ocean GEOSECS cruise.

Table 3.4

Amount of ^{210}Po and ^{210}Pb lost during storage of acidified (pH ~ 2.0) water samples for at least 3 months in storage cubitainers.

Sample #	Collection date	Analysis of In-situ ^{210}Po date	Leaching date	Collection to Leaching Interval days	^{210}Po Activity (Spike and Blank subtracted) dpm	% Loss of ^{210}Po	^{210}Pb Activity dpm	% Loss of ^{210}Pb
UDNA 46-AW	11/20/2011	2/21/2014	2/21/2014	824	0.064 ± 0.007	3.47 ± 0.004	0.053 ± 0.024	2.90 ± 0.013
2091-AW	10/29/2013	2/27/2014	5/28/2014	211	0.036 ± 0.004	4.39 ± 0.007		
2212-AW	10/31/2013	3/1/2014	5/28/2014	209	0.054 ± 0.006	1.44 ± 0.002		
8404-AW	11/20/2013	3/5/2014	5/28/2014	189	0.017 ± 0.002	5.79 ± 0.012		
8547-AW	11/22/2013	3/6/2014	5/28/2014	187	0.030 ± 0.004	0.89 ± 0.001		
Blank- 1- AW			8/1/2014		0.047 ± 0.007			
Blank- 2- AW			8/1/2014		0.052 ± 0.007			
Average Pacific leach of ^{210}Po (dpm)					0.034 ± 0.004			

3.3 Distribution of ^{210}Po and ^{210}Pb

The activities of dissolved ^{210}Po ($^{210}\text{Po}_d$) and ^{210}Pb ($^{210}\text{Pb}_d$) were measured at Wayne State University (WSU), whereas the activities of particulate (small particulate, 1 – 51 μm and large particulate, $> 51 \mu\text{m}$) activities of ^{210}Po ($^{210}\text{Po}_{sp}$ and $^{210}\text{Po}_{lp}$) and ^{210}Pb ($^{210}\text{Pb}_{sp}$ and $^{210}\text{Pb}_{lp}$) were measured at Queens College, NY by Yi Tang under the supervision of Dr. Gillian Stewart (collaborating Principal Investigator for the ^{210}Po and ^{210}Pb work funded by National Science Foundation). To interpret ^{210}Pb distribution and the disequilibrium between total ^{210}Pb ($^{210}\text{Pb}_T$) and ^{226}Ra , ^{226}Ra data was obtained from Drs. Matthew Charette (Woods Hole Oceanographic Institution) and Willard S. Moore (University of South Carolina). The activities of dissolved and

particulate ^{210}Po and ^{210}Pb for all six stations are given in Table 3.5 and shown in Figures 3.1, 3.2, 3.3. The errors associated with the values are the propagated error arising from counting statistics (on ^{210}Po), error associated with the ^{209}Po spike and error associated with blanks. All the errors reported are 1σ errors.

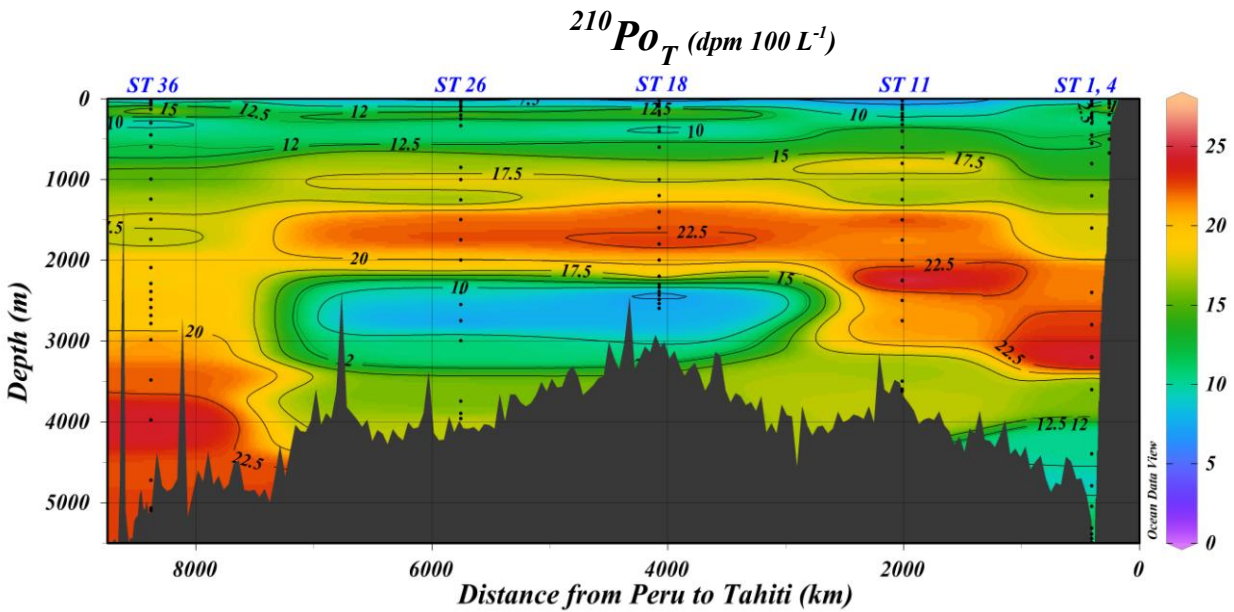


Figure 3.1. Section of $^{210}\text{Pb}_T$ activity (vertical profile), Ocean Data View (ODV).

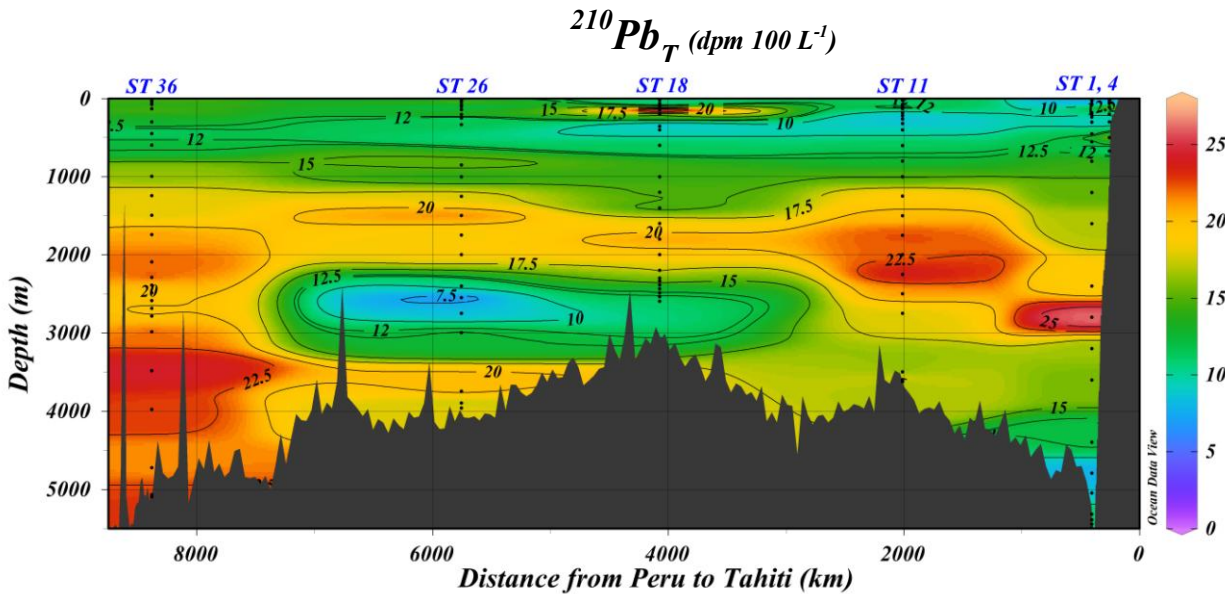


Figure 3.2. Section of $^{210}\text{Po}_T$ activity (vertical profile) Ocean Data View (ODV).

3.3.1 Activity Ratios of $^{210}\text{Po}/^{210}\text{Pb}$ and $^{210}\text{Pb}/^{226}\text{Ra}$ in the Upper 60 m and Mixed Layers

The total ^{210}Po and ^{210}Pb activity ratios, $(^{210}\text{Po}/^{210}\text{Pb})_{\text{T}}$ in the upper 60 m and mixed layers as seen in Table 3.5 varied between 0.24 and 0.83 (mean: 0.56, n=14; note that the values in the continental shelf station (STN 4) vary between 1.46 and 2.07). There is excess ^{210}Pb activity, with $^{210}\text{Pb}/^{226}\text{Ra}$ activity ratio, $\text{AR} > 1.0$ in the mixed layer, mainly due to atmospheric depositional input. The depth where $^{210}\text{Pb}_{\text{total}}/^{226}\text{Ra}$ AR is < 1.0 varies, depending on the location (ST 4, 18, 36: > 200 m; ST 11: 225-260 m; ST 1: > 300 m; ST 26: > 335 m). The activities of dissolved, particulate and total activities of ^{210}Pb depends on two factors, assuming the advective and diffusion transport terms are negligible: 1) Atmospheric depositional flux and 2) scavenging intensity from the water by suspended particulate matter.

Table 3.5

Activities of particulate and dissolved and total ^{210}Po , ^{210}Pb and activity ratios of $^{210}\text{Po}/^{210}\text{Pb}$ and $^{210}\text{Pb}/^{226}\text{Ra}$

ST #	depth (m)	$^{210}\text{PO}_p$ ^[+] dpm 100L ⁻¹	$^{210}\text{PO}_d$ dpm 100L ⁻¹	$^{210}\text{PO}_T$ dpm 100L ⁻¹	$^{210}\text{Pb}_p$ ^[+] dpm 100L ⁻¹	$^{210}\text{Pb}_d$ dpm 100L ⁻¹	$^{210}\text{Pb}_T$ dpm 100L ⁻¹	$^{210}\text{PO}_T/^{210}\text{Pb}_T$ AR	^{226}Ra ^[++] dpm 100L ⁻¹	$^{210}\text{Pb}_T/^{226}\text{Ra}$ AR
ST 4 12.0448(°S) Latitude, 77.8181(°W) Longitude; Total Depth 755 (m)	20	0.74 ± 0.06	10.67 ± 0.70	11.4 ± 0.7	0.15 ± 0.02	5.36 ± 0.23	5.51 ± 0.23	2.07 ± 0.15	6.59 ± 0.28	0.84 ± 0.05
	48	0.46 ± 0.05	13.2 ± 1.0	13.7 ± 1.0	0.38 ± 0.03	7.59 ± 0.28	7.98 ± 0.28	1.72 ± 0.14	6.14 ± 0.23	1.29 ± 0.07
	68	0.69 ± 0.06	11.2 ± 0.8	11.9 ± 0.8	0.52 ± 0.03	7.68 ± 0.30	8.20 ± 0.31	1.46 ± 0.11	7.21 ± 0.20	1.14 ± 0.06
	110	0.77 ± 0.07	25.1 ± 2.2	25.9 ± 2.2	0.74 ± 0.04	27.5 ± 1.1	28.2 ± 1.1	0.92 ± 0.09	7.13 ± 0.15	3.96 ± 0.18
	200	0.74 ± 0.05	11.2 ± 0.9	11.9 ± 0.9	0.38 ± 0.02	8.42 ± 0.33	8.80 ± 0.33	1.36 ± 0.11	8.36 ± 0.18	1.04 ± 0.05
	300	0.75 ± 0.05	9.99 ± 0.79	10.7 ± 0.8	0.34 ± 0.02	9.38 ± 0.37	9.73 ± 0.37	1.10 ± 0.09	9.74 ± 0.33	1.01 ± 0.05
	500	0.77 ± 0.05	14.4 ± 1.4	15.2 ± 1.4	0.15 ± 0.01	17.4 ± 0.7	17.6 ± 0.7	0.86 ± 0.09	12.3 ± 0.4	1.43 ± 0.08
675	NM	11.8 ± 1.0	13.5 ± 1.0	NM	9.57 ± 0.34	10.65 ± 0.42	1.27 ± 0.11	13.7 ± 0.55	0.78 ± 0.04	
ST 1 12.0054(°S) Latitude, 79.1955(°W) Longitude; Total Depth 5533 (m)	3	NM	4.22 ± 0.47	4.22 ± 0.47	NM	7.20 ± 0.29	7.20 ± 0.29	0.59 ± 0.07	7.40 ± 0.24	0.97 ± 0.05
	15	NM	6.43 ± 1.07	7.41 ± 1.08	NM	9.07 ± 0.38	9.47 ± 0.38	0.78 ± 0.12	7.40 ± 0.24	1.28 ± 0.07
	35	0.48 ± 0.08	3.87 ± 0.48	4.35 ± 0.49	0.26 ± 0.03	6.52 ± 0.33	6.77 ± 0.33	0.64 ± 0.08	6.15 ± 0.26	1.10 ± 0.07
	60	0.40 ± 0.04	7.43 ± 0.59	7.83 ± 0.59	0.20 ± 0.02	5.35 ± 0.30	5.55 ± 0.30	1.41 ± 0.13	7.12 ± 0.32	0.78 ± 0.05
	80	1.11 ± 0.07	11.6 ± 0.8	12.7 ± 0.8	0.58 ± 0.05	8.12 ± 0.35	8.70 ± 0.36	1.46 ± 0.11	6.60 ± 0.25	1.32 ± 0.07
	180	0.58 ± 0.05	9.47 ± 0.81	10.0 ± 0.8	0.31 ± 0.03	11.00 ± 0.42	11.3 ± 0.4	0.89 ± 0.08	7.04 ± 0.21	1.61 ± 0.08
	210	0.67 ± 0.05	11.3 ± 0.8	11.9 ± 0.8	0.32 ± 0.02	9.19 ± 0.40	9.51 ± 0.40	1.25 ± 0.10	8.17 ± 0.20	1.16 ± 0.06
	235	0.61 ± 0.06	8.79 ± 0.78	9.40 ± 0.78	0.48 ± 0.05	8.81 ± 0.36	9.29 ± 0.36	1.01 ± 0.09	8.55 ± 0.18	1.09 ± 0.05
	300	0.74 ± 0.05	10.4 ± 0.8	11.1 ± 0.8	0.24 ± 0.02	8.67 ± 0.44	8.91 ± 0.44	1.25 ± 0.11	7.77 ± 0.20	1.15 ± 0.06
	450	0.90 ± 0.05	10.4 ± 0.9	11.3 ± 0.9	0.13 ± 0.02	10.23 ± 0.42	10.36 ± 0.42	1.09 ± 0.09	11.0 ± 0.3	0.94 ± 0.04
	550	0.86 ± 0.05	10.4 ± 0.9	11.3 ± 0.9	0.10 ± 0.01	11.3 ± 0.5	11.4 ± 0.5	1.00 ± 0.09	12.7 ± 0.3	0.90 ± 0.04
	800	0.87 ± 0.05	12.6 ± 1.0	13.5 ± 1.0	0.13 ± 0.01	14.4 ± 0.5	14.6 ± 0.5	0.93 ± 0.07	15.5 ± 0.4	0.94 ± 0.04
	1200	1.45 ± 0.08	14.7 ± 1.1	16.1 ± 1.1	0.39 ± 0.03	15.0 ± 0.5	15.4 ± 0.5	1.05 ± 0.08	20.7 ± 0.7	0.74 ± 0.03
	1600	1.63 ± 0.07	16.4 ± 1.3	18.0 ± 1.3	0.47 ± 0.02	16.5 ± 0.5	17.0 ± 0.5	1.06 ± 0.08	23.1 ± 0.6	0.74 ± 0.03
	2400	2.20 ± 0.10	19.5 ± 1.5	21.8 ± 1.5	0.93 ± 0.04	17.9 ± 0.6	18.8 ± 0.6	1.15 ± 0.09	27.2 ± 0.5	0.69 ± 0.03
	2800	2.36 ± 0.11	20.5 ± 1.9	22.9 ± 1.9	1.15 ± 0.04	25.2 ± 1.1	26.3 ± 1.1	0.87 ± 0.08	30.1 ± 1.2	0.88 ± 0.05
	3200	2.11 ± 0.11	22.4 ± 1.5	24.5 ± 1.5	0.98 ± 0.04	15.6 ± 0.5	16.5 ± 0.5	1.48 ± 0.10	30.8 ± 1.2	0.54 ± 0.03
3600	2.04 ± 0.10	13.9 ± 1.2	16.0 ± 1.2	1.01 ± 0.04	14.9 ± 0.5	15.9 ± 0.5	1.00 ± 0.08	31.9 ± 0.8	0.50 ± 0.02	
4200	3.17 ± 0.13	7.07 ± 0.73	10.2 ± 0.7	1.34 ± 0.05	10.83 ± 0.46	12.2 ± 0.5	0.84 ± 0.07	32.9 ± 1.4	0.37 ± 0.02	
4800	3.46 ± 0.15	5.83 ± 0.54	9.29 ± 0.56	1.71 ± 0.06	6.16 ± 0.29	7.88 ± 0.30	1.18 ± 0.08	32.5 ± 1.2	0.24 ± 0.01	
5080	3.74 ± 0.16	6.95 ± 0.58	10.7 ± 0.6	2.29 ± 0.07	6.13 ± 0.27	8.42 ± 0.28	1.27 ± 0.08	31.0 ± 0.6	0.27 ± 0.01	
5325	2.85 ± 0.13	10.7 ± 0.7	13.5 ± 0.7	2.30 ± 0.07	7.14 ± 0.31	9.44 ± 0.32	1.43 ± 0.09	28.8 ± 1.2	0.33 ± 0.02	
5400	3.33 ± 0.16	5.71 ± 0.67	9.04 ± 0.69	2.20 ± 0.08	10.06 ± 0.41	12.3 ± 0.4	0.74 ± 0.06	30.0 ± 0.9	0.41 ± 0.02	
5450	3.34 ± 0.15	7.57 ± 0.91	10.9 ± 0.9	2.12 ± 0.10	12.9 ± 0.6	15.0 ± 0.6	0.73 ± 0.07	28.6 ± 0.7	0.52 ± 0.02	
5525	4.19 ± 0.16	7.10 ± 0.57	11.3 ± 0.6	1.01 ± 0.04	5.75 ± 0.32	6.76 ± 0.32	1.67 ± 0.12	27.7 ± 1.0	0.24 ± 0.01	

ST #	depth (m)	$^{210}\text{PO}_p$ ^[+]	$^{210}\text{PO}_d$	$^{210}\text{PO}_T$	$^{210}\text{Pb}_p$ ^[+]	$^{210}\text{Pb}_d$	$^{210}\text{Pb}_T$	$^{210}\text{PO}_T/^{210}\text{Pb}_T$	^{226}Ra ^[++]	$^{210}\text{Pb}_T/^{226}\text{Ra}$
		dpm 100L ⁻¹	dpm 100L ⁻¹	dpm 100L ⁻¹	dpm 100L ⁻¹	dpm 100L ⁻¹	dpm 100L ⁻¹	AR	dpm 100L ⁻¹	AR
ST 11 11.9999(°S) Latitude, 94.0001(°W) Longitude; Total Depth 3663 (m)	3	NM	4.59 ± 0.88	4.59 ± 0.88	NM	14.4 ± 0.6	14.4 ± 0.6	0.32 ± 0.06	6.86 ± 0.20*	2.11 ± 0.11
	20	1.32 ± 0.09	5.14 ± 0.63	6.45 ± 0.64	0.33 ± 0.03	9.50 ± 0.40	9.83 ± 0.40	0.66 ± 0.07	6.86 ± 0.20	1.44 ± 0.07
	75	0.62 ± 0.05	6.49 ± 0.63	7.11 ± 0.63	0.31 ± 0.02	7.01 ± 0.31	7.32 ± 0.31	0.97 ± 0.10	7.02 ± 0.16	1.04 ± 0.05
	110	0.36 ± 0.04	5.79 ± 1.14	6.16 ± 1.14	0.40 ± 0.02	20.5 ± 0.9	20.9 ± 0.9	0.30 ± 0.06	6.47 ± 0.17	3.22 ± 0.16
	130	0.38 ± 0.04	11.9 ± 0.9	12.3 ± 0.9	0.26 ± 0.02	7.41 ± 0.31	7.66 ± 0.31	1.60 ± 0.13	6.54 ± 0.18	1.17 ± 0.06
	180	0.35 ± 0.03	9.90 ± 0.82	10.3 ± 0.8	0.09 ± 0.01	8.34 ± 0.35	8.43 ± 0.35	1.22 ± 0.11	7.16 ± 0.16	1.18 ± 0.06
	225	0.57 ± 0.06	9.06 ± 0.77	9.62 ± 0.77	0.28 ± 0.02	8.48 ± 0.36	8.76 ± 0.36	1.10 ± 0.10	6.87 ± 0.17	1.28 ± 0.06
	260	0.48 ± 0.04	9.51 ± 0.76	9.98 ± 0.76	0.11 ± 0.01	8.31 ± 0.35	8.42 ± 0.35	1.19 ± 0.10	9.39 ± 0.34	0.90 ± 0.05
	320	0.65 ± 0.04	11.3 ± 0.8	11.9 ± 0.8	0.13 ± 0.01	8.61 ± 0.38	8.74 ± 0.38	1.37 ± 0.11	10.4 ± 0.4	0.84 ± 0.05
	400	0.69 ± 0.05	13.7 ± 1.0	14.4 ± 1.0	0.26 ± 0.02	9.58 ± 0.42	9.84 ± 0.42	1.46 ± 0.12	11.6 ± 0.5	0.85 ± 0.05
	600	0.75 ± 0.04	13.0 ± 1.0	13.7 ± 1.0	0.15 ± 0.01	11.3 ± 0.4	11.4 ± 0.4	1.20 ± 0.10	13.8 ± 0.5	0.83 ± 0.04
	800	0.92 ± 0.05	17.7 ± 1.4	18.6 ± 1.4	0.22 ± 0.02	12.3 ± 0.5	12.6 ± 0.5	1.48 ± 0.12	16.1 ± 0.5	0.78 ± 0.04
	1000	1.16 ± 0.07	15.9 ± 1.3	17.1 ± 1.3	0.34 ± 0.02	14.6 ± 0.6	15.0 ± 0.6	1.14 ± 0.10	17.9 ± 0.5	0.84 ± 0.04
	1250	1.34 ± 0.10	15.0 ± 1.4	16.4 ± 1.4	0.46 ± 0.04	18.5 ± 0.8	19.0 ± 0.8	0.86 ± 0.08	19.5 ± 0.4	0.97 ± 0.04
	1500	1.41 ± 0.07	21.2 ± 1.9	22.7 ± 1.9	0.65 ± 0.04	19.7 ± 0.8	20.3 ± 0.8	1.12 ± 0.10	22.8 ± 0.5	0.89 ± 0.04
	1750	1.61 ± 0.09	19.9 ± 1.7	21.5 ± 1.7	0.85 ± 0.04	21.7 ± 0.9	22.5 ± 0.9	0.95 ± 0.08	24.2 ± 0.8	0.93 ± 0.05
	2000	2.12 ± 0.10	19.7 ± 1.5	21.8 ± 1.5	1.00 ± 0.05	21.2 ± 0.8	22.2 ± 0.8	0.98 ± 0.08	23.3 ± 0.7	0.95 ± 0.04
	2250	1.99 ± 0.11	23.4 ± 1.7	25.4 ± 1.7	1.20 ± 0.04	23.0 ± 0.9	24.2 ± 0.9	1.05 ± 0.08	27.0 ± 1.1	0.90 ± 0.05
	2500	3.44 ± 0.14	17.9 ± 1.6	21.4 ± 1.6	1.34 ± 0.04	19.9 ± 0.8	21.2 ± 0.8	1.01 ± 0.09	26.2 ± 0.8	0.81 ± 0.04
	2750	3.62 ± 0.15	17.6 ± 1.3	21.2 ± 1.3	1.33 ± 0.04	16.6 ± 0.6	17.9 ± 0.6	1.19 ± 0.09	27.6 ± 1.1	0.65 ± 0.03
3500	4.41 ± 0.17	12.1 ± 1.0	16.5 ± 1.0	2.28 ± 0.07	13.5 ± 0.5	15.7 ± 0.5	1.05 ± 0.07	30.9 ± 1.1	0.51 ± 0.03	
3600	4.57 ± 0.18	12.0 ± 1.2	16.6 ± 1.2	2.73 ± 0.08	17.6 ± 0.7	20.3 ± 0.7	0.82 ± 0.06	33.9 ± 1.0	0.60 ± 0.03	
3625	4.92 ± 0.21	12.8 ± 1.0	17.7 ± 1.0	2.62 ± 0.09	12.2 ± 0.5	14.8 ± 0.5	1.20 ± 0.08	32.8 ± 0.8	0.45 ± 0.02	
ST 18 14.9835(°S) Latitude, 112.7504(°W) Longitude; Total Depth 2972 (m)	3	NM	4.08 ± 0.69	4.08 ± 0.69	NM	8.40 ± 0.37	8.40 ± 0.37	0.49 ± 0.08	6.59 ± 0.24*	1.28 ± 0.07
	20	1.80 ± 0.13	5.81 ± 0.64	7.61 ± 0.65	0.84 ± 0.06	10.57 ± 0.44	11.4 ± 0.4	0.67 ± 0.06	6.59 ± 0.24	1.75 ± 0.08
	60	1.31 ± 0.09	5.79 ± 0.59	7.10 ± 0.60	0.74 ± 0.05	7.81 ± 0.33	8.55 ± 0.34	0.83 ± 0.08	6.35 ± 0.22	1.35 ± 0.07
	95	1.29 ± 0.07	7.28 ± 0.65	8.57 ± 0.65	0.44 ± 0.03	7.97 ± 0.33	8.41 ± 0.33	1.02 ± 0.09	6.71 ± 0.28	1.25 ± 0.07
	150	0.49 ± 0.04	18.7 ± 2.7	19.2 ± 2.7	0.38 ± 0.02	39.8 ± 1.5	40.2 ± 1.5	0.48 ± 0.07	7.64 ± 0.35	5.26 ± 0.32
	200	0.45 ± 0.04	12.3 ± 0.9	12.7 ± 0.9	0.29 ± 0.02	9.23 ± 0.37	9.52 ± 0.37	1.34 ± 0.11	6.95 ± 0.26	1.37 ± 0.07
	355	0.56 ± 0.05	9.17 ± 0.74	9.73 ± 0.74	0.28 ± 0.02	7.95 ± 0.32	8.23 ± 0.32	1.18 ± 0.10	9.47 ± 0.28	0.87 ± 0.04
	400	0.62 ± 0.04	9.22 ± 0.77	9.84 ± 0.77	0.32 ± 0.02	9.37 ± 0.38	9.69 ± 0.38	1.02 ± 0.09	9.05 ± 0.22	1.07 ± 0.05
	600	1.01 ± 0.09	12.2 ± 0.9	13.2 ± 0.9	0.28 ± 0.02	10.98 ± 0.40	11.3 ± 0.4	1.17 ± 0.09	12.7 ± 0.4	0.89 ± 0.04
	1000	1.24 ± 0.06	16.0 ± 1.4	17.3 ± 1.4	0.37 ± 0.03	13.9 ± 0.5	14.2 ± 0.5	1.21 ± 0.10	15.2 ± 0.6	0.94 ± 0.05
	1200	1.09 ± 0.07	17.8 ± 1.2	18.9 ± 1.2	0.58 ± 0.03	14.2 ± 0.6	14.8 ± 0.6	1.28 ± 0.09	17.4 ± 0.5	0.85 ± 0.04
	1400	1.02 ± 0.07	21.5 ± 1.4	22.5 ± 1.4	0.61 ± 0.03	13.5 ± 0.5	14.1 ± 0.5	1.59 ± 0.12	18.5 ± 0.7	0.76 ± 0.04
	1600	1.56 ± 0.08	20.8 ± 1.6	22.4 ± 1.6	0.64 ± 0.03	17.9 ± 0.8	18.5 ± 0.8	1.21 ± 0.10	20.8 ± 0.9	0.89 ± 0.05
	1800	1.98 ± 0.09	21.3 ± 1.6	23.2 ± 1.6	0.74 ± 0.04	20.6 ± 0.9	21.3 ± 0.9	1.09 ± 0.09	22.4 ± 0.6	0.95 ± 0.05
	2000	2.73 ± 0.12	18.0 ± 1.5	20.7 ± 1.5	1.01 ± 0.05	18.8 ± 0.8	19.8 ± 0.8	1.05 ± 0.09	23.8 ± 0.5	0.83 ± 0.04
	2200	5.35 ± 0.21	18.8 ± 1.5	24.1 ± 1.5	1.80 ± 0.10	17.1 ± 0.7	18.9 ± 0.7	1.28 ± 0.09	23.2 ± 0.5	0.81 ± 0.03
	2300	8.05 ± 0.33	5.92 ± 0.58	14.0 ± 0.7	6.51 ± 0.17	8.96 ± 0.35	15.5 ± 0.4	0.90 ± 0.05	24.3 ± 0.8	0.64 ± 0.03
	2350	3.73 ± 0.24	5.78 ± 0.65	9.51 ± 0.69	9.39 ± 0.25	10.43 ± 0.42	19.8 ± 0.5	0.48 ± 0.04	25.4 ± 1.0	0.78 ± 0.04
	2400	2.88 ± 0.26	2.49 ± 0.22	5.37 ± 0.34	10.1 ± 0.3	2.95 ± 0.16	13.1 ± 0.4	0.41 ± 0.03	28.0 ± 1.2	0.47 ± 0.02
	2450	1.88 ± 0.18	1.54 ± 0.22	3.42 ± 0.28	7.32 ± 0.22	1.87 ± 0.23	9.19 ± 0.32	0.37 ± 0.03	27.9 ± 1.0	0.33 ± 0.02
2500	5.74 ± 0.26	3.49 ± 0.69	9.23 ± 0.74	6.82 ± 0.21	7.63 ± 0.61	14.5 ± 0.6	0.64 ± 0.06	26.9 ± 0.8	0.54 ± 0.03	
2550	5.00 ± 0.25	2.01 ± 0.26	7.01 ± 0.36	7.50 ± 0.20	3.14 ± 0.23	10.6 ± 0.3	0.66 ± 0.04	26.8 ± 0.6	0.40 ± 0.01	
2610	5.52 ± 0.29	2.28 ± 0.26	7.81 ± 0.38	7.87 ± 0.23	2.37 ± 0.18	10.2 ± 0.3	0.76 ± 0.04	26.5 ± 0.7	0.39 ± 0.01	

ST #	depth (m)	²¹⁰ PO _p ^[+]	²¹⁰ PO _d	²¹⁰ PO _T	²¹⁰ Pb _p ^[+]	²¹⁰ Pb _d	²¹⁰ Pb _T	²¹⁰ PO _T / ²¹⁰ Pb _T	²²⁶ Ra ^[++]	²¹⁰ Pb _T / ²²⁶ Ra
		dpm 100L ⁻¹	dpm 100L ⁻¹	dpm 100L ⁻¹	dpm 100L ⁻¹	dpm 100L ⁻¹	dpm 100L ⁻¹	dpm 100L ⁻¹	AR	dpm 100L ⁻¹
	3	NM	2.55 ± 0.49	2.55 ± 0.49	NM	10.50 ± 0.43	10.50 ± 0.43	0.24 ± 0.05	6.69 ± 0.23 [*]	1.57 ± 0.09
	20	1.25 ± 0.08	3.64 ± 0.50	4.89 ± 0.50	0.35 ± 0.15	9.81 ± 0.38	10.15 ± 0.41	0.48 ± 0.05	6.69 ± 0.23	1.54 ± 0.07
	45	1.46 ± 0.08	13.0 ± 1.4	14.5 ± 1.4	0.55 ± 0.17	21.9 ± 0.8	22.4 ± 0.9	0.65 ± 0.07	6.80 ± 0.16	3.30 ± 0.15
	80	1.15 ± 0.06	5.85 ± 0.56	7.00 ± 0.57	0.32 ± 0.14	9.56 ± 0.33	9.88 ± 0.36	0.71 ± 0.06	6.25 ± 0.17	1.58 ± 0.07
	100	0.97 ± 0.06	10.2 ± 0.9	11.2 ± 0.9	0.60 ± 0.17	11.4 ± 0.4	12.0 ± 0.4	0.93 ± 0.08	7.05 ± 0.19	1.70 ± 0.07
	140	0.56 ± 0.05	10.2 ± 0.9	10.7 ± 0.9	0.51 ± 0.16	11.1 ± 0.4	11.6 ± 0.5	0.92 ± 0.09	8.42 ± 0.19	1.38 ± 0.06
	200	0.44 ± 0.04	18.2 ± 1.5	18.7 ± 1.5	0.27 ± 0.13	15.4 ± 0.5	15.7 ± 0.5	1.19 ± 0.11	6.89 ± 0.21	2.28 ± 0.10
	250	0.46 ± 0.04	10.05 ± 0.76	10.5 ± 0.8	0.22 ± 0.13	9.25 ± 0.33	9.46 ± 0.36	1.11 ± 0.09	7.53 ± 0.28	1.26 ± 0.07
	335	0.46 ± 0.04	10.1 ± 0.9	10.6 ± 0.9	0.15 ± 0.12	11.7 ± 0.4	11.9 ± 0.4	0.89 ± 0.08	9.55 ± 0.25	1.24 ± 0.05
	850	0.91 ± 0.06	15.5 ± 1.4	16.4 ± 1.4	0.24 ± 0.13	15.1 ± 0.5	15.4 ± 0.5	1.07 ± 0.09	14.8 ± 0.3	1.04 ± 0.04
	1000	1.06 ± 0.07	17.4 ± 1.3	18.5 ± 1.3	0.24 ± 0.10	13.7 ± 0.5	13.9 ± 0.5	1.33 ± 0.11	15.8 ± 0.5	0.88 ± 0.04
	1250	1.20 ± 0.10	15.1 ± 1.3	16.3 ± 1.3	0.53 ± 0.16	17.7 ± 0.5	18.2 ± 0.5	0.90 ± 0.08	20.6 ± 0.7	0.88 ± 0.04
	1500	1.24 ± 0.10	21.0 ± 2.0	22.3 ± 2.0	0.75 ± 0.17	21.0 ± 0.7	21.7 ± 0.7	1.02 ± 0.10	18.5 ± 0.5	1.18 ± 0.05
	1750	NM	20.7 ± 1.4	20.7 ± 1.4	NM	17.6 ± 0.6	17.6 ± 0.6	1.18 ± 0.09	20.7 ± 0.7 ^{**}	0.85 ± 0.04
	2000	2.57 ± 0.14	17.4 ± 1.5	20.0 ± 1.5	0.96 ± 0.18	17.9 ± 0.6	18.8 ± 0.6	1.06 ± 0.09	23.0 ± 1.0	0.82 ± 0.04
	2200	5.38 ± 0.25	6.68 ± 0.87	12.06 ± 0.90	2.85 ± 0.27	13.0 ± 0.8	15.9 ± 0.8	0.76 ± 0.07	27.2 ± 1.1	0.58 ± 0.04
	2400	3.99 ± 0.23	5.87 ± 0.51	9.85 ± 0.56	3.28 ± 0.29	7.16 ± 0.31	10.4 ± 0.4	0.94 ± 0.07	28.5 ± 1.0	0.37 ± 0.02
	2550	5.57 ± 0.25	2.49 ± 0.29	8.06 ± 0.38	0.95 ± 0.15	4.17 ± 0.18	5.12 ± 0.23	1.57 ± 0.10	30.9 ± 1.2	0.17 ± 0.01
	2750	3.93 ± 0.27	3.31 ± 0.34	7.25 ± 0.44	3.52 ± 0.32	4.87 ± 0.22	8.39 ± 0.38	0.86 ± 0.07	27.8 ± 0.8	0.30 ± 0.02
	3000	4.19 ± 0.29	6.78 ± 0.58	11.0 ± 0.6	4.08 ± 0.33	8.74 ± 0.36	12.8 ± 0.5	0.86 ± 0.06	30.8 ± 1.1	0.42 ± 0.02
	3750	4.35 ± 0.30	11.4 ± 1.2	15.8 ± 1.2	4.18 ± 0.34	16.8 ± 0.7	21.0 ± 0.8	0.75 ± 0.06	32.2 ± 1.3	0.65 ± 0.04
	3900	4.19 ± 0.52	11.3 ± 0.9	15.4 ± 1.0	4.36 ± 0.32	12.3 ± 0.5	16.7 ± 0.6	0.93 ± 0.07	32.9 ± 1.3	0.51 ± 0.03
	3960	4.61 ± 0.29	13.3 ± 1.1	17.9 ± 1.2	2.95 ± 0.29	15.2 ± 0.6	18.2 ± 0.7	0.98 ± 0.07	29.5 ± 0.9	0.62 ± 0.03

ST 26
11.6706(°S)
Latitude,
127.9998(°W)
Longitude;
Total Depth
4008 (m)

ST #	depth (m)	²¹⁰ PO _p ^[+]	²¹⁰ PO _d	²¹⁰ PO _T	²¹⁰ Pb _p ^[+]	²¹⁰ Pb _d	²¹⁰ Pb _T	²¹⁰ PO _T / ²¹⁰ Pb _T	²²⁶ Ra ^[++]	²¹⁰ Pb _T / ²²⁶ Ra
		dpm 100L ⁻¹	dpm 100L ⁻¹	dpm 100L ⁻¹	dpm 100L ⁻¹	dpm 100L ⁻¹	dpm 100L ⁻¹	AR	dpm 100L ⁻¹	AR
	2	NM	6.15 ± 0.63	6.15 ± 0.63	NM	14.0 ± 0.5	14.0 ± 0.5	0.44 ± 0.05	5.78 ± 0.17*	2.43 ± 0.11
	30	1.48 ± 0.09	6.86 ± 0.65	8.35 ± 0.66	0.71 ± 0.03	13.1 ± 0.5	13.8 ± 0.5	0.61 ± 0.05	5.78 ± 0.17	2.40 ± 0.11
	45	1.28 ± 0.09	6.31 ± 0.70	7.59 ± 0.70	0.97 ± 0.04	14.6 ± 0.5	15.5 ± 0.5	0.49 ± 0.05	6.76 ± 0.17	2.30 ± 0.10
	75	1.96 ± 0.09	12.4 ± 1.1	14.4 ± 1.1	0.33 ± 0.02	12.5 ± 0.4	12.9 ± 0.4	1.12 ± 0.09	6.55 ± 0.15	1.96 ± 0.08
	130	1.16 ± 0.06	17.0 ± 1.4	18.2 ± 1.4	0.25 ± 0.02	14.5 ± 0.6	14.8 ± 0.6	1.23 ± 0.10	6.86 ± 0.29	2.16 ± 0.12
	300	0.57 ± 0.05	8.84 ± 0.70	9.41 ± 0.70	0.18 ± 0.02	12.8 ± 0.5	13.0 ± 0.5	0.72 ± 0.06	6.99 ± 0.31	1.86 ± 0.11
	450	0.64 ± 0.06	10.03 ± 0.71	10.7 ± 0.7	0.16 ± 0.02	11.2 ± 0.5	11.3 ± 0.5	0.94 ± 0.07	12.1 ± 0.4	0.93 ± 0.05
	600	0.60 ± 0.05	11.6 ± 0.8	12.2 ± 0.8	0.38 ± 0.02	12.1 ± 0.5	12.5 ± 0.5	0.97 ± 0.08	12.7 ± 0.3	0.99 ± 0.04
	1000	0.95 ± 0.08	14.2 ± 1.2	15.2 ± 1.2	0.70 ± 0.03	15.6 ± 0.5	16.3 ± 0.5	0.93 ± 0.08	16.9 ± 0.4	0.96 ± 0.04
ST 36	1250	NM	15.6 ± 1.3	15.6 ± 1.3	NM	17.6 ± 0.7	17.6 ± 0.7	0.89 ± 0.08	18.5 ± 0.5	0.95 ± 0.05
10.5002(°S)	1500	NM	16.7 ± 1.3	16.7 ± 1.3	NM	17.4 ± 0.7	17.4 ± 0.7	0.96 ± 0.08	21.4 ± 0.5	0.81 ± 0.04
Latitude,	1750	1.05 ± 0.06	16.2 ± 1.2	17.3 ± 1.2	0.61 ± 0.03	20.5 ± 0.8	21.1 ± 0.8	0.82 ± 0.07	24.7 ± 0.5	0.85 ± 0.04
152.0004(°W)	2100	2.90 ± 0.12	16.7 ± 1.2	19.6 ± 1.2	0.73 ± 0.04	21.3 ± 0.8	22.0 ± 0.8	0.89 ± 0.06	24.4 ± 0.8	0.90 ± 0.04
Longitude;	2300	2.97 ± 0.12	14.7 ± 1.2	17.6 ± 1.2	1.15 ± 0.04	22.0 ± 0.8	23.1 ± 0.8	0.76 ± 0.06	26.43 ± 0.67	0.87 ± 0.04
Total Depth	2400	3.89 ± 0.15	16.7 ± 1.2	20.6 ± 1.2	1.45 ± 0.05	18.7 ± 0.7	20.1 ± 0.7	1.02 ± 0.07	28.5 ± 0.6	0.71 ± 0.03
5162 (m)	2500	3.82 ± 0.16	15.5 ± 1.1	19.3 ± 1.1	1.23 ± 0.06	18.1 ± 0.7	19.3 ± 0.7	1.00 ± 0.07	27.9 ± 1.0	0.69 ± 0.03
	2600	4.52 ± 0.17	15.5 ± 1.3	20.0 ± 1.3	1.84 ± 0.07	18.6 ± 0.7	20.5 ± 0.7	0.98 ± 0.07	28.9 ± 0.8	0.71 ± 0.03
	2700	3.53 ± 0.15	16.2 ± 1.2	19.7 ± 1.2	1.90 ± 0.07	17.8 ± 0.7	19.7 ± 0.7	1.00 ± 0.07	28.6 ± 0.9	0.69 ± 0.03
	2800	3.75 ± 0.15	15.2 ± 1.1	19.0 ± 1.1	1.71 ± 0.06	18.2 ± 0.6	19.9 ± 0.6	0.95 ± 0.06	30.2 ± 0.8	0.66 ± 0.03
	3000	4.02 ± 0.15	17.4 ± 1.5	21.4 ± 1.5	1.13 ± 0.05	21.1 ± 0.6	22.2 ± 0.6	0.96 ± 0.07	31.5 ± 1.1	0.71 ± 0.03
	3500	2.83 ± 0.13	19.4 ± 1.8	22.3 ± 1.8	0.98 ± 0.05	23.3 ± 0.8	24.2 ± 0.8	0.92 ± 0.08	28.0 ± 0.8	0.86 ± 0.04
	4000	2.10 ± 0.10	22.2 ± 1.8	24.3 ± 1.8	0.87 ± 0.05	22.0 ± 0.6	22.8 ± 0.6	1.06 ± 0.08	29.1 ± 0.7	0.79 ± 0.03
	4750	3.02 ± 0.15	19.6 ± 1.6	22.6 ± 1.6	2.09 ± 0.07	19.4 ± 0.8	21.4 ± 0.8	1.05 ± 0.08	23.1 ± 0.7	0.93 ± 0.05
	5000	3.83 ± 0.18	19.2 ± 1.4	23.1 ± 1.4	1.53 ± 0.06	20.1 ± 0.7	21.6 ± 0.7	1.07 ± 0.08	25.5 ± 1.0	0.85 ± 0.04
	5105	4.11 ± 0.19	18.2 ± 1.6	22.3 ± 1.6	2.25 ± 0.09	21.9 ± 0.8	24.1 ± 0.8	0.93 ± 0.07	27.8 ± 1.2	0.87 ± 0.05

NM = Not measured (no sample was collected)

For Po-210 and Pb-210, p: particulate (>1µm); d: dissolved (<0.45 µm)

For both ²¹⁰Po & ²¹⁰Pb, when no particulate data available, total activity = dissolved activity is assumed

* = Taken from layer below

** = average value of the layers above and below

+ Data collected and processed by Stewart, G.M.

++ Data collected and processed by Charette, Matthew and crew - EPZT cruise participant, Sanial et al., 2017

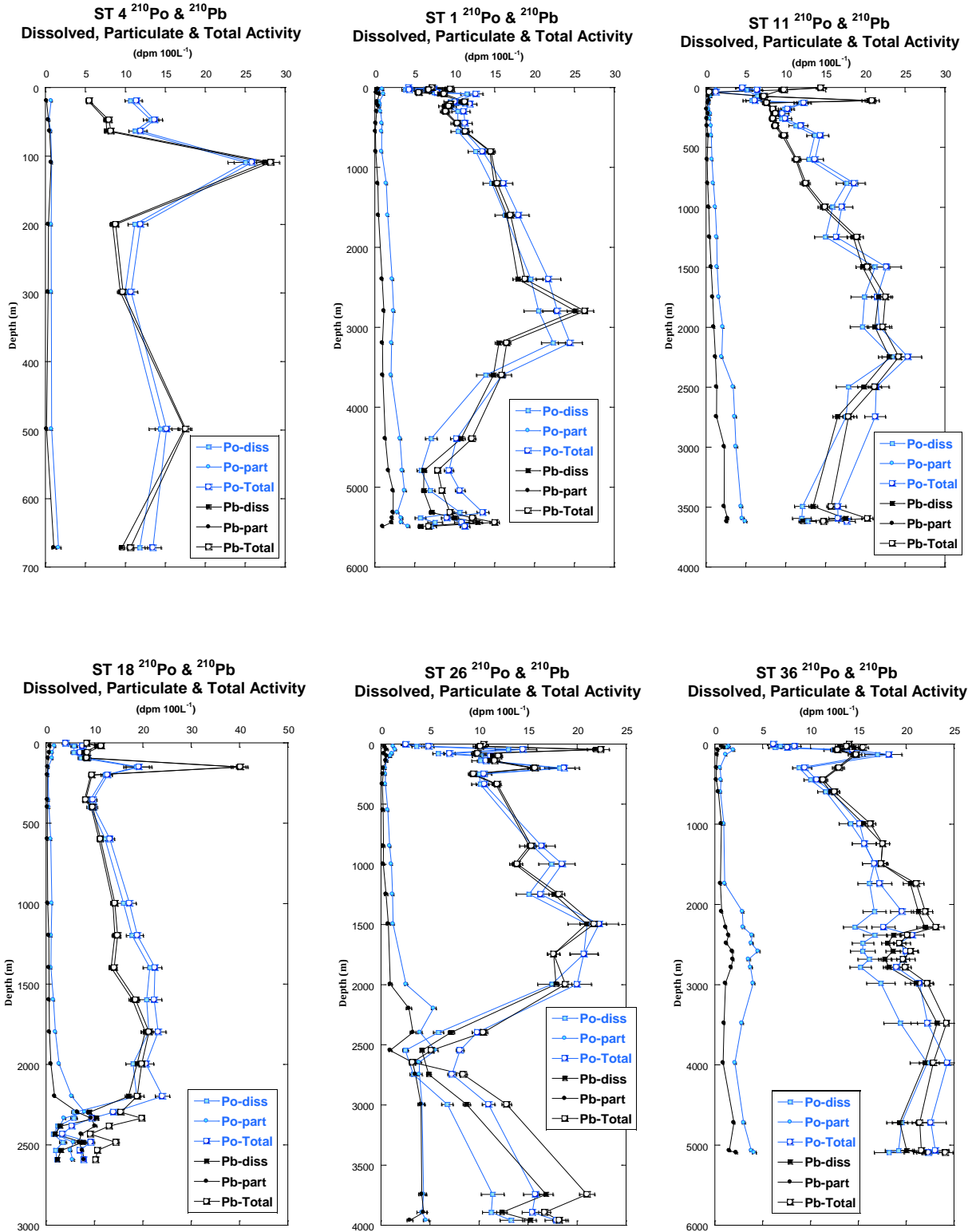


Figure 3.3. Activities of dissolved and particulate ^{210}Po and ^{210}Pb for all six stations are given in Table 3.5.

3.4 Variations in Activities and Inventories of ^{210}Po and ^{210}Pb , Activity Ratios of $^{210}\text{Po}/^{210}\text{Pb}$ and $^{210}\text{Pb}/^{226}\text{Ra}$

3.4.1 Full Water Column

The activities of particulate and dissolved ^{210}Po and ^{210}Pb are given in Table 3.5 and Figure 3.3. The vertical profiles across the EPZT transect are depicted in Ocean Data View (ODV) Figure 3.1 and 3.2 and show total ^{210}Po ($^{210}\text{Po}_T$) and ^{210}Pb ($^{210}\text{Pb}_T$) for all 6 stations (ST 4, 1, 11, 18, 26 and 36). The vertical profiles for the full water column of ($^{210}\text{Po}/^{210}\text{Pb}$)_T and ($^{210}\text{Pb}_T/^{226}\text{Ra}$) are shown in Figures 3.4, 3.5 and 3.6, 3.7. The dissolved ^{210}Po and ^{210}Pb AR range between 1.5 and 25.1 and 1.9 and 39.8 dpm 100L^{-1} , respectively, with average values of 12.2 ± 5.7 and 13.3 ± 6.0 dpm 100L^{-1} , respectively. The total (dissolved + small and large particulate) ^{210}Po and ^{210}Pb ranged between 3.4 and 25.9 (mean: 14.2 ± 5.8) and 5.1 and 40.2 (mean: 14.6 ± 5.8) dpm 100L^{-1} , respectively. The overall vertical profiles of ^{210}Po and ^{210}Pb are similar to other published results from the Equatorial and South Pacific (Thomson and Turekian, 1976; Nozaki et al., 1997), North Pacific (Nozaki and Tsunogai, 1976; Cochran et al., 1990), Indian Ocean (Cochran et al., 1983) and Atlantic Ocean (Bacon et al., 1976, Cochran et al., 1990; Rigaud et al., 2015), although there are large variations in the distribution of these nuclides in different basins, depending on the concentration and composition of particulate matter, rates of upwelling, diapycnal and isopycnal mixing of water (variation or vertical distribution of water density), etc.

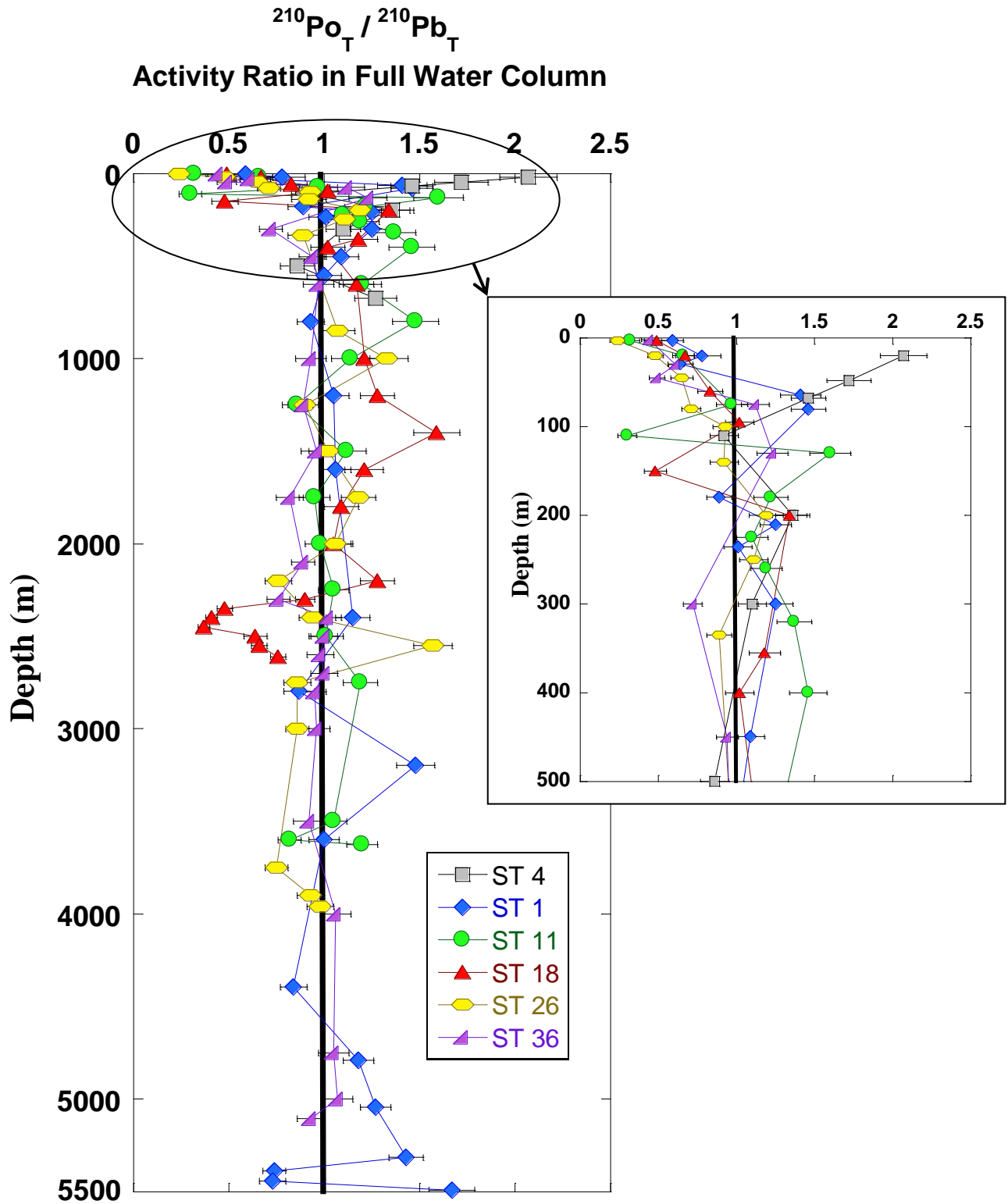


Figure 3.4. Vertical profile of total $^{210}\text{Po}/^{210}\text{Pb}$ activity ratio in full water column.

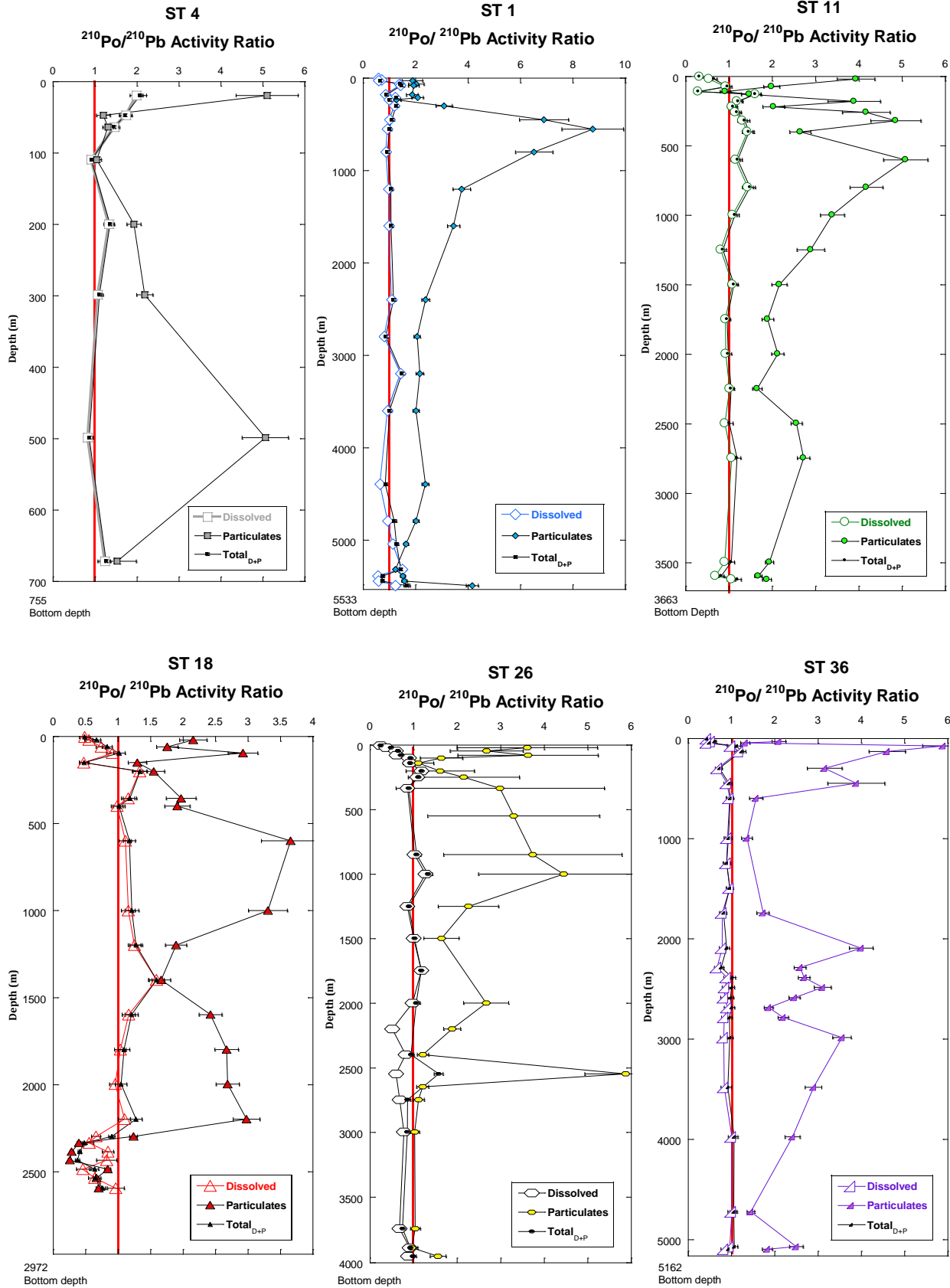


Figure 3.5. Activity ratios of dissolved and particulate $^{210}\text{Po}/^{210}\text{Pb}$ in full water column for all six stations shown in Table 3.5.

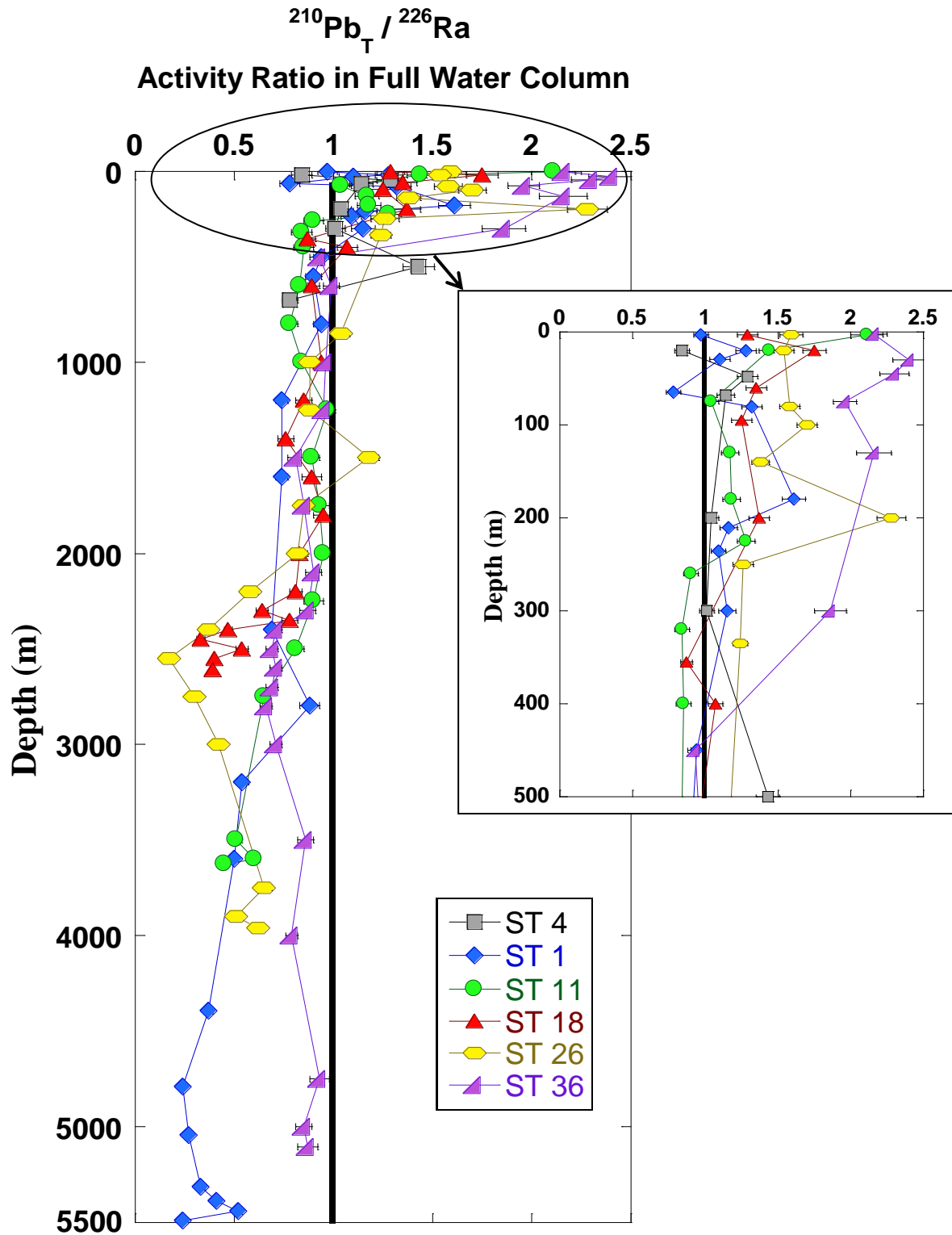


Figure 3.6. Vertical profile of $^{210}\text{Pb}_T/^{226}\text{Ra}$ activity ratio in full water column. ST 4, 11, 18, 26 at depths 110, 110, 115, 45 and AR 3.96, 3.22, 5.26, 3.30 respectively were excluded from the plot. Center black line is the equilibrium line ($^{210}\text{Po}_T/^{210}\text{Pb}_T$ activity ratio = 1).

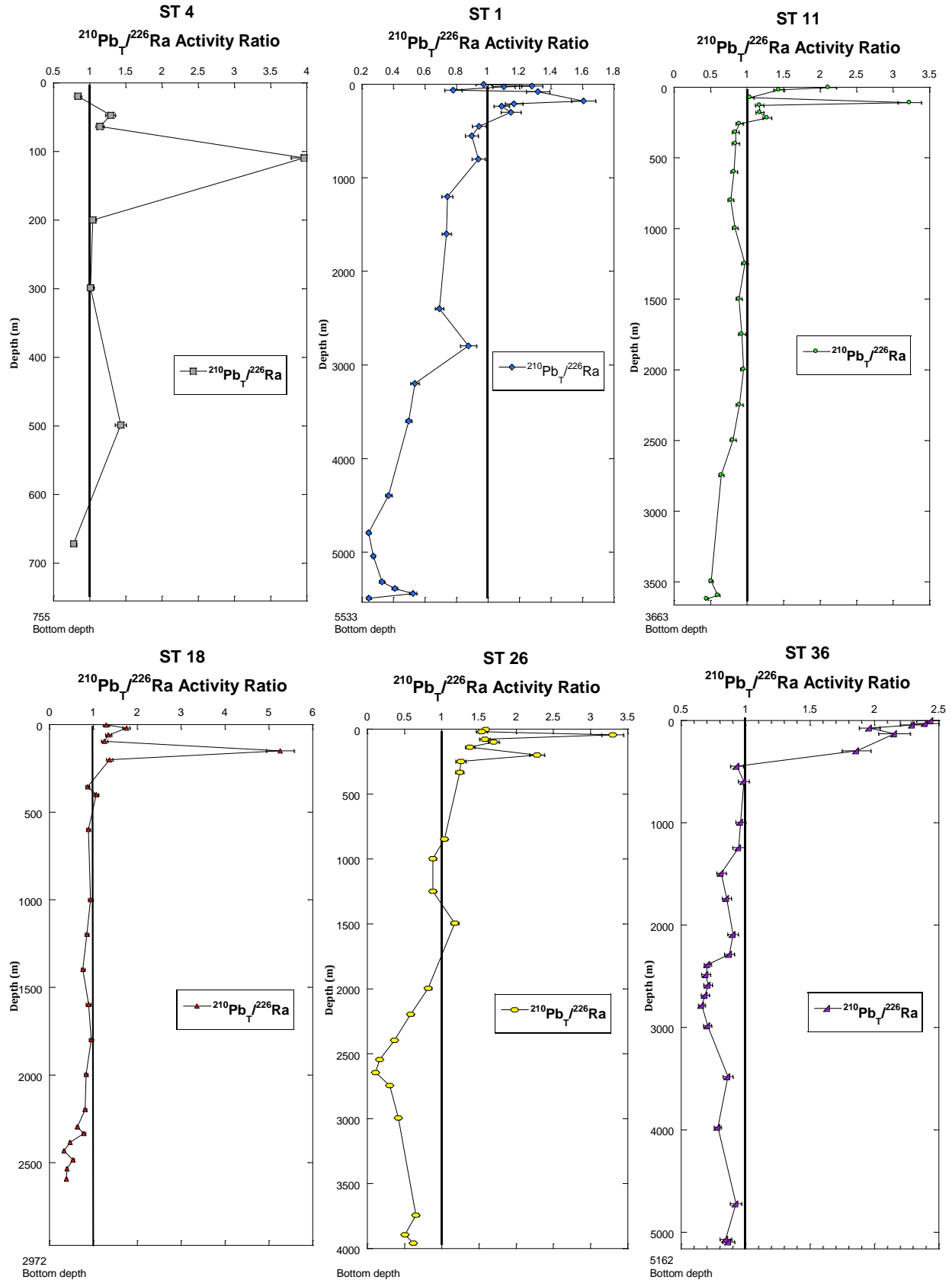


Figure 3.7. Vertical profiles of $^{210}\text{Pb}_{\text{Total}}/^{226}\text{Ra}$ AR in full water column for all six stations shown in Table 3.5.

The particulate ($\geq 1 \mu\text{m}$) ^{210}Po or ^{210}Pb fraction of the total (particulate ^{210}Po or ^{210}Pb % = $100 \times \frac{^{210}\text{Po or } ^{210}\text{Pb particulate (small particulate + large particulate) activity}}{^{210}\text{Po or } ^{210}\text{Pb total (particulate + dissolved) activity}}$, in all samples at stations 4, 1, 11, 18, 26 and 36, ranged between 3.0-7.0% (mean 5.3%), 5.2-37.3% (mean 16.0%), 3.1-27.7% (mean 10.6%), 2.6-71.4% (mean 25.5%), 2.4-69.1% (mean 19.8%), and 4.9-22.8% (mean 13.8%) respectively (shown in Table 3.6 calculated from data given in Table 3.5). At stations 4, 1, 11, 18, 26 and 36 the corresponding values for ^{210}Pb varied between 0.9-6.4% (mean 3.6%), 0.9-27.2% (mean 8.3%), 1.1-17.7% (mean 4.8%), 0.9-79.6% (mean 23.1%), 1.3-42.0% (mean 11.2%), and 1.4-9.7% (mean 5.3%), respectively. The percentage of particulate / total ^{210}Po in all stations ranged between 2.4 and 71.4 (mean 16.4%) and the percentage of particulate / total ^{210}Pb in all stations range between 0.9 and 79.6 (mean 10.1%) respectively. The overall distribution of ^{210}Po and ^{210}Pb in the particulate and dissolved phases indicate that both nuclides are mainly present in the dissolved phase ($\leq 0.45 \mu\text{m}$), similar to earlier observations reported (e.g., Craig et al., 1973; Bacon et al., 1976; Hong et al., 2013; Rigaud et al., 2015). From the percentage of particulate ^{210}Po ($^{210}\text{Po}_p$) and ^{210}Pb ($^{210}\text{Pb}_p$), the following was inferred: 1) the fraction of particulate ^{210}Pb is always lower than that for ^{210}Po in every sample at every station; 2) the range of particulate ^{210}Po fraction is generally larger compared to ^{210}Pb , except at the Eastern Pacific Rise (EPR) site (ST 18); 3) the highest particulate activity is found in the EPR site (ST 18), with mean or average particulate ^{210}Po and ^{210}Pb activity values of 25.5 and 23.1% of the total, and (5) a much lower value for $^{210}\text{Po}_p$ and for $^{210}\text{Pb}_p$ of the total were found in the most oligotrophic station (ST 36).

From the activity ratio of total (= particulate ($\geq 1 \mu\text{m}$) + dissolved ($\leq 0.45 \mu\text{m}$)) ^{210}Po and ^{210}Pb [$(^{210}\text{Po}/^{210}\text{Pb})_T$] and activity ratio of total (= particulate ($\geq 1 \mu\text{m}$) + dissolved ($\leq 0.45 \mu\text{m}$)) ^{210}Pb and ^{226}Ra [$^{210}\text{Pb}_T/^{226}\text{Ra}$], (Figures 3.4, 3.5 and Table 3.5), it is inferred that the

$(^{210}\text{Po}/^{210}\text{Pb})_{\text{T}}$ activity ratio (AR) is < 1.0 in the mixed-layer (except at ST 4) due to preferential removal of ^{210}Po by suspended and sinking particulate matter by scavenging (Table 3.5, Figure 3.4). A substantial fraction of the sinking particulate matter undergoes remineralization in the thermocline releasing ^{210}Po (and some ^{210}Pb) back to the dissolved fraction resulting in $(^{210}\text{Po}/^{210}\text{Pb})_{\text{T}}$ AR > 1.0 (Figure 3.4). In a majority of discrete depth layers (82%, 103 out of 126 samples in all 6 super stations, with absolute AR values between 0.95 and 1.05), it was found that the ^{210}Po - ^{210}Pb pair was in radioactive equilibrium between total ^{210}Po and total ^{210}Pb activities. Earlier studies generally reported that ^{210}Po and ^{210}Pb were essentially to be in radioactive equilibrium below thermocline in the interior of the ocean (Bacon et al., 1976; Nozaki and Tsunogai, 1976; Nozaki et al., 1976; Thomson and Turekian, 1976; Rigaud et al., 2015), although significant regional variations in the ^{210}Po - ^{210}Pb relationship have also been reported (e.g. Chung and Finkel, 1988; Nozaki et al., 1990; Kim, 2001; Chung and Wu, 2005; Su et al., 2017).

In most surface waters (< 100 m), the $^{210}\text{Pb}_{\text{T}}/^{226}\text{Ra}$ AR is greater > 1.0 because of atmospheric input and this excess AR decreases with depth until the activities become approximately equal between 300-500 m where a pseudo-equilibrium cross-over point is reported (Figure 3.6; Chung and Craig, 1983). The $^{210}\text{Pb}_{\text{T}}/^{226}\text{Ra}$ AR continues to decrease with depth, mostly with activity ratios varying between 0.5 and 0.9 (Figure 3.6). The particulate activities of ^{210}Pb generally increased with depth (Table 3.5), with a steep increase in the hydrothermal station (Figure 3.5), and the overall increasing trend is consistent with ^{210}Pb being scavenged by sinking particulate matter observed in the Pacific, Atlantic and Indian Oceans (Craig et al., 1973; Somayajulu and Craig, 1976; Chung and Craig, 1983).

Table 3.6
EPZT ^{210}Po , ^{210}Pb (Particulate & Dissolved) %

	Depth (m)	$^{210}\text{Po}_p/^{210}\text{Po}_{p+d}$				$^{210}\text{Pb}_p/^{210}\text{Pb}_{p+d}$				
		Mean μ	Std Dev σ	Range min to max		Mean μ	Std Dev σ	Range min to max		
Station 4 Peru Shelf	19.5	6.49	10.47	12.42	1.88 — 28.89	2.64	7.43	11.37	0.64	— 24.44
	47.4	3.36	7.68	10.93	0.81 — 24.00	4.81	8.52	10.73	1.18	— 24.45
	63.8	5.75	7.25	7.14	1.01 — 17.51	6.37	7.77	7.40	1.17	— 18.35
	109.5	2.99	7.13	10.31	0.67 — 22.52	2.63	6.50	9.54	0.55	— 20.75
	199.9	6.21	8.32	8.62	1.30 — 20.87	4.37	2.36	2.31	0.03	— 4.37
	298.7	7.02	6.91	5.19	0.95 — 13.60	3.54	5.96	7.30	0.59	— 16.75
	498.7	5.11	6.52	6.51	0.81 — 15.88	0.87	5.48	9.80	0.18	— 20.17
671.7										
		5.28			2.99 — 7.02	3.60			0.87	— 6.37
		Mean				Mean				
	3.0									
	20.2									
	29.3	11.06	8.91	5.21	1.50 — 13.53	3.78	3.88	3.15	0.30	— 7.97
	64.6	5.16	8.93	11.08	1.31 — 25.37	3.59	7.81	10.90	0.86	— 24.08
	80.5									
	179.7	5.73	7.17	7.01	0.99 — 17.23	2.72	6.93	10.27	0.61	— 22.27
	210.6	5.58	5.99	5.02	0.71 — 12.79	3.37	9.29	14.13	1.02	— 30.44
	235.5	6.49	7.34	6.48	1.06 — 16.40	5.18	6.37	6.15	0.78	— 15.13
	300.1	6.67	6.67	5.11	0.89 — 13.32	2.70	7.68	11.78	0.68	— 25.30
	449.6	7.92	5.84	3.51	0.60 — 7.92	1.25	7.42	13.17	0.34	— 27.17
	551.7	7.61	5.16	3.30	0.41 — 7.61	0.86	3.81	6.47	0.12	— 13.51
	801.9	6.44	5.06	3.11	0.48 — 7.37	0.92	4.33	7.44	0.14	— 15.48
Station 1 Peru Margin	1200.5	8.99	6.45	3.86	0.71 — 8.99	2.51	2.72	2.35	0.15	— 5.85
	1599.9	9.05	5.87	3.94	0.49 — 9.05	2.77	3.03	2.64	0.18	— 6.58
	2398.7	10.13	6.02	4.74	0.39 — 10.13	4.91	4.33	2.95	0.37	— 7.51
	2797.0	10.30	6.60	4.47	0.60 — 10.30	4.36	3.96	2.80	0.31	— 7.14
	3197.1	8.62	7.96	5.46	1.26 — 14.58	5.91	7.33	7.11	1.04	— 17.52
	3599.1	12.81	7.91	5.64	0.77 — 12.81	6.38	5.09	3.15	0.48	— 7.59
	4394.0	30.96	20.77	10.32	6.55 — 30.96	10.98	12.30	10.48	2.99	— 27.23
	4792.1	37.25	21.58	15.95	4.40 — 37.25	21.77	13.35	9.09	2.15	— 21.77
	5043.7	34.97	22.57	11.91	7.11 — 34.97	27.20	17.77	9.82	4.54	— 27.20
	5316.3	21.03	16.85	8.63	5.33 — 25.32	24.37	16.55	8.67	4.26	— 24.37
	5387.2	36.79	24.11	11.93	8.41 — 36.79	17.94	13.49	7.01	3.24	— 18.06
	5442.1	30.63	20.59	10.22	6.46 — 30.63	14.13	12.21	7.33	2.91	— 20.59
	5491.5	37.14	22.44	14.42	5.74 — 37.14	14.90	28.51	37.54	2.35	— 84.23
			15.97			5.16 — 37.25	8.30			0.86
		Mean				Mean				
	2.9									
	20.6	20.41	15.62	7.86	4.42 — 21.68	3.40	14.85	25.18	1.61	— 52.61
	74.5	8.71	7.31	4.54	1.03 — 11.81	4.26	9.01	12.40	1.17	— 27.51
	109.9	5.91	5.38	3.75	0.57 — 9.71	1.90	7.04	11.56	0.46	— 24.36
	129.1	3.05	4.11	4.32	0.31 — 10.32	3.33	8.96	13.51	0.97	— 29.16
	180.5	3.42	4.67	4.97	0.41 — 11.86	1.07	10.29	19.15	0.42	— 39.00
	218.1	5.88	5.60	4.10	0.63 — 10.65	3.18	7.83	11.46	0.79	— 24.96
	259.6	4.76	4.95	4.02	0.49 — 10.26	1.35	5.18	8.57	0.24	— 18.02
	319.7	5.42	5.17	3.80	0.53 — 9.82	1.53	6.79	11.55	0.37	— 24.10
	400.0	4.84	4.40	3.09	0.38 — 7.92	2.66	3.56	3.73	0.24	— 8.92
Station 11 OMZ Galapagos Rise	600.4	5.48	4.97	3.46	0.49 — 8.92	1.30	4.81	7.91	0.22	— 16.66
	799.3	4.93	4.90	3.78	0.48 — 9.72	1.75	4.67	7.04	0.27	— 15.18
	998.6	6.82	5.60	3.51	0.60 — 8.77	2.30	4.51	6.02	0.31	— 13.45
	1248.5	8.19	6.94	4.38	0.93 — 11.40	2.44	7.24	11.25	0.59	— 24.07
	1498.7	6.21	5.42	3.59	0.57 — 9.24	3.20	4.61	5.10	0.38	— 12.02
	1747.9	7.49	6.30	3.98	0.76 — 10.21	3.77	5.39	5.93	0.53	— 14.03
	1997.3	9.74	7.88	4.70	1.17 — 12.04	4.48	5.31	4.96	0.55	— 12.29
	2248.4	7.83	7.01	4.69	0.97 — 12.37	4.96	5.46	4.72	0.59	— 11.91
	2497.4	16.08	10.61	6.45	1.66 — 16.08	6.33	5.98	4.31	0.71	— 11.25
	2746.1	17.06	11.49	6.67	2.02 — 17.06	7.43	7.15	5.22	1.02	— 13.74
	3495.2	26.66	17.82	9.39	4.79 — 26.66	14.51	12.53	7.48	3.06	— 21.09
3594.5	27.53	18.95	9.32	5.71 — 27.53	13.44	11.96	7.49	2.82	— 20.94	
3620.2	27.74	18.85	9.47	5.53 — 27.74	17.74	15.39	8.96	4.63	— 26.08	
		10.64			3.05 — 27.74	4.83			1.07	— 17.74
		Mean				Mean				

	20.2	23.67	14.09	10.25	2.14 — 23.67	7.33	5.47	3.30	0.53	—	7.33
	60	18.41	10.79	8.41	1.17 — 18.41	8.69	5.58	3.82	0.43	—	8.69
	95.2	15.04	9.00	6.79	0.89 — 15.04	5.24	4.31	2.76	0.35	—	6.76
	150.3	2.57	3.83	4.37	0.26 — 10.20	0.95	3.01	4.77	0.10	—	10.14
	200.2	3.52	2.82	1.82	0.15 — 4.22	3.04	7.11	10.22	0.68	—	22.37
	355.3	5.74	4.98	3.31	0.48 — 8.44	3.44	7.05	9.58	0.73	—	21.32
	400	6.29	5.64	3.84	0.63 — 9.97	3.34	5.78	7.21	0.55	—	16.44
	599.1	7.63	7.77	6.05	1.21 — 15.82	2.45	5.15	7.08	0.38	—	15.69
	998.9	7.16	6.14	3.96	0.73 — 10.23	2.63	5.95	8.45	0.49	—	18.56
	1198.5	5.77	5.74	4.42	0.66 — 11.42	3.89	5.67	6.32	0.58	—	14.90
Station 18	1398.4	4.53	6.66	7.45	0.80 — 17.58	4.34	6.01	6.44	0.67	—	15.36
Pacific Rise	1597.4	6.98	7.62	6.43	1.15 — 16.49	3.47	5.74	6.97	0.56	—	16.02
	1798	8.53	8.02	5.63	1.28 — 15.02	3.49	5.82	7.11	0.57	—	16.32
	1997.1	13.14	10.55	5.98	2.09 — 15.90	5.11	6.24	5.97	0.75	—	14.73
	2198	22.20	15.50	7.99	3.91 — 22.20	9.53	11.37	10.45	2.52	—	26.43
	2296.7	57.63	32.39	24.74	8.24 — 57.63	42.06	23.96	18.37	4.94	—	42.06
	2334.2	39.22	27.94	11.26	13.08 — 39.22	47.36	28.27	17.82	8.70	—	47.36
	2383.8	53.68	39.60	14.78	26.29 — 53.68	77.45	43.62	30.98	15.17	—	77.45
	2433.2	54.98	29.06	28.01	3.44 — 54.98	79.63	47.90	24.34	25.73	—	79.63
	2484.5	62.15	38.01	19.73	17.23 — 62.15	47.22	30.71	13.99	13.41	—	47.22
	2534.2	71.35	43.15	22.32	21.33 — 71.35	70.47	41.73	24.02	18.32	—	70.47
	2593.7	70.77	42.16	23.55	19.17 — 70.77	76.85	46.08	24.12	23.54	—	76.85
		25.50			2.57 — 71.35	23.09			0.95	—	79.63
		Mean				Mean					
	20.2	25.55	14.14	12.49	1.40 — 25.55	3.41	3.89	3.53	0.30	—	8.76
	45.5	10.08	6.35	4.45	0.53 — 10.08	2.43	3.82	4.50	0.25	—	10.42
	79.7	16.46	9.74	7.48	1.00 — 16.46	3.21	4.54	4.95	0.38	—	11.72
	100.4	8.72	6.49	3.84	0.74 — 8.72	4.97	3.51	2.24	0.20	—	4.97
	140	5.25	5.13	3.88	0.53 — 10.01	4.38	6.41	7.16	0.74	—	16.90
	200.5	2.36	3.69	4.34	0.24 — 10.03	1.74	7.96	13.61	0.49	—	28.35
	248.9	4.41	5.66	5.68	0.61 — 13.81	2.28	6.43	9.86	0.48	—	21.18
Station 26	334	4.31	4.41	3.55	0.39 — 9.03	1.28	6.53	11.36	0.30	—	23.57
S. of	848.5	5.52	5.92	4.96	0.70 — 12.65	1.58	4.38	6.68	0.23	—	14.35
Marquesas	998.5	5.74	5.96	4.82	0.71 — 12.37	1.71	8.06	13.85	0.49	—	28.82
Fracture	1249.6	7.34	6.81	4.77	0.92 — 12.56	2.91	5.96	8.11	0.52	—	18.02
Zone	1496.3	5.55	5.56	4.32	0.62 — 11.14	3.46	4.72	5.02	0.41	—	11.98
	1996.9	12.83	9.83	5.49	1.75 — 13.65	5.11	6.89	7.20	0.89	—	17.34
	2397.6	40.46	24.61	15.12	7.08 — 40.46	31.38	20.59	10.76	6.15	—	31.38
	2546.3	69.12	37.92	30.93	9.31 — 69.12	18.54	26.78	29.33	5.55	—	70.04
	2746.1	54.30	32.01	20.44	10.55 — 54.30	41.96	25.52	15.51	7.63	—	41.96
	2996.3	38.22	23.39	14.27	6.55 — 38.22	31.85	20.77	10.98	6.17	—	31.85
	3743.5	27.62	17.30	10.65	3.86 — 27.62	19.87	14.21	7.36	3.40	—	19.87
	3893.3	27.12	20.62	9.48	7.66 — 28.25	26.11	17.64	9.14	4.79	—	26.11
	3958.6	25.73	17.76	8.89	5.04 — 25.73	16.22	12.74	6.84	3.00	—	18.51
		19.83			2.36 — 69.12	11.22			1.28	—	41.96
		Mean				Mean					
	29.4	17.76	11.76	6.98	2.05 — 17.76	5.13	4.24	2.73	0.34	—	6.71
	44.1	16.87	10.38	7.25	1.31 — 16.87	6.25	5.22	3.33	0.52	—	8.38
	74.4	13.57	8.67	5.74	1.02 — 13.57	2.58	3.94	4.56	0.27	—	10.60
	130.4	6.37	5.33	3.40	0.55 — 8.56	1.70	3.17	4.13	0.16	—	9.27
	298	6.06	6.50	5.43	0.84 — 13.89	1.39	6.44	11.04	0.32	—	22.99
	448.2	6.00	5.78	4.28	0.67 — 11.12	1.45	7.85	13.77	0.41	—	28.51
	595.7	4.93	6.89	7.41	0.87 — 17.69	3.06	6.57	9.12	0.62	—	20.15
	994.3	6.26	7.73	7.44	1.15 — 18.40	4.30	5.12	4.81	0.51	—	11.87
	1739.8	6.10	6.43	5.26	0.82 — 13.50	2.89	4.48	5.24	0.35	—	12.16
Station 36	2089.8	14.80	10.55	5.87	1.86 — 14.80	3.29	5.82	7.35	0.55	—	16.70
S. of Vostok	2285.6	16.85	12.90	6.81	3.01 — 17.88	4.98	5.87	5.44	0.67	—	13.53
Island	2385.6	18.85	12.93	7.14	2.65 — 18.85	7.21	6.66	4.65	0.88	—	12.23
	2484.1	19.77	13.50	7.42	2.86 — 19.77	6.37	7.03	6.04	0.98	—	15.38
	2585	22.61	14.78	8.56	3.14 — 22.61	8.99	9.41	7.50	1.77	—	19.67
	2684.3	17.92	13.11	6.87	2.98 — 17.92	9.65	9.01	6.22	1.62	—	16.75
	2782.7	19.73	13.79	7.33	3.10 — 19.73	8.57	8.23	5.94	1.35	—	15.80
	2983.4	18.79	12.85	7.13	2.60 — 18.79	5.09	6.25	6.03	0.75	—	14.84
	3480.5	12.73	10.82	6.48	2.27 — 17.82	4.04	7.71	10.12	0.92	—	22.77
	3975.7	8.64	7.65	5.01	1.15 — 13.32	3.82	4.72	4.60	0.43	—	11.24
	4721.4	13.38	12.15	7.82	2.92 — 21.83	9.73	8.76	5.79	1.52	—	15.59
	5069	16.59	15.09	9.47	4.51 — 27.16	7.09	12.56	15.78	2.56	—	36.07
	5094.6	18.40	13.09	6.95	2.86 — 18.40	9.31	11.43	10.82	2.52	—	27.11
		13.77			4.93 — 22.61	5.31			1.39	—	9.73
		Mean				Mean					

3.4.2 Upper 60 m and Mixed Layer

The mixed-layer depths for all 5 deep water stations (ST 1, 11, 18, 26 and 36) ranged between 36 and 60 m and was calculated from the CTD data (Table 2.1, Ohmemus et al., 2016). Since the deepest mixed-layer depth is ≤ 60 m, the inventories were calculated (details given below) of total ^{210}Pb ($^{210}\text{Po}_T$) and ^{210}Po ($^{210}\text{Pb}_T$) in the upper 60 m (Table 3.5). From the measured ^{210}Po and ^{210}Pb activities in the dissolved phase ($^{210}\text{Po}_d$, $^{210}\text{Pb}_d$), particulate phase ($^{210}\text{Po}_p$, $^{210}\text{Pb}_p$) and total ($^{210}\text{Po}_T$, $^{210}\text{Pb}_T$, total = particulate + dissolved) phase in the upper 60 m (Table 3.5, Figures 3.1, 3.2, 3.4 and 3.6), the following observations are made: 1) the activities of dissolved and total ^{210}Po are highest in the Peru Shelf (ST-4), 11.4 and 13.7 dpm 100L⁻¹) and generally lower (as low as 2.55 dpm 100L⁻¹ in ST 26) in the open water stations west of this site; 2) the ^{210}Po and ^{210}Pb activities in the upper 3 m in all six super stations varied considerably (by a factor of ~ 3 for dissolved ^{210}Pb and ~ 2 for dissolved ^{210}Po), with ^{210}Pb activities $>$ ^{210}Po activities ($^{210}\text{Po}/^{210}\text{Pb}$ AR $<$ 1.0); 3) unlike standard oceanic parameters (temperature, density, conductivity) that generally remain constant within the mixed layer, the activities of both ^{210}Po and ^{210}Pb varied considerably (by more than a factor of 4) as well as $^{210}\text{Pb}_T/^{226}\text{Ra}$ AR (by a factor of ~ 2); 4) the activities of dissolved and total ^{210}Pb were distinctly higher (10.2 - 22.4 dpm 100 L⁻¹) in the upper 60 m of the open ocean waters west of the continental margins (Table 3.5); and 5) the $^{210}\text{Pb}_T/^{226}\text{Ra}$ AR values from analyzed water samples near the mixed layer that were removed in Figure 3.6, show large AR value (circled in red) near the 100 m depth (Figure 3.8 and 3.9).

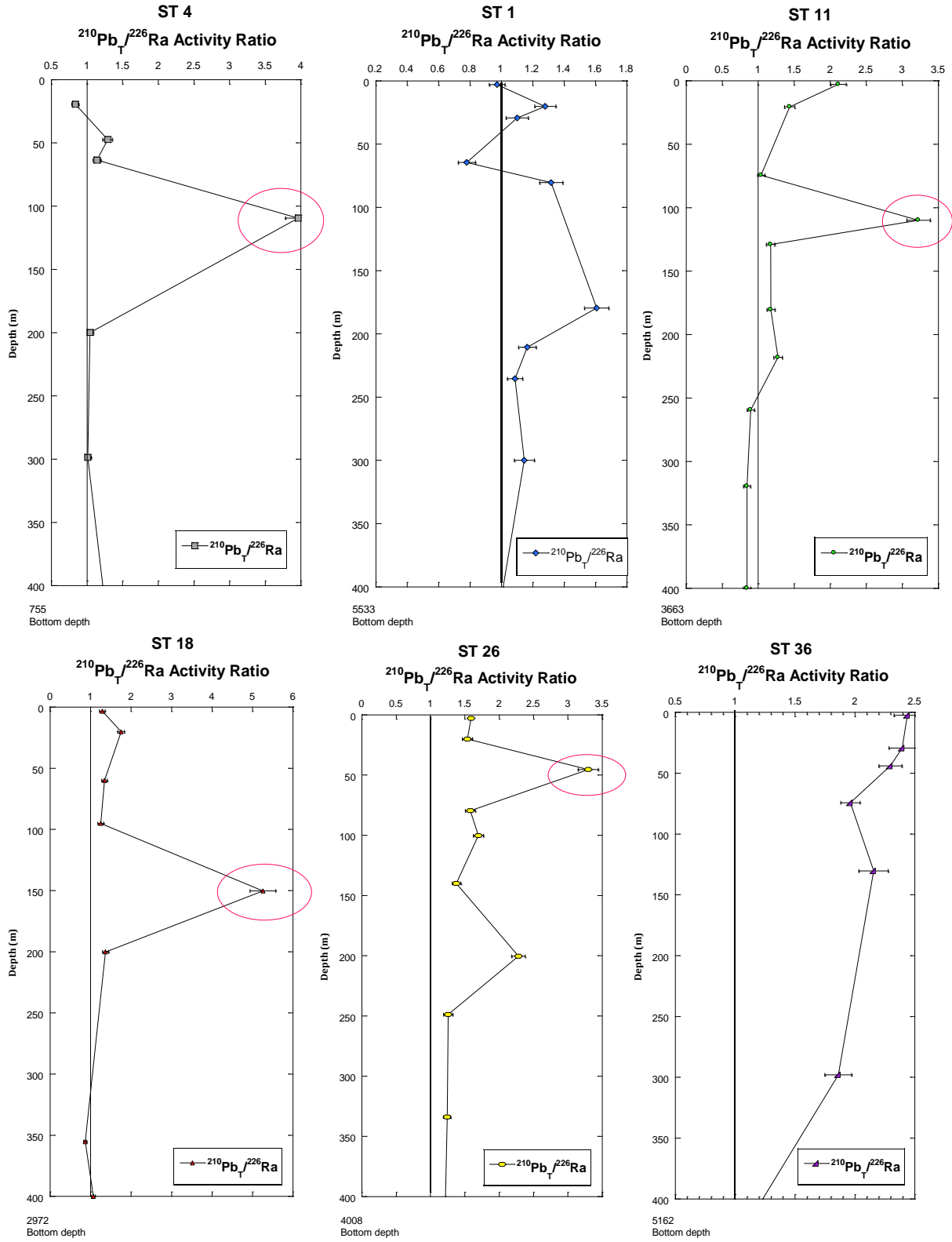


Figure 3.8. Vertical profiles of $^{210}\text{Pb}_{\text{Total}}/^{226}\text{Ra}$ of AR to 400 m depth, Detail of Figures 3.6, 3.7.

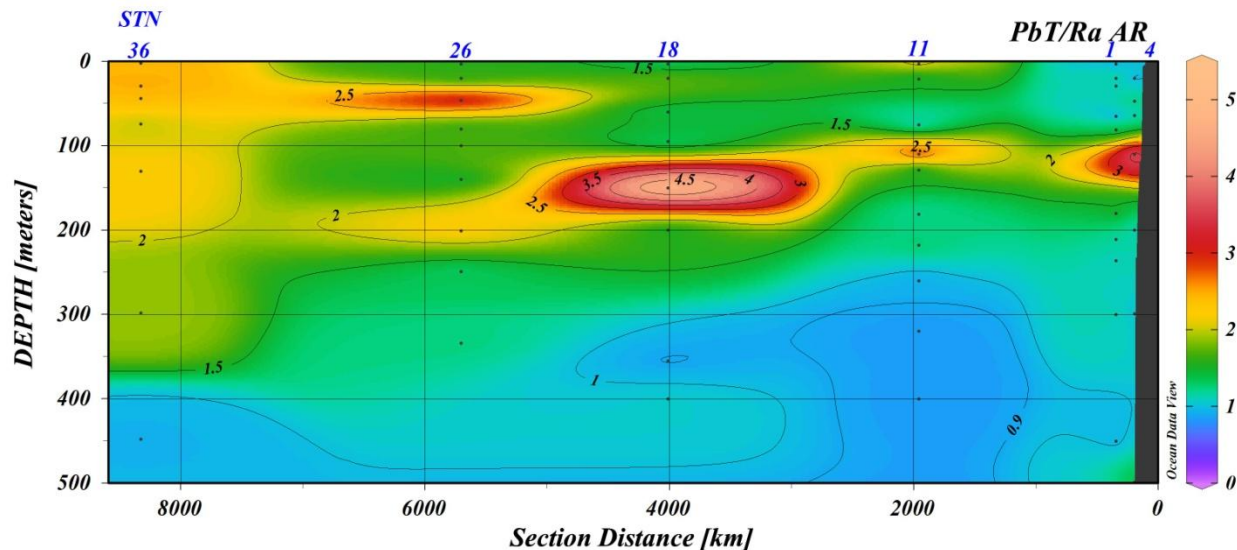


Figure 3.9. Vertical section of $^{210}\text{Pb}_T/^{226}\text{Ra}$ activity ratio down to 500m, Ocean Data View (ODV), Detail of Figures 3.6, 3.7, Ocean Data View (ODV).

The inventories of ^{210}Po and ^{210}Pb were calculated from the integration of their measured activities and linear interpolation for layers in between (e.g. at ST 1 for upper 300 m, the ^{210}Po and ^{210}Pb activities were measured at depths: 3, 15, 35, 60, 80, 180, 210, 235, 300 m; for the upper 3 m, the value at 3-m layer was used; for 3 to 15 m, the average value of 3 and 15 m for the 12 m thick layer (3 to 15 m), and so on; for 235-300 m, the average value at 235 and 300 m for that 65 m layer and summing up the total inventories in the 300 m). As seen in Table 3.7 and Figure 3.10, the total ^{210}Po inventory in the upper 60 m ranged from 3.65×10^3 to 7.34×10^3 dpm m^{-2} , with the highest value found in the waters of the Peru shelf (ST 4). The inventories of total ^{210}Pb ($^{210}\text{Pb}_T$) in the upper 60 m ranged between 3.97×10^3 and 8.62×10^3 dpm m^{-2} (factor of 2.2 difference) with the highest inventory at the most oligotrophic station (ST 36), and lowest in the most productive shelf station waters (ST 4), showing an overall increase in inventory with distance from the Peru margin.

Table 3.7

Inventories in the **upper 60m** of $^{210}\text{Po}_T$, $^{210}\text{Pb}_T$ and ^{226}Ra , DO, SiO_4^{2-} , NO_3^- , PO_4^{3-} , particulate Al, Mn and Fe and $(^{210}\text{Po}/^{210}\text{Pb})_T$ AR and $(^{210}\text{Pb}_T/^{226}\text{Ra})$ AR at the GEOTRACES EPZT (October -- December 2013).

Super Station #	GT #	East		$^{210}\text{Po}_T/^{210}\text{Pb}_T$ Inv. AR	^{226}Ra dpm m ⁻²	$^{210}\text{Pb}_T/^{226}\text{Ra}$ Inv. AR	$\text{Al}_p^{[++]}$ Inv μmol m ⁻²	Mn_p Inv μmol m ⁻²	Fe_p Inv μmol m ⁻²	O_2 Inv μmol m ⁻²	SiO_4^{2-} Inv mmol m ⁻²	NO_3^- Inv mmol m ⁻²	PO_4^{3-} Inv mmol m ⁻²
		$^{210}\text{Po}_T$ dpm m ⁻²	$^{210}\text{Pb}_T$ dpm m ⁻²										
4	2300	7341 ± 230	3972 ± 73	1.85 ± 0.07	3901 ± 76	1.02 ± 0.03	39.0	4.80	52.9	5.41	1049	654	146
1	2100	3649 ± 165	4330 ± 84	0.84 ± 0.04	4145 ± 68	1.04 ± 0.03	98.1	13.1	66.8	13.5	150	476	60.1
11	3600	3995 ± 160	6007 ± 96	0.67 ± 0.03	3904 ± 41	1.54 ± 0.03	3.35	1.86	1.29	13.5	193	529	49.9
18	8400	4261 ± 195	6018 ± 121	0.71 ± 0.04	3906 ± 71	1.54 ± 0.04	5.66	3.86	27.7	12.8	92.4	191	24.8
26	9400	4870 ± 224	8594 ± 143	0.57 ± 0.03	3991 ± 48	2.15 ± 0.04	1.05	0.95	1.12	12.2	81.9	140	22.7
36	10300	5259 ± 175	8620 ± 115	0.61 ± 0.02	3668 ± 42	2.35 ± 0.04	3.95	0.88	6.20	11.8	73.0	38.0	14.1

Total = dissolved (<0.45 μm), + particulate (>1 μm) GEOTRACES EPZT (25 October - 20 December, 2013)

+ ^{226}Ra data collected and processed by Charett, Matthew and crew - EPZT cruise participant, Sanial et al. submitted

++ Al_p , Mn_p , Fe_p , particulate data was collected and processed by Lam, Phoebe J. and crew - EPZT cruise participant

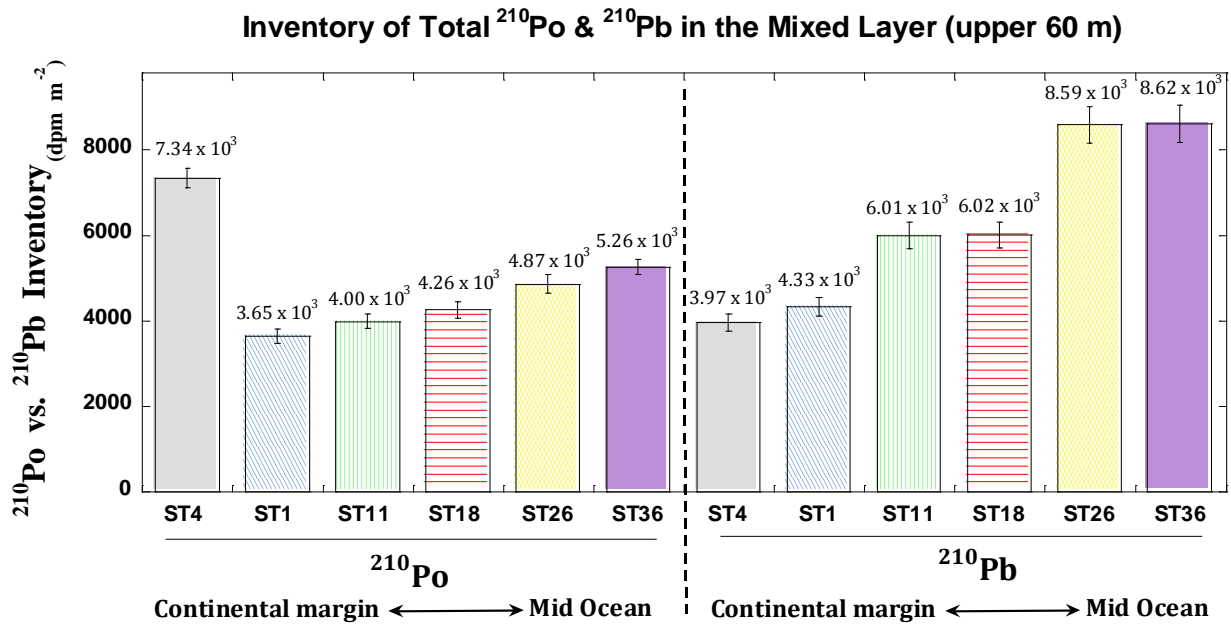


Figure 3.10. Bar diagram of total ^{210}Po and ^{210}Pb inventories in the upper 60 m of 6 super stations in U.S. GEOTRACES GP16 EPZT.

Although there is no ^{210}Pb depositional flux data, one can use the ^{210}Pb concentrations in aerosols. The atmospheric depositional flux is anticipated to be much higher in ST 4 compared to ST 36 due to the distance from the coastline of these two stations. The ^{210}Pb concentrations in aerosols and the inventories of ^{210}Pb in the upper 60 m mixed layer are plotted in Figure 3.11.

There seems no correlation between the two. It is likely that aerosol data is a snapshot and may not reflect the annual fallout data.

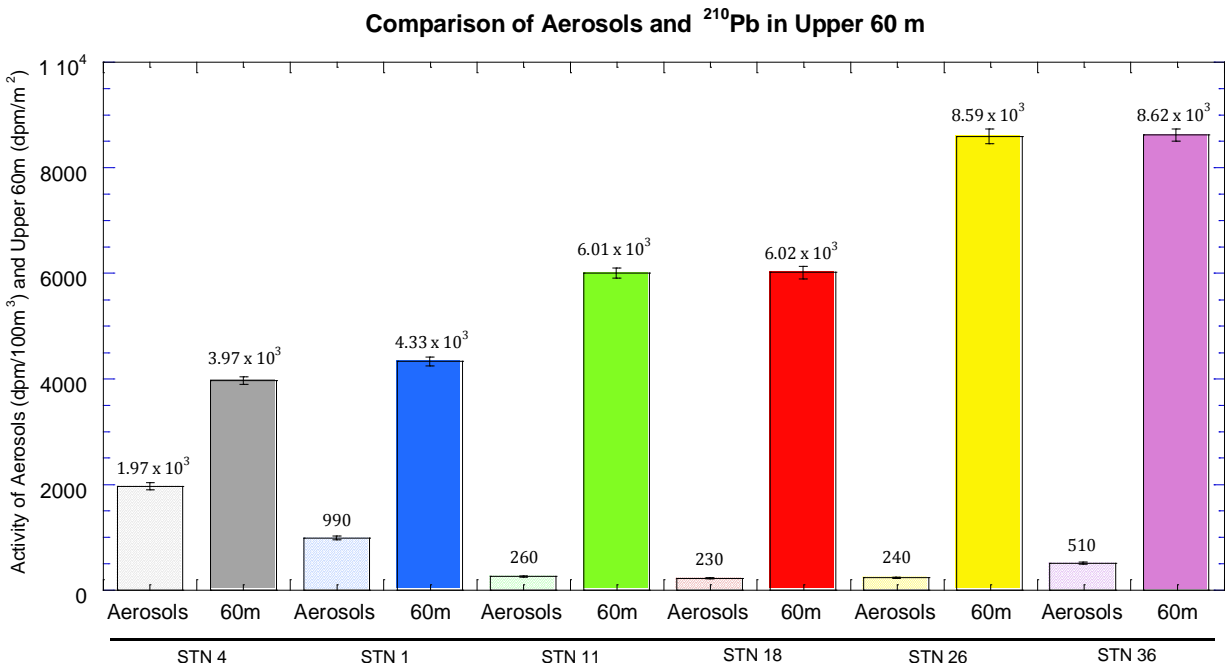


Figure 3.11. Comparison of aerosols and upper 60 m for all six stations.

The differences in the total ^{210}Pb inventories in the mixed layer can be attributed to two factors: 1) differences in the atmospheric depositional fluxes and 2) differences in the scavenging intensities. In contrast, the inventory of ^{226}Ra remained constant ($\pm 6\%$) in the upper 60 m at all 6 stations ($3.91 \pm 0.24 \times 10^3 \text{ dpm m}^{-2}$) as seen in Table 3.7.

The inventory-based ($^{210}\text{Po}_T / ^{210}\text{Pb}_T$) AR in the mixed layer varied between 0.57 and 0.84 (mean 0.68, $n=5$) (except in ST 4 where it was found to be 1.85. Table 3.7), again indicating active scavenging in the mixed layer. This is in agreement with earlier published results on discrete layers from the Pacific, Atlantic and Indian Oceans (Bacon et al., 1976; Nozaki et al., 1976; Thomson and Turekian, 1976; Cochran et al., 1983, 1986; Rigaud et al., 2015). The $^{210}\text{Pb}_T / ^{226}\text{Ra}$ activity ratio in the mixed layer varied between 1.02 and 2.35, with the lowest value

found in the highly productive waters of the Peru shelf (ST 4) due to active scavenging of ^{210}Pb . Excess ^{210}Pb activity, with $^{210}\text{Pb}/^{226}\text{Ra}$ activity ratios (AR) varying between 1.54 and 2.35, was found in the mixed layer of the four open ocean stations (ST 11, 18, 26 and 36; Table 3.7), and this is mainly attributed to the direct atmospheric depositional input.

3.4.3 Biotic, Sediment-water and Hydrothermal (Upper and Bottom 300 m) Interfaces

The inventories of total ^{210}Po and ^{210}Pb activity in the upper 300 m varied between 2.71×10^4 and 4.49×10^4 dpm m^{-2} and between 2.71×10^4 and 4.37×10^4 dpm m^{-2} , respectively. As can be seen in Table 3.8, the highest ^{210}Po inventory was found in the Peru shelf station (ST 4) and the lowest value was found ST 11, the OMZ (Oxygen Minimal Zone). The highest inventory of total ^{210}Pb in the upper 300 m was found in the EPR (Eastern Pacific Rise) site, ST 18 followed by the most oligotrophic station (ST 36) due to poor scavenging. The lowest inventory of ^{210}Pb was found in the Peru margin. The inventory-based $(^{210}\text{Po}/^{210}\text{Pb})_{\text{T}}$ AR in the upper 300 m varied between 0.78 and 1.16, with the highest value found in the Peru shelf station and the lowest value found at the EPR station (Table 3.8).

The inventories of total ^{210}Po and ^{210}Pb in the bottom 300 m of the water column varied between 2.25×10^4 and 6.63×10^4 dpm m^{-2} and between 3.15×10^4 and 6.50×10^4 dpm m^{-2} , respectively, with the highest ^{210}Po inventory found in the oligotrophic water, ST 36 and the lowest value at the OMZ station, ST 11 (Table 3.8). Due to low biological particle production rate in the upper 300 m in ST 36, and expected lower particle inventory in the whole water column, it was anticipated that the scavenging intensity of ^{210}Po in the bottom 300 m would be low, resulting in a higher inventory of ^{210}Po . Also, the highest inventory of total ^{210}Pb was found in the most oligotrophic station (ST 36) due to poor scavenging. The lowest inventory was found in the Peru margin (ST 1) due to intense scavenging likely due to higher particle flux.

The inventory-based ($^{210}\text{Po}/^{210}\text{Pb}$)_T AR in the bottom 300 m varied between 0.57 and 1.08, with the highest value found in the most productive Peru margin, (ST 1) water, again indicating poor scavenging intensity.

Table 3.8
Inventories and activity ratios of ^{210}Po , ^{210}Pb , ^{226}Ra , particulate Al, Mn, Fe and the residence times at the **top and bottom 300 m** of all six super stations at the GEOTRACES EPZT (October -- December 2013).

Depth	Station		$^{210}\text{Po}_T$		$^{210}\text{Pb}_T$		$^{210}\text{Po}_T/^{210}\text{Pb}_T$	^{226}Ra		$^{210}\text{Pb}_T/^{226}\text{Ra}$	$^{210}\text{Po}_\tau$	$^{210}\text{Pb}_\tau$	Al _p	Mn _p	Fe _p
	#	GT #	dpm	m ⁻²	dpm	m ⁻²	Inv. AR	dpm	m ⁻²	Inv. AR	τ (y)	τ (y)	μmol m ⁻²	μmol m ⁻²	μmol m ⁻²
Upper 300 m	** 4	2300	44918 ± 1633	38665 ± 625	1.16 ± 0.04	23483 ± 235	1.65 ± 0.03	-	-	477	7	756			
	1	2100	29521 ± 740	27108 ± 362	1.09 ± 0.03	21989 ± 212	1.23 ± 0.02	-	-	712	18	1103			
	11	3600	27163 ± 596	29296 ± 306	0.93 ± 0.02	22413 ± 177	1.31 ± 0.02	7.0 ± 2.2	-	39	14	39			
	18	8400	33850 ± 1214	43657 ± 649	0.78 ± 0.03	21967 ± 257	1.99 ± 0.04	1.9 ± 0.3	-	30	29	101			
	26	9400	34512 ± 858	38512 ± 360	0.90 ± 0.02	20405 ± 164	1.89 ± 0.02	4.7 ± 1.1	-	11	15	8			
	36	10300	39378 ± 1405	41973 ± 709	0.94 ± 0.04	20084 ± 352	2.09 ± 0.05	8.3 ± 5.0	-	30	14	34			
Lower 300 m	** 4	2300	41245 ± 1831	41730 ± 912	0.99 ± 0.05	36492 ± 669	1.14 ± 0.03	-	-	2960	11	883			
	1	2100	34186 ± 808	31525 ± 408	1.08 ± 0.03	87492 ± 925	0.36 ± 0.01	-	18 ± 0.4	5800	109	1469			
	11	3600	54059 ± 1673	52655 ± 863	1.03 ± 0.04	95512 ± 1518	0.55 ± 0.01	-	40 ± 2	332	45	163			
	18	8400	22488 ± 437	39443 ± 363	0.57 ± 0.01	80312 ± 748	0.49 ± 0.01	0.7 ± 0.0	31 ± 1	54	382	6264			
	26	9400	45588 ± 1428	54033 ± 787	0.84 ± 0.03	95586 ± 3288	0.57 ± 0.02	3.0 ± 0.6	42 ± 3	97	38	162			
	36	10300	66340 ± 1930	64996 ± 1513	1.02 ± 0.05	70247 ± 1329	0.93 ± 0.03	-	398 ± 153	NM	NM	NM			

** = Depth to only 672 meters, NM = Not measured (no sample was collected)

Total = ^{210}Po dissolved (<0.45 μm), + particulate (>1 μm)

τ = Residence time in years

3.4.4 Activity Ratios of ($^{210}\text{Po}/^{210}\text{Pb}$)_T and ($^{210}\text{Pb}_T/^{226}\text{Ra}$) Based on the Integrated Activities of $^{210}\text{Po}_T$, $^{210}\text{Pb}_T$ and ^{226}Ra in the Whole Water Column

The ($^{210}\text{Po}/^{210}\text{Pb}$)_T AR based on the integrated activities of $^{210}\text{Po}_T$ and $^{210}\text{Pb}_T$ over the whole water column varied between 0.97 ± 0.02 and 1.09 ± 0.02 (Table 3.9), with the highest value found at the EPR site, ST 18. Remineralization of biogenic particulate matter containing $^{210}\text{Po}/^{210}\text{Pb}$ AR of >1.0 at various depths of water column will result in higher activities of dissolved ^{210}Po compared to ^{210}Pb , but such redistribution of ^{210}Po will not affect the whole water column inventory of total ^{210}Po . In stations ST 26 and 36, ^{210}Po and ^{210}Pb are in secular

equilibrium for the whole water column. The $^{210}\text{Pb}_T/^{226}\text{Ra}$ AR in the five open ocean stations (excluding the Peruvian margin, ST 4) varied between 0.57 and 1.32 with highest the value was found in the most oligotrophic water (ST 36) where the biological productivity was minimal and hence the least intensity of scavenging. The lowest AR value was measured at the Peru margin due to the highest biological productivity and active scavenging of ^{210}Pb . The higher $^{210}\text{Pb}_T/^{226}\text{Ra}$ activity ratio at the EPR site (ST 18) could have been due to partial removal of Ra as RaSO_4 near the hydrothermal vent.

Table 3.9

Whole column inventory of total ^{210}Po , ^{210}Pb , ^{226}Ra inventories and residence times

Station #	$^{210}\text{Po}_T$ Inv dpm m^{-2}	$^{210}\text{Pb}_T$ Inv dpm m^{-2}	^{226}Ra Inv dpm m^{-2}	$^{210}\text{Po}_T/^{210}\text{Pb}_T$ Inv. AR	$^{210}\text{Pb}_T/^{226}\text{Ra}_T$ Inv. AR	$^{210}\text{Po}_\tau$ τ (y)	$^{210}\text{Pb}_\tau$ τ (y)
**							
4	95478 ± 2609	90183 ± 1279	68233 ± 812	1.06 ± 0.03	1.32 ± 0.02		
1	862650 ± 13695	811397 ± 6104	1416053 ± 9797	1.06 ± 0.02	0.75 ± 0.01		43 ± 1
11	664480 ± 9260	624125 ± 4626	806683 ± 5693	1.06 ± 0.02	0.77 ± 0.01		110 ± 4
18	426602 ± 6382	391391 ± 2938	459813 ± 2753	1.09 ± 0.02	0.85 ± 0.01		184 ± 11
26	584288 ± 8708	600170 ± 4142	880620 ± 7243	0.97 ± 0.02	0.68 ± 0.01	20 ± 12	69 ± 2
36	978759 ± 14511	1011783 ± 6689	1177071 ± 6535	0.97 ± 0.02	0.86 ± 0.01	16 ± 8	197 ± 11

** = Depth to only 672 meters, τ = Residence time

3.4.5 Inventories of ^{210}Po , ^{210}Pb , and Inventories of Al, Mn, Fe and Other Major Nutrients in the Mixed Layer

Inventories of ^{210}Po and ^{210}Pb were compared to calculated inventories of Al, Mn, Fe and other major nutrients in the upper 60 m and mixed layer. Table 3.7 shows for ST 1 that Al_p , Mn_p and Fe_p have their highest inventory levels of 98.1, 13.1 and 66.8 $\mu\text{mol m}^{-2}$ respectively, corresponding to the lowest inventory value of $3.65 \pm 0.17 \times 10^3$ dpm m^{-2} also at ST 1.

The inventory values at the EPR, ST 18 for Al_p , Mn_p and Fe_p are 5.66, 3.86, and 27.7 $\mu\text{mol m}^{-2}$ respectively. The particulate Al inventory decreases from the Peru margin to offshore by more than order of magnitude. While Al inventories in the 6 stations vary by ~ 2 orders of magnitude.

With respect to dissolved oxygen and nutrients in the mixed layer, the inventory of O_2 decreases westward from ST 1 to ST 36, 13.5 to 11.8 $\mu\text{mol m}^{-2}$, respectively; but there is a lower inventory of 5.41 $\mu\text{mol m}^{-2}$ for the Peru Shelf (ST 4). The other major nutrients of silicates, nitrates and phosphates with values of 1049, 654 and 146 mmol m^{-2} respectively, display a decrease westward with the highest inventories at Peru shelf (ST 4). After a decrease by a factor of 7 for silicates and a factor of 1.4 for nitrates, silicate and nitrate values show a slight increase at ST 11 before decreasing westward to station 36. Furthermore, dissolved nitrate inventory varies by a factor of 17. Clearly, biological activity as assessed by nitrate inventory decreases from Peru margin to the most oligotrophic waters.

CHAPTER 4

DISCUSSION

4.1 Introduction

The major source of most of the ^{210}Pb in surface waters is derived from atmospheric deposition. The ^{210}Pb depositional fluxes vary both spatially and temporally. In the continental/coastal stations, the ^{210}Pb depositional fluxes almost vary by an order of magnitude, $\sim 2.0 \text{ dpm cm}^{-2} \text{ y}^{-1}$ in Japan and $0.15\text{-}0.30 \text{ dpm cm}^{-2} \text{ y}^{-1}$ in the west coast of San Francisco and Los Angeles, CA; (Fuller and Hammond, 1983; summarized in Baskaran, 2011). Such large variations are attributed to the differences in frequency and amount of precipitation, sources of air masses (continental versus oceanic) and radon escape rate in the surrounding areas (Figure 4.1). While there are large amounts of directly-measured depositional flux published data over the continents, there is virtually no data from over the ocean and long-term (>1 year) ^{210}Pb depositional flux data from direct fallout studies do not exist. It is possible to estimate the atmospheric depositional flux by assessing the scavenging intensity and residence times of ^{210}Pb in the surface waters with its required source function, by the measured concentrations of ^{210}Pb in the water column. Hence, details on the estimation of atmospheric depositional flux are given in the next section.

The disequilibrium between ^{210}Po and ^{210}Pb (Bacon et al., 1976) as well as between ^{210}Pb and ^{226}Ra was demonstrated (Craig et al., 1973) several decades ago. The disequilibrium between ^{210}Pb and its granddaughter, ^{210}Po , has been widely utilized to estimate rates of removal of ^{210}Po , POC from upper waters, residence times of ^{210}Po and the extent of remineralization of biogenic particulate matter. The overall patterns of $^{210}\text{Po} - ^{210}\text{Pb}$ and $^{210}\text{Pb} - ^{226}\text{Ra}$ disequilibria in the East Pacific Zonal Transect cruise are similar to the eastern South Pacific, North Pacific, Atlantic and

central and eastern Indian Oceans (Atlantic: Craig et al., 1973; Bacon et al., 1976; Hong et al., 2013; Rigaud et al., 2015; Pacific: Nozaki and Tsunogai, 1973, 1976; Nozaki et al., 1976, 1980; Thomson and Turekian, 1976; Chung and Craig, 1983; Indian Ocean: Cochran et al., 1983). The observed overall trend is as follows: upper mixed layer with excess ^{210}Pb over ^{226}Ra ($^{210}\text{Pb}/^{226}\text{Ra}$ AR >1.0) due to atmospheric depositional flux of ^{210}Pb , $^{210}\text{Pb}/^{226}\text{Ra}$ AR < 1.0 in most layers below 300 m.

4.2 Atmospheric Depositional Flux Estimation using ^{210}Pb in Aerosols and the Upper 500 m Water

There is no directly measured atmospheric flux data for ^{210}Pb over the Pacific Ocean. This flux can be determined by two different methods: 1) from the measured ^{210}Pb activity (C_a) in aerosols and assuming a constant aerosol deposition velocity (V_d); and 2) from a mass balance of ^{210}Pb at the depth where the atmospheric fallout of ^{210}Pb can penetrate into the oceanic water column. In the first method, the atmospheric depositional flux (I_A^0) is calculated from the relationship:

$$I_A^0 \text{ (dpm cm}^{-2} \text{ y}^{-1}\text{)} = V_d \text{ (cm y}^{-1}\text{)} \times C_a \text{ (dpm cm}^{-3}\text{)} \quad (4.1)$$

In the calculation of atmospheric deposition flux, a constant deposition velocity of 1 cm s^{-1} is commonly used (Turekian et al., 1977, Baskaran, 2011). The atmospheric depositional flux calculated using equation 4.1 varied from 0.07 to 0.62 $\text{dpm cm}^{-2} \text{ y}^{-1}$ and generally decreased from the continental slope station (ST 4) to offshore stations (ST 1, 11, 18, 26 and 36), as expected (Figure 4.2). The calculated atmospheric depositional flux using equation 4.1 from east to west of the cruise transect indicates a generally decreasing trend (Figure 4.2). An earlier study by Nozaki and Tsunogai (1973) indicated a geographical variation of ^{210}Pb in Pacific surface water, which was well correlated with the geographical distribution of arid land area. There are

two caveats in the calculation of the atmospheric depositional flux using equation 4.1; 1) the assumed constant deposition velocity and 2) the assumption that the ^{210}Pb activity in aerosols measured over 1-2 days is a representative value for the whole year. The average depositional velocities reported in literature ranged between 0.6 and 1.9 cm s^{-1} , with a commonly used value of 1 cm s^{-1} (Baskaran, 2011). For assessing the constancy of ^{210}Pb concentration in aerosols, one needs to evaluate the variations in the sources of air masses, if any. This is because the atmospheric depositional flux of ^{210}Pb primarily depends on the sources of air masses, (continental versus oceanic), mainly because average global ^{222}Rn flux from continents ($7.8 - 10.8 \text{ dpm cm}^{-2} \text{ d}^{-1}$) is about two orders of magnitude higher than that from the ocean surface ($0.10 \text{ dpm cm}^{-2} \text{ d}^{-1}$) (Baskaran, 2011). Thus, the temporal variations of ^{210}Pb in the ‘planetary boundary layer’ which is the lowest level of the atmosphere above the ocean surface is expected to remain relatively constant (Turekian et al., 1977; Baskaran, 2011). It has been shown that ^{210}Pb activity in aerosols collected from the South Pacific are about half of what was found in North Pacific, reflecting lower land/sea ratios in the Southern Hemisphere compared to the Northern Hemisphere (Turekian et al., 1989; Baskaran, 2011), and therefore, lower atmospheric depositional flux of ^{210}Pb in South Pacific is expected.

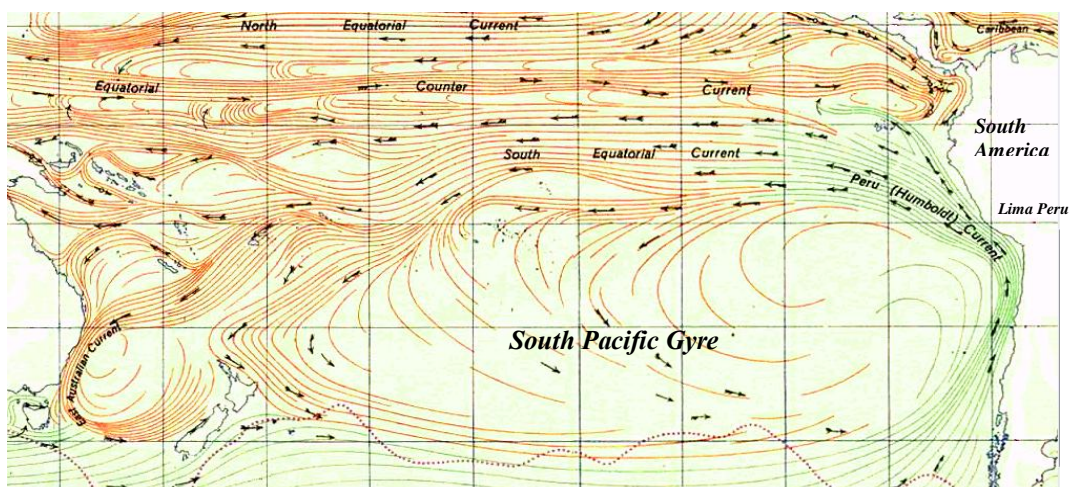


Figure 4.1. Equatorial trade winds and the South Pacific Gyre. Inventory of ^{210}Pb activity decreases in samples taken from east (Peru) toward the west (Tahiti), coincides with less lithogenic input from the South American Continent.
https://en.wikipedia.org/wiki/File:South_Pacific_Gyre.png

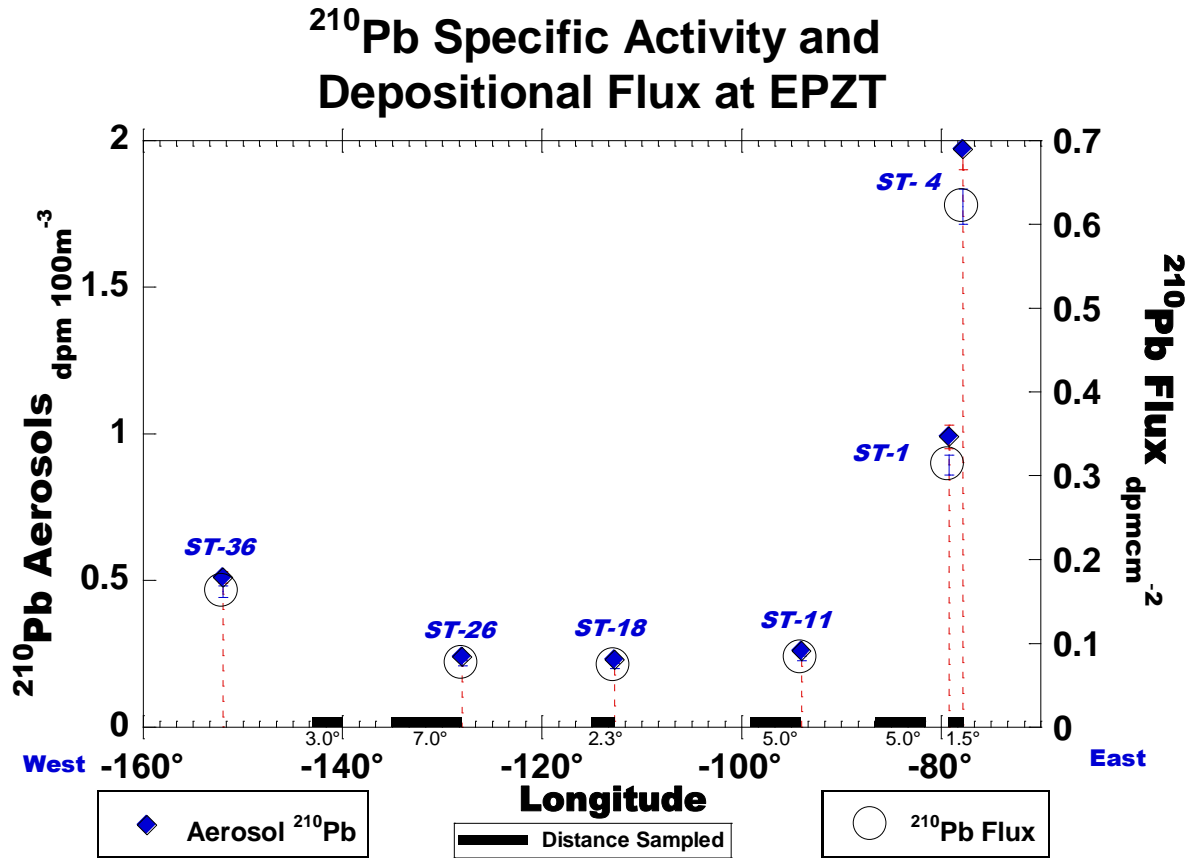


Figure 4.2. Specific activity of ^{210}Pb (dpm 100m⁻³) in aerosols and calculated ^{210}Pb atmospheric depositional flux.

In the second method, the atmospheric deposition flux of ^{210}Pb can be estimated from a simple box model calculation for the open ocean stations. A box of 500 m depth was chosen primarily because earlier works have shown that the penetration depth of atmospherically-delivered ^{210}Pb is ~500 m (Bacon et al., 1976). Furthermore, the nuclear-weapons tests derived fallout nuclides peak ($^{239,240}\text{Pu}$, ^{90}Sr , ^{137}Cs ; corresponding to 1963) also correspond to ~ 500 m (Hong et al., 2011 summarized in Baskaran (2011); Kenna, personal communication).

The sources of total (dissolved + particulate) ^{210}Pb in the upper 500 m of the water column in the open ocean include: 1) the annual atmospheric depositional flux, I_A^0 ; and 2) production from dissolved in situ ^{226}Ra . The sinks of total ^{210}Pb are: 1) removal by scavenging

on to particulate matter and eventual removal (characterized by scavenging removal rate constant, ψ_c^0) from the 500 m thick layer; and 2) radioactive decay. Since stations 11, 18, 26 and 36 are far away from continental margins, it is assumed that the vertical and horizontal advection input into and out of the box were relatively small and were ignored. It is noted that ST 1 and 4 are highly influenced by the fractional continental air mass due to their proximity to the landmass, as well as high productivity and advective transport of water masses. Therefore, this study did not attempt to estimate atmospheric depositional fluxes for those two stations. The mass balance of total ^{210}Pb for a parcel of 500 m layer water from air-sea interface can thus be written as follows:

$$\lambda_{Pb} I_{Ra} + I_A^0 = \lambda_{Pb} I_{Pb}^T + \psi_c^0 I_{Pb}^T \quad (4.2)$$

where λ_{Pb} is the decay constant of ^{210}Pb (0.03136 yr^{-1}), $I_{Ra} = ^{226}\text{Ra}$ inventory (dpm m^{-2}) in the 500 m layer, I_{Pb}^T is the total (dissolved + particulate) ^{210}Pb inventory measured in dpm m^{-2} ; and ψ_c^0 is the first-order removal rate constant from the 500 m layer (yr^{-1}).

From equation (4.2), the residence time ($\tau_c = 1/\psi_c^0$) for total ^{210}Pb can be calculated as follows:

$$\tau_c = 1/\psi_c^0 = I_{Pb}^T / [\lambda_{Pb} (I_{Ra} + (I_A^0/\lambda_{Pb}) - I_{Pb}^T)] \quad (4.3)$$

Residence time of ^{210}Pb in the water column requires data on its atmospheric depositional flux. Using the atmospheric depositional flux data (Table 4.1) obtained using equation 4.1, the calculated residence time of ^{210}Pb in the upper 500 m for ST 4, 1, 11, 18, 26 and 36 are 11.8 ± 0.4 , 14.4 ± 0.5 , 64 ± 4 , 110 ± 6 , 486 ± 141 , and 66 ± 5 y, respectively (Note that the + and – errors calculated using equation 4.3 is asymmetric and the upper value is given here as well as in other places in this article). The sensitivity of the atmospheric depositional flux on the model-derived

residence time of ^{210}Pb is illustrated in Figure 4.3. For residence times of > 20 years, the variations in atmospheric depositional fluxes are relatively small whereas the ^{210}Pb depositional flux estimates drastically increase for residence times of < 20 years (Figure 4.3).

Table 4.1
Activity of ^{210}Pb in aerosols and calculated flux for the six super stations of the EPZT

Aerosols Start-end average			EPZT Water Sample Locations			^{210}Pb Aerosols	^{210}Pb flux
ST #	lat.	long.	ST #	lat.	long.	dpm 100m^{-3}	dpm $\text{cm}^{-2}\text{y}^{-1}$
1 E. to 4	-12.0253	-78.4261	EPZT-4	-12.0448	-77.8181	1.97 ± 0.07	0.62 ± 0.02
1 W. toward 11	-11.9993	-84.0007	EPZT-1	-12.0054	-79.1955	0.99 ± 0.04	0.31 ± 0.012
11 W. toward 18	-13.0003	-96.5008	EPZT-11	-11.9999	-94.0001	0.26 ± 0.01	0.082 ± 0.003
W. toward 18	-15.5001	-106.5955				0.29 ± 0.01	0.090 ± 0.004
18 W. toward 26	-14.8766	-113.8750	EPZT-18	-14.9835	-112.7504	0.23 ± 0.01	0.073 ± 0.003
W. toward 26	-13.2728	-122.5008				1.02 ± 0.04	0.323 ± 0.012
26 W. toward 36	-11.6352	-131.5002	EPZT-26	-11.6706	-127.9998	0.24 ± 0.01	0.076 ± 0.003
W. toward 36	-11.1682	-141.4758	EPZT-36	-10.5002	-152.0004	0.51 ± 0.02	0.162 ± 0.007

From the inventory of ^{210}Pb in the upper 500 m and assuming a residence time of ^{210}Pb in the upper 500 m, the atmospheric depositional flux can be estimated. If all the atmospheric depositional flux in the stations is derived from oceanic air mass, then, the ^{210}Pb flux is expected to be much lower when compared to continental-derived air masses. The atmospheric flux can be calculated using the equation:

$$(I_A^0) = \lambda_{Pb} (I_{Pb}^T - I_{Ra}) + I_{Pb}^T / \tau_s \quad (4.4)$$

Note that the atmospheric depositional flux depends on the residence time of ^{210}Pb in the upper 500 m. Using the atmospheric depositional fluxes calculated using aerosol ^{210}Pb data (corresponding atmospheric depositional fluxes of 1.27 ± 0.04 dpm $\text{cm}^{-2} \text{y}^{-1}$ (n=1), for ST 1, 0.64 ± 0.02 dpm $\text{cm}^{-2} \text{y}^{-1}$ (n=1) for ST 11, 0.19 ± 0.02 dpm $\text{cm}^{-2} \text{y}^{-1}$ (n=2) for ST 18, 0.41 ± 0.25

dpm cm⁻² y⁻¹ (n=2) for ST 26 and 0.31±0.01 dpm cm⁻² y⁻¹ (n=1) for ST 36), the residence times calculated for ST 1, 11, 18, 26 and 36 are 3.6±0.1, 7.8±0.2, 51±7, 19+47±8, 26±1 years, respectively. The calculated atmospheric depositional flux from east to west of the cruise transect indicates a decreasing trend (Figure 2.1). Earlier study by Tsunogai and Nozaki (1973) indicated a latitudinal variation of ²¹⁰Pb in Pacific surface water which was well correlated with the geographical distribution of arid land area.

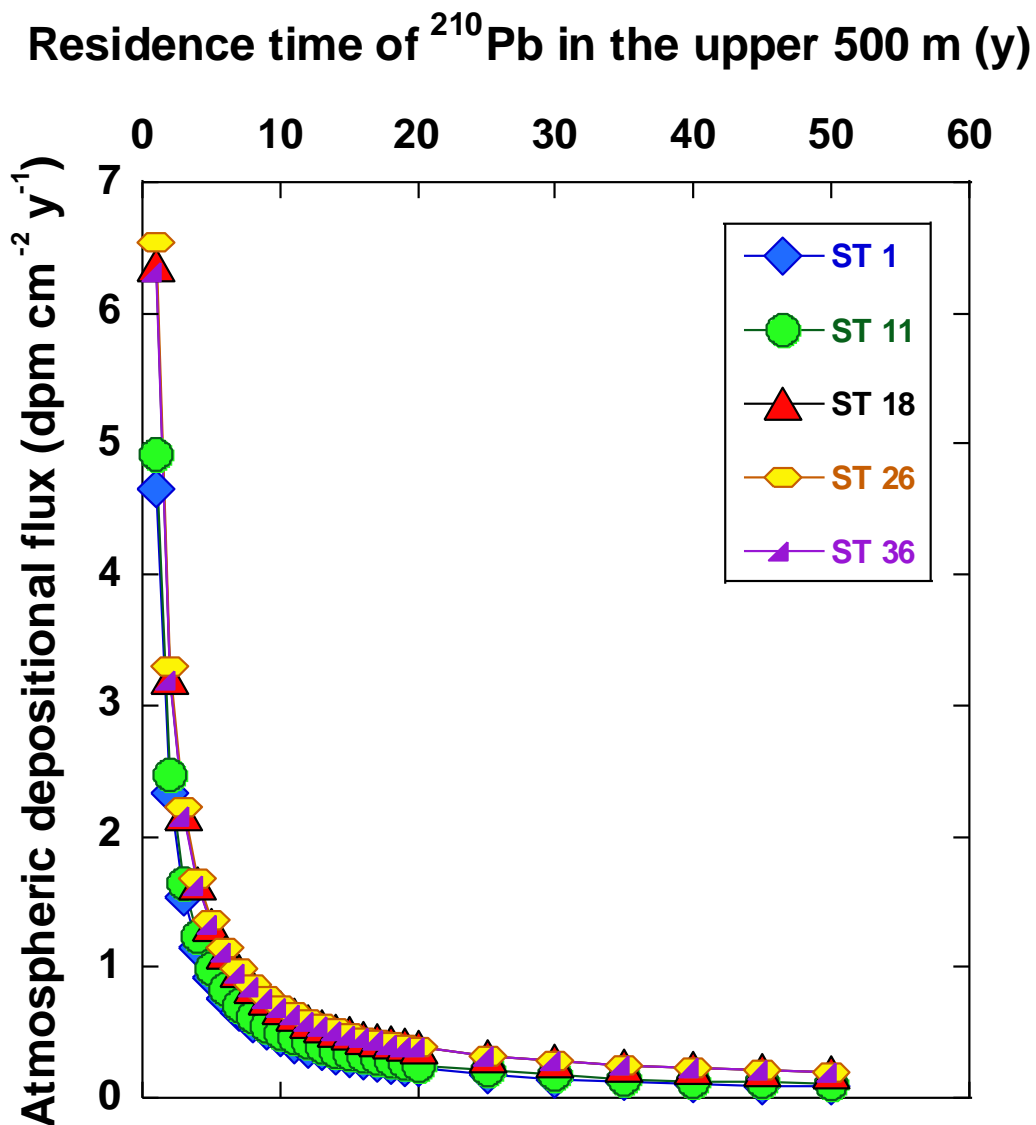


Figure 4.3. Model-derived ²¹⁰Pb atmospheric depositional flux using Equation 4.3 for various residence times (1 to 50 y) of ²¹⁰Pb in the upper 500 m.

4.3 Variations of Fraction of Particulate ^{210}Po and ^{210}Pb Activities at Key Interfaces

The relative distribution of ^{210}Po and ^{210}Pb between particulate and dissolved phases is related to the concentration and composition of particulate matter. Specifically, the lower fraction of particulate ^{210}Po and ^{210}Pb activities at biotic interfaces is attributed to higher biological activity. The OMZ (ST 11) and the most oligotrophic station (ST 36) have the lowest fractional activities (average for the whole water column) of particulate ^{210}Po and ^{210}Pb , namely 10.6% in ST 11 and 13.8% in ST 36 for ^{210}Po and 4.8% in ST 11 and 5.3% in ST 36 for ^{210}Pb . The inventory of nutrients in the mixed layer are the lowest in ST 36 (73.0, 38.0 and 14.1 mmol m^{-2} of SiO_4^{2-} , NO_3^- and PO_4^{3-} , respectively, (Table 3.7) and therefore biogenic particulate concentration is expected to be much lower due to lower biological activity. Furthermore, the lower biogenic particle concentration leads to lower fraction of particulate activity (Figure 4.4). Many of the biogenic organic particulate matter likely will undergo degradation in the oxygen minimum zone and therefore, the particulate matter below OMZ is expected to have lower particulate ^{210}Po and ^{210}Pb activity. At the volcanic interface, the fraction of particulate ^{210}Po and ^{210}Pb activity is the highest (Table 4.2). It has been documented that the dissolved Fe from the EPR vent site, ST 18 escapes from scavenging over the travel distance of up to ~4,000 - 6,000 km (Fitzsimmons et al., 2014, 2017) and one of the speculations made to interpret such an observation is the binding of Fe with organic ligands that protects the Fe from precipitation/scavenging. Such a complexation of Fe (and possibly Mn) with organic ligand could form sites for sorption of ^{210}Po and ^{210}Pb , as is evidenced by highest particulate activity at 2300 m ($^{210}\text{Po}_p$) and 2400 m in ST 18 ($^{210}\text{Pb}_p$, Table 3.5 and Figure 4.4). Fitzsimmons et al. (2014) suggested that dissolved Fe could reach the biologically euphotic zone and this study's inventory calculation indicates that particulate Fe in the upper 60 m of the EPR station is the

highest among the four deep-water stations (27.7 $\mu\text{mol m}^{-2}$ in ST 18 compared to 1.12 – 6.20 $\mu\text{mol m}^{-2}$ in stations 11, 26 and 36 (Table 4.2).

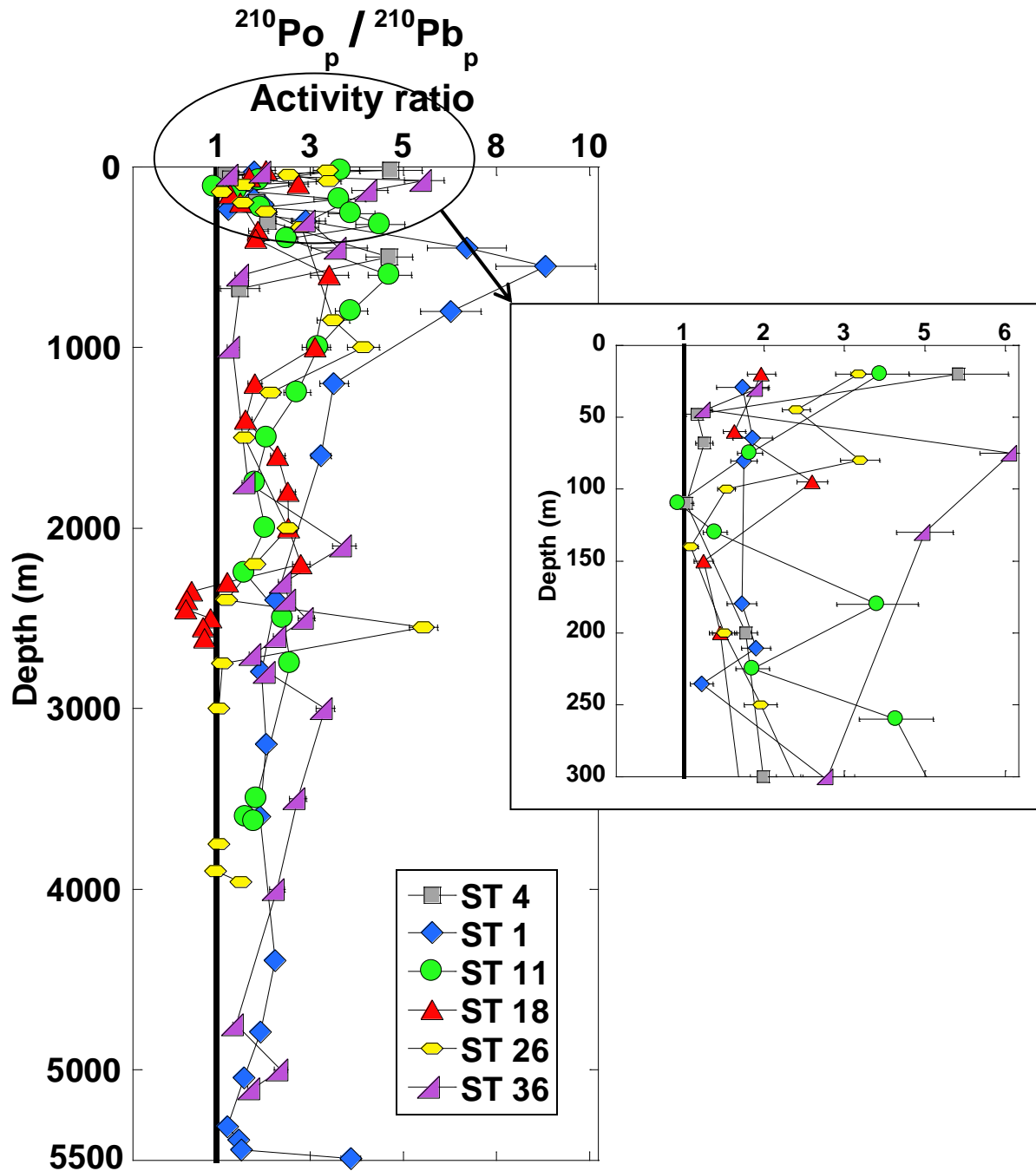


Figure 4.4. Vertical profiles particulate ($\geq 1 \mu\text{m}$) $(^{210}\text{Po}/^{210}\text{Pb})_T$ activity ratio indicating overall higher ratios in surface waters and decreasing with depth, indicating remineralization of biogenic particulate matter throughout the water column.

Table 4.2

Inventories of particulate and dissolved ^{210}Po , ^{210}Pb and Ra, Al, Mn and Fe at the top 60m of all six super stations at the GEOTRACES EPZT (October -- December 2013).

STN #	$^{210}\text{Po}_p$		$^{210}\text{Po}_d$		$^{210}\text{Po}_T$		$^{210}\text{Po}_p$ %	$^{210}\text{Pb}_p$		$^{210}\text{Pb}_d$		$^{210}\text{Pb}_T$		$^{210}\text{Pb}_p$ %	Al_p	Al_d	Fe_p	Fe_d	Mn_p	Mn_d	
	dpm	m^{-2}	dpm	m^{-2}	dpm	m^{-2}		dpm	m^{-2}	dpm	m^{-2}	dpm	m^{-2}		dpm	m^{-2}	μmol	μmol	μmol	μmol	μmol
**																					
4	385 ± 17	6956 ± 229	7341 ± 230	5.2	157 ± 6	3814 ± 73	3972 ± 73	4.0	39	149	53	56	5	152							
1	404 ± 18	3245 ± 164	3649 ± 165	11.1	184 ± 10	4146 ± 83	4330 ± 84	4.2	98	94	67	13	13	234							
11	710 ± 18	3285 ± 159	3995 ± 160	17.8	221 ± 6	5785 ± 96	6007 ± 96	3.7	3	111	1	5	2	134							
18	982 ± 35	3279 ± 192	4261 ± 195	23.1	483 ± 17	5535 ± 120	6018 ± 121	8.0	6	1168	28	6	4	73							
26	785 ± 19	4085 ± 224	4870 ± 224	16.1	245 ± 6	8349 ± 143	8594 ± 143	2.9	1	241	1	9	1	40							
36	895 ± 21	4364 ± 174	5259 ± 175	17.0	436 ± 8	8184 ± 114	8620 ± 115	5.1	4	136	6	8	1	32							

** = Depth to only 672 meters

Total = ^{210}Po dissolved (<0.45 μm), + Small particulate (0.8-51 μm), + large particulate (>51 μm)

Dissolved metal data obtained from Resing et al., 2015, Particulate metal data obtained for Phoebe Lamb

4.4 Residence Time of ^{210}Po and ^{210}Pb at Key Interfaces and Relationship between Activities and Inventories of ^{210}Po , ^{210}Pb , Nutrients and Trace Elements

4.4.1 Upper 60 m and Mixed Layer

The activities of ^{210}Pb in the upper 3 m in all six super stations vary widely (by a factor of ~3 for dissolved ^{210}Pb and ~2 for dissolved ^{210}Po), with ^{210}Pb activities > ^{210}Po activities. Such variations can be attributed to varying atmospheric input of ^{210}Pb (decreasing atmospheric flux with increasing distance from continent). It is noted that the $^{210}\text{Po}/^{210}\text{Pb}$ AR in bulk precipitation is <0.1 and there are variations in scavenging intensities due to differences in the concentration and composition of particulate matter, as well as possible differences in upwelling. The residence time of ^{210}Po or ^{210}Pb ($\tau_{\text{Po or Pb}}$) is calculated from the simple equation below, assuming that there is no net advective and/or diffusive input into a one-dimensional box.

$$\tau_{\text{Po or Pb}} = \tau_i [R_i / (1 - R_i)] \quad (4.4)$$

where τ_i is the mean-life of ^{210}Po (0.5467 y) or ^{210}Pb (32.18 y) and R_i is activity ratio of $(^{210}\text{Po}/^{210}\text{Pb})_T$ or $(^{210}\text{Pb}_T/^{226}\text{Ra})$.

The mean $(^{210}\text{Po}/^{210}\text{Pb})_{\text{T}}$ AR of 0.7 corresponds to a residence time (τ_{Po}) of 1.2 years for ^{210}Po , which is in general agreement with earlier published results from the Pacific, Atlantic and Indian Oceans (Bacon et al., 1976; Nozaki et al., 1980; Chung and Craig, 1983; Cochran, 1992; Sarin et al., 1999; Hong et al., 2013; Rigaud et al., 2015). The activities of ^{210}Po in the mixed layer are the highest in the most productive waters off of Peru (ST 1 and 4) compared to other stations.

The $^{210}\text{Pb}_{\text{T}}/^{226}\text{Ra}$ activity ratio in the mixed layer that varied between 0.78 and 3.30 with the lowest values found in the most productive waters off of Peru (ST 1 and ST 4) is attributed to intense scavenging (also evidenced by low ^{210}Pb activities) and also is attributed to higher upwelling of ^{210}Pb -deficient deeper water, although higher atmospheric depositional flux is expected at ST 1 and ST 4 which are nearer to the continent (Figure 2.1). A similar lack of excess ^{210}Pb in surface waters from the eastern South Pacific and high southern latitudes have been previously reported (Thomson and Turekian, 1976; Turekian and Nozaki, 1980; Chung, 1981; Chung and Craig, 1983) and was attributed to upwelling and enhanced scavenging associated with high productivity (eastern South Pacific) and low atmospheric flux (high latitude southern oceans). Although standard oceanographic parameters such as conductivity, temperature, and dissolved oxygen remained constant within the mixed layer, the $^{210}\text{Pb}_{\text{T}}/^{226}\text{Ra}$ activity ratios vary as high as a factor of ~ 2 . In the most oligotrophic station (ST 36), the $^{210}\text{Pb}_{\text{T}}/^{226}\text{Ra}$ AR remain relatively constant (within 2σ) in the mixed layer and thus the vertical profiles of $^{210}\text{Pb}_{\text{T}}/^{226}\text{Ra}$ ratios in the mixed layer reflect the biological activity (Figure 3.6). In all the mixed layer samples in the open ocean (ST 11 to 36), the $^{210}\text{Pb}_{\text{T}}/^{226}\text{Ra}$ AR are >1.0 , similar to what was found commonly in other ocean basins (Nozaki et al., 1980; Chung and Craig, 1983; Rigaud et al., 2015).

The inventories of total ^{210}Po ($^{210}\text{Po}_T$) in the upper 60 m ranged between 3.65×10^3 and 7.34×10^3 dpm m^{-2} (factor 2.0 difference) with the highest ^{210}Po inventory in the most productive water (ST-4), as evidenced by the highest nitrate, phosphate and silicate inventories (Figure 3.10). In contrast, the total inventories of total ^{210}Pb ($^{210}\text{Pb}_T$) ranged between 3.97×10^3 and 8.62×10^3 dpm m^{-2} (factor 2.2 difference) with the highest inventory at the most oligotrophic station, and lowest at the most productive waters, although the atmospheric depositional flux is much higher in ST 4 compared to ST 36 due to the distance between coastline and to these two stations. Note that the inventory of ^{226}Ra remained constant in the upper 60 m in all 6 stations ($3.91 \pm 0.24 \times 10^3$ dpm m^{-2} , within 6.1%) in the upper 60 m. The ($^{210}\text{Po}_T / ^{210}\text{Pb}_T$) AR in the mixed layer varied between 0.57 and 0.84 (mean 0.68, $n=5$), except in ST 4 where it was found to be 1.85, again indicating intense remineralization of ^{210}Po in the mixed layer of the most-productive waters off of Peru margin. The ($^{210}\text{Pb}_T / ^{226}\text{Ra}$) AR in the mixed layer varied between 1.02 and 2.35 with the lowest values found in the slope and margins water off of Peru where active scavenging of ^{210}Pb is observed based on the inventory of $^{210}\text{Pb}_T$ (Figure 3.7).

Higher nutrient concentrations in the upper waters, namely the euphotic zone, is anticipated to result in higher biological productivity leading to higher generation and regeneration of particulate organic matter and biogenic elements such as ^{210}Po , and thus a relationship between the inventories of ^{210}Po and nutrients is expected. This is evidenced by the highest observed inventory of dissolved nitrate in the euphotic zone among all six stations, varying between 38 mmol m^{-2} - 654 mmol m^{-2} . Phosphate and silicate have the highest inventory, but oxygen has the lowest inventory value in the Peru shelf (ST 4) as seen in Table 3.7. In the euphotic zone, high biological activity is likely directly linked to the remineralization/recycling of ^{210}Po in the water column. In the upper 60 m, the linkage between

nutrient concentrations and activities of ^{210}Po and ^{210}Pb were assessed using correlation between them. There was a significant inverse correlation between the inventories of total ^{210}Po and nutrients (SiO_4 : $R = -0.85$, $n = 5$; NO_3^- : $R = -0.94$ and PO_4 : $R = -0.95$, $n = 5$, (Figure 4.5). It has been shown that there is a correlation between Chlorophyll a (used in oxygenic photosynthesis) and the activity of ^{210}Po at discrete layers (Nozaki et al. 1997). In this study a strong inverse correlation is seen between the inventories of $^{210}\text{Po}_T$ and inventories of nutrients. Higher nutrients in the surface waters promote higher productivity leading to larger removal of ^{210}Po by biogenic particulate matter, which in turn, results in lower inventory of $^{210}\text{Po}_T$ in the mixed layer. Therefore, such inverse relationship between ^{210}Po inventory and nutrients were expected.

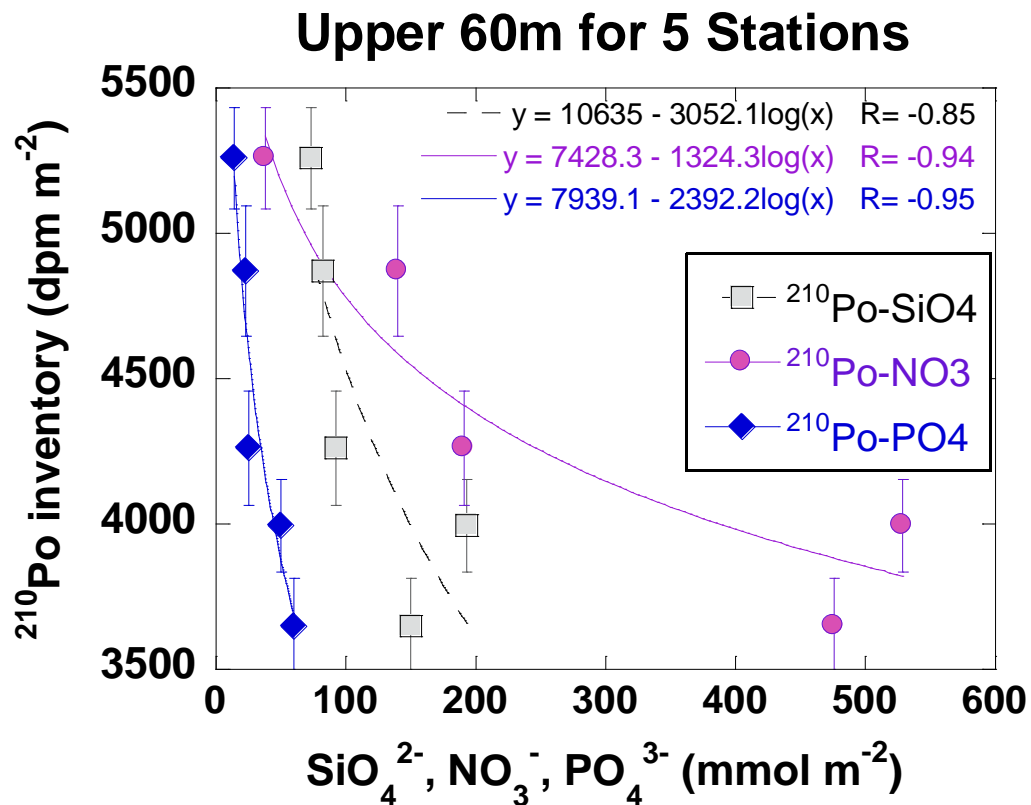


Figure 4.5. Inventory of ^{210}Po vs. inventory of nutrients (SiO_4^{2-} , NO_3^- , PO_4^{3-}) in the upper 60 m (mixed layer)

The correlation between the inventories of total ^{210}Pb and nutrients, in contrast to ^{210}Po , as seen in Figure 4.6, was weaker ($R = -0.89$) compared to the correlations with ^{210}Po ($R = -0.94$). There is also a significant negative correlation ($R = -0.85$) as seen in Figure 4.7 between the inventory of total ^{210}Pb and inventory of particulate Al, but there is weak correlation between inventory of total ^{210}Po and inventory of particulate Al ($R = -0.67$ (Figure 4.7), suggesting that there is much less efficient removal of ^{210}Po by lithogenic matter compared to ^{210}Pb . When the mass flux of sinking particulate matter increases, the removal fluxes of ^{210}Pb is also expected to be higher (Moore and Dymond, 1988).

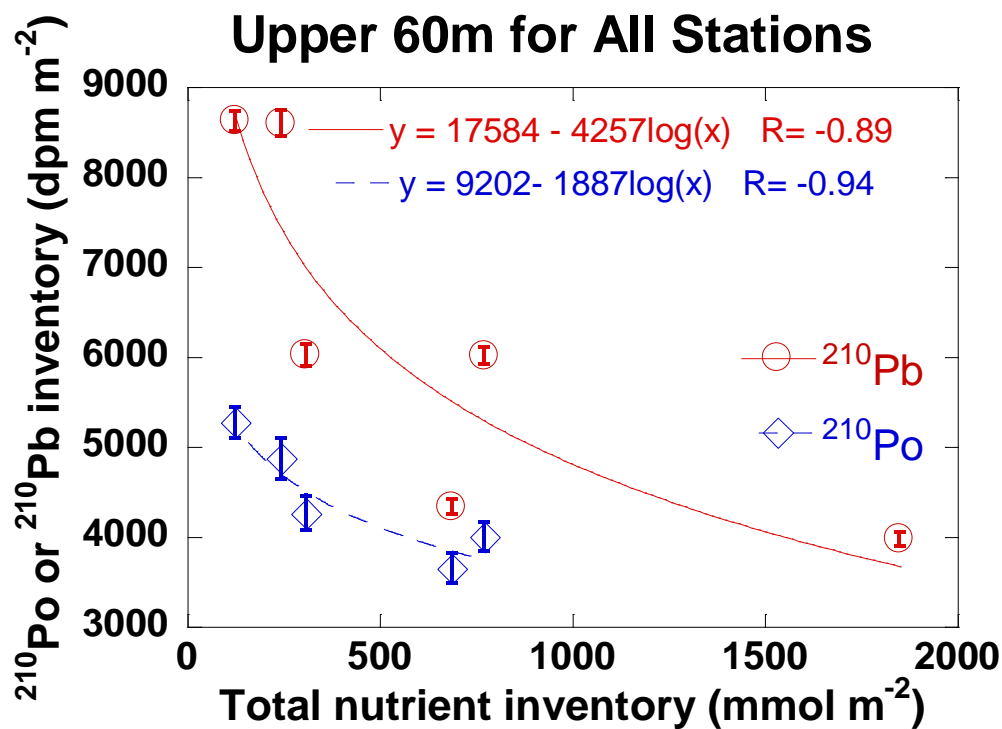


Figure 4.6. Inventory of ^{210}Po or ^{210}Pb vs. total nutrients ($\text{SiO}_4^{2-} + \text{NO}_3^- + \text{PO}_4^{3-}$) inventory in the upper 60 m mixed layer. (^{210}Po inventory for ST 4 is excluded).

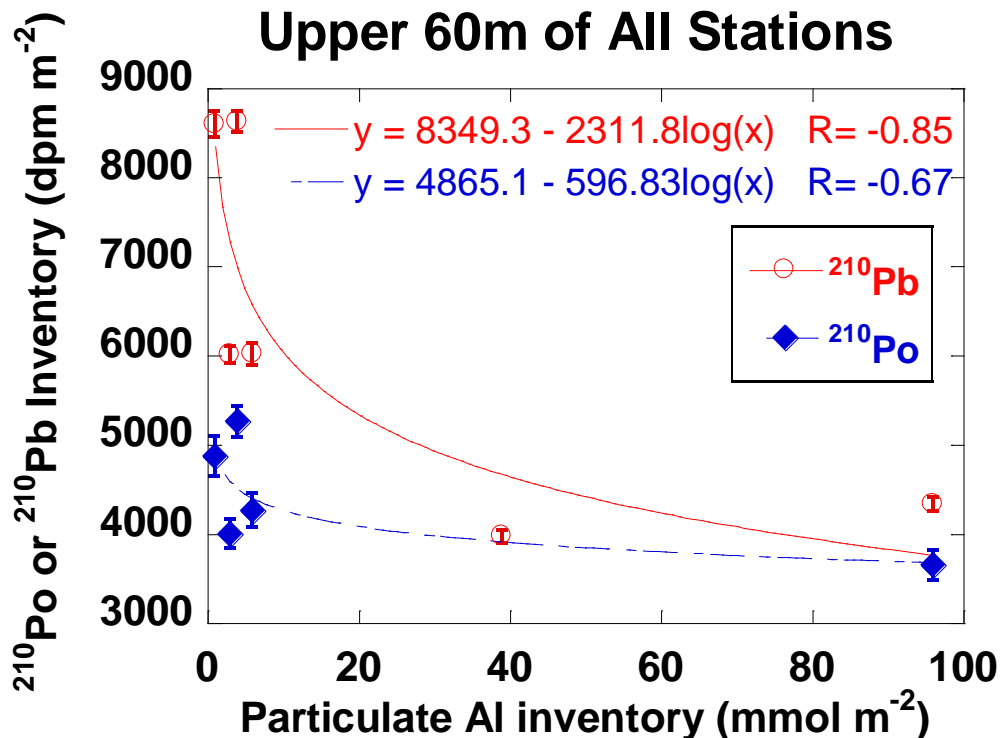


Figure 4.7. Inventory of ^{210}Po or ^{210}Pb vs. particulate Al inventory in the upper 60 m mixed layer.

It was also observed that the highest inventories of particulate Fe and Mn were found in ST 1 and ST 4, coinciding with the lowest inventories of particulate ^{210}Po and ^{210}Pb in the upper 60 m, thereby establishing a possible link between the particulate ^{210}Po , ^{210}Pb activities and abundance of Fe and Mn. Due to high productivity in the continental shelf and margins waters (Table 4.2), the Fe and Mn oxidation-reduction cycling in shelf and slope sediments could result in higher particulate and dissolved Fe and Mn in the water column, which could result in more intense scavenging of ^{210}Po and ^{210}Pb . The importance of oxidation-reduction cycling of Fe and Mn in sediments has been proposed to affect the removal of particle-reactive radionuclides (Todd et al., 1986; Swarzenski et al., 1999). This is the first time in this study that the inventories of particulate Fe and Mn are shown to be directly related to the inventories of particulate ^{210}Po and ^{210}Pb .

4.4.2 Residence Time of ^{210}Po and ^{210}Pb in the Biotic, Sediment-water and Hydrothermal Interfaces (Upper and Bottom 300 m)

The residence time of ^{210}Po calculated using inventories of total ^{210}Po and ^{210}Pb in the upper 300 m, ranged between 1.9 and 8.3 y in four of the six stations (the same approach cannot be made in ST 1 and 4 because the $^{210}\text{Po}/^{210}\text{Pb}$ AR is >1.0) (Table 3.8). The highest $^{210}\text{Po}/^{210}\text{Pb}$ AR value was found in the most productive waters, indicating that the ^{210}Po inventory could be a measure of productivity and the extent of remineralization in the upper 300 m and hence an index of biological activity of the surface ocean (Table 3.8). The $^{210}\text{Pb}_T/^{226}\text{Ra}$ AR is >1.0 in the upper 300 m in all six stations, and results in a more robust residence time calculation requires the precise atmospheric depositional flux of ^{210}Pb and the downward export flux of ^{210}Pb from the upper 300 m. If the global average upwelling rate at mid-ocean depth of about 3 m per year is considered (Toole, 1996), it will take approximately 1,000 y for the Fe and Mn derived from vent water to reach the surface ocean vertically above the vent, assuming that Fe and Mn are insulated from the scavenging, similar to the observation reported in the transport of horizontal distance of ~4,000 - 6,000 km (Fitzsimmons et al. 2014, 2017). In the oligotrophic station there is equilibrium between ^{210}Po and ^{210}Pb (equation 4.4 will yield a residence time of ∞ and thus cannot be calculated). Note that the commonly reported 0.5-0.7 y residence time of ^{210}Po in the surface waters (mixed layer or in the upper 100 m; Bacon et al., 1976; Cochran et al. 1983; Sarin et al., 1999; Hong et al., 2013; Rigaud et al., 2015) is significantly lower than those observed in the upper 300 m due to the limited extent of remineralization in the mixed layer.

The shortest residence time of ^{210}Po (0.7 y) in the bottom 300 m was observed at EPR (ST 18) whereas in the oligotrophic station the residence time is much longer ($^{210}\text{Po}/^{210}\text{Pb}$ AR ~ 1.0 , causing the residence time of ^{210}Po to be >3 years (Table 3.8). The residence time of ^{210}Po in the bottom 300 m at the EPR site is comparable to its residence in the surface water (< 100 m).

Since the $^{210}\text{Po}_T/^{210}\text{Pb}_T$ AR in ST 1, 11 and 36 are >1.0 in the bottom 300 m, the residence time cannot be determined using equation 4.4. The residence time of total ^{210}Po in bottom 300 m of ST 26 is 3.0 ± 0.6 y corresponding to $^{210}\text{Po}_T/^{210}\text{Pb}_T$ AR = 0.84 ± 0.03 . It is likely that the chemistry of the water (dissolved Fe, Mn, etc) in ST 26 could have been influenced by the transport of dissolved/colloidal Fe/Mn from the EPR site which is ~ 1700 km away from ST 26.

In the EPR site, the preferential removal of ^{210}Po is observed at both upper and bottom 300 m and both seem to be influenced by the dissolved/colloidal Mn from the vent fluid discharge. In ST 36, the low biological activity (and hence biogenic particle production rate and particle flux) results in lower scavenging intensity in the upper 300 m and which leads to lower particle flux and lower scavenging intensity in the bottom 300 m. Thus, it seems the scavenging in the upper 300 m of ^{210}Po and ^{210}Pb in ST 18 and ST 36 are coupled to the bottom 300 m.

The $^{210}\text{Pb}_T/^{226}\text{Ra}$ AR in the bottom 300 m varied between 0.36 (ST 1) and 0.93 (ST 36) along the transect, corresponding to a residence time of 18 years (ST 1) to 398 years for the total ^{210}Pb . The lowest residence time (among the four open ocean stations) of 31 years was found in the EPR site, ST 18 and the longest was found in the most-oligotrophic site, ST 36 (Table 3.8 and Table 4.3 on the following page).

It is also possible that the iron sulfide from the vent could serve as a carrier phase for ^{210}Pb , as was shown in the anoxic waters of the Orca Basin, with a residence time of ~ 1 year for ^{210}Pb , and at the Cariaco Trench, of 2 years for ^{210}Pb (Bacon et al., 1980; Todd et al., 1986). It is also likely that the preferential association of ^{210}Po onto refractory biogenic organic particles, which are more refractory to reducing conditions (e.g., reduction of Fe^{+3} to Fe^{+2}) near the vent than MnO_2 oxy-hydroxides could result in longer residence time of particulate phase resulting in travel to farther distances.

Table 4.3
Dissolved & Total Residence Time

		²¹⁰ Po Dissolved Residence time			²¹⁰ Pb Dissolved Residence time		
Station #	GEOTRACE #	Upper 300 m	Lower 300 m	Whole column	Upper 300 m	Lower 300 m	Whole column
4	2300		9.6 ± 8.9				
1	2100		11.0 ± 8.1	28.5 ± 29.9		13.1 ± 0.3	37.0 ± 0.7
11	3600	4.2 ± 0.9	5.3 ± 2.3	269.8 ± 2345.0		29.2 ± 1.2	85.9 ± 2.9
18	8400	1.5 ± 0.2	0.9 ± 0.1			7.6 ± 0.2	101.8 ± 3.8
26	9400	3.4 ± 0.6	2.0 ± 0.3	5.6 ± 1.2		24.9 ± 1.6	47.1 ± 1.2
36	10300	3.9 ± 1.2	21.9 ± 49.5	4.5 ± 0.7		177.8 ± 33.5	142.8 ± 6.2

		²¹⁰ Po Total Residence time			²¹⁰ Pb Total Residence time		
Station #	GEOTRACE #	Upper 300 m	Lower 300 m	Whole column	Upper 300 m	Lower 300 m	Whole column
4	2300		46.5 ± 196.1				
1	2100					18.1 ± 0.4	43.2 ± 0.9
11	3600	7.0 ± 2.2				39.5 ± 1.7	110.0 ± 4.5
18	8400	1.9 ± 0.3	0.7 ± 0.028			31.0 ± 0.7	184.0 ± 10.9
26	9400	4.7 ± 1.1	3.0 ± 0.6	20.1 ± 12.2		41.8 ± 3.5	68.8 ± 2.1
36	10300	8.3 ± 5.0		16.2 ± 7.8		398.2 ± 153.0	196.9 ± 11.2

Total = ²¹⁰Po dissolved (<0.45µm), + Small particulate (0.8-51µm), + large particulate (>51µm)

4.4.3 Vertical Variations in ²¹⁰Po_T/²¹⁰Pb_T Activity Ratios, Depth-normalized Inventories of ²¹⁰Po and ²¹⁰Pb and Residence Time of ²¹⁰Pb in the Whole Water and Implications Deep-water Remineralization of Particulate ²¹⁰Po

The inventories of total ²¹⁰Po and ²¹⁰Pb in the whole water column depend on the water depth and hence normalization to a finite depth is required to assess the variations in scavenging intensity in the whole water column. The 1000 m depth-normalized inventories of total ²¹⁰Po and ²¹⁰Pb (= total inventory in the whole water column × (1000 m/total water depth calculated from Tables 2.1 and 3.9) for all six stations varied between 1.48 × 10⁵ and 1.92 × 10⁵ dpm m⁻² and 1.47 × 10⁵ and 1.98 × 10⁵ dpm m⁻², respectively, with the lowest ²¹⁰Po_T inventory at ST 26 and highest at ST 36 while for ²¹⁰Pb_T, the corresponding stations are ST 1 (lowest) and ST 36

(highest), respectively (Figure 4.8). The 1000 m depth-normalized inventory of ^{226}Ra varied between $1.76 \times 10^5 \text{ dpm m}^{-2}$ (ST 18) and $2.56 \times 10^5 \text{ dpm m}^{-2}$ (ST 1). The lowest ^{226}Ra inventory in the water column may be attributed to RaSO_4 precipitation at and near the hydrothermal vent site. Except at ST 1 and ST 18, the Ra inventories at the other three stations were constant, $(2.27 \pm 0.05) \times 10^5 \text{ dpm m}^{-2}$.

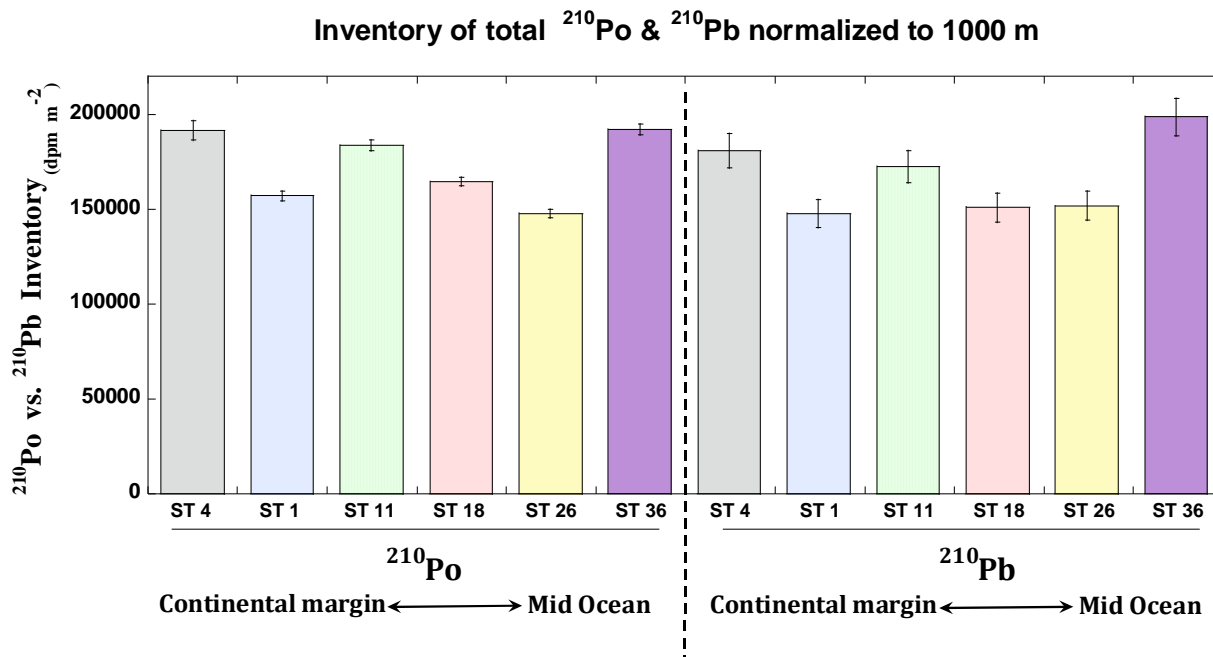


Figure 4.8. Bar diagram of total ^{210}Po and ^{210}Pb inventories in 1,000m-normalized depths of 6 super stations in US GEOTRACES GP16 EPZT.

The $^{210}\text{Po}_T/^{210}\text{Pb}_T$ AR for the whole water column (= inventory of $^{210}\text{Po}_T/^{210}\text{Pb}_T$) ranged between 0.97 ± 0.02 and 1.09 ± 0.02 , with the highest value found at ST 18, indicating active recycling of ^{210}Po compared to ^{210}Pb in the water column (Table 3.9). Deficiency of ^{210}Po at discrete layers in deep waters have been attributed to efficient uptake by cyanobacteria and successive transfer to higher trophic levels rather than downward transport by sinking particulate matter (e.g. $^{210}\text{Po}/^{210}\text{Pb}$ AR at 3,500 m: 0.64-0.70 (n=3); 0.37 at 2,500 m (n=1); 0.69 at 1,400 m (n=1) in South China Sea, Chung and Wu, 2005; $^{210}\text{Po}/^{210}\text{Pb}$ AR of 0.86 and 0.68 at 2,038 m and

1913 m, respectively in East China and Philippine seas (Nozaki et al., 1990; Kim, 2001). It is suggested that all these earlier observations of excesses/deficiencies of ^{210}Po were reported for discrete layers, but did not take into account variable extent of the redistribution of ^{210}Po and ^{210}Pb from remineralization in the whole water column. Observations in this study show that there is < 10% deficiency of ^{210}Po in the whole water column, but gross disequilibrium between ^{210}Po and ^{210}Pb (32% ^{210}Po excess at 500-1000 m, ST 11; 35% ^{210}Po excess at 1000-1500 m, ST 18; and 21% ^{210}Po deficiency at 3500-4000 m, ST 26; all these three 500 m layers are at much above sediment-water interface; Tables 3.5 and 4.4) is due to redistribution of these nuclides in the vertical water column due to deep-water remineralization of biogenic particulate matter and preferential scavenging of ^{210}Po and ^{210}Pb at deep ocean.

The ratio of the inventories of $^{210}\text{Pb}_T$ and ^{226}Ra for the whole water column, $^{210}\text{Pb}_T/^{226}\text{Ra}$, varied between 0.57 ± 0.01 to 0.86 ± 0.01 , with the lowest ratio at ST 1 (Table 3.9). The $^{210}\text{Pb}_T/^{226}\text{Ra}$ AR is >1.0 for the shallow water station (ST 4) and hence no estimate on residence time is possible. The residence time of total ^{210}Pb in the five open-ocean stations (ST 1, 11, 18, 26 and 36) (calculated using equation 4.4) varied between 43 and 197 years (Tables 3.9 and 4.3). This range of values is comparable to a range of values reported for the deep water (no residence time seems available for the whole water column in literature) in the Atlantic, Pacific and Indian Ocean of 30 and 150 years (Craig et al., 1973; Bacon et al., 1976; Nozaki and Tsunogai, 1976; Nozaki et al., 1980; Cochran et al., 1983; Rigaud et al., 2015). The residence time of total ^{210}Pb in the Peru margin water column of 43 ± 1 years is higher than a range of values reported in the continental margin waters (depths 1,000-1,500 m) in the Gulf of Mexico of 3.2-4.4 years and such large difference was attributed to higher suspended particle concentration and particle flux (Baskaran and Santschi, 2002). Significant concentration gradients of ^{210}Pb along shelf-slope

gradients have been reported earlier in the Middle Atlantic Bight (Bacon et al., 1988). Furthermore, boundary scavenging is more important in areas near the continental margins while in open-ocean, in situ scavenging is likely the major removal process (Chung and Craig, 1983).

4.5 $^{210}\text{Po}/^{210}\text{Pb}$ Activity Ratios in 500 m Thick Layers in Deeper Waters to Evaluate Extent of Remineralization and Preferential Removal of ^{210}Po by Particulate Matter

It is well known that ^{210}Po is more particle-reactive than ^{210}Pb in the marine system ($K_d^{210}\text{Po} > K_d^{210}\text{Pb}$; K_d = specific activity of ^{210}Pb in particles (dpm g^{-1}) / activity of ^{210}Pb in the dissolved phase, dpm cm^{-3}) resulting in a longer residence time of ^{210}Pb (~2.5 years in the mixed layer) compared to ^{210}Po (0.5 - 1.2 years in the mixed layer) (Bacon et al., 1976; Cochran, 1992; Sarin et al., 1999; Hong et al., 2013). If the residence time of ^{210}Po at depths > 500 m is ≥ 2 years, then, it is expected that the $^{210}\text{Po}_T/^{210}\text{Pb}_T$ AR will be ~ 1.0 [$(^{210}\text{Po}/^{210}\text{Pb})_T$ AR at any time 't' = $(1 - \exp(-\lambda t))$ where 't' is the time elapsed since ^{210}Po is quantitatively stripped, and in-growth takes place from the decay of ^{210}Pb ; λ is the decay constant of ^{210}Po], because ^{210}Po and ^{210}Pb will reach secular equilibrium. However, if remineralization of biogenic particulate matter derived from the upper 300 m with $(^{210}\text{Po}/^{210}\text{Pb})_p$ activity ratios > 1.0 takes place at depths > 500 m in less than 2 years prior to field sampling, then, the $(^{210}\text{Po}/^{210}\text{Pb})_T$ AR is anticipated to be > 1.0 . In contrast, if there is active preferential removal of ^{210}Po by suspended and/or sinking particulate matter at depths > 500 m in less than last 2 years, then secular equilibrium between ^{210}Po and ^{210}Pb at depths below 500 m is not expected, with $(^{210}\text{Po}/^{210}\text{Pb})_T < 1.0$. Although slight disequilibrium between total ^{210}Po and ^{210}Pb in deep ocean waters (> 500 m) have been reported previously, no estimate on the residence time of ^{210}Po in deep waters has been attempted. Since the residence time of ^{210}Pb in deep-ocean is much longer than 2 years (Craig et al., 1973; Bacon et al., 1976; Nozaki and Tsunogai, 1976; Cochran et al., 1983; Rigaud et al.,

2015) there is no additional possible inputs of ^{210}Pb to the deep ocean waters (ST 11, 18, 26 and 36) in open ocean (farther from the continental margins).

In order to assess if there is preferential removal of ^{210}Po from the water column (leading to $(^{210}\text{Po}/^{210}\text{Pb})_{\text{T}} \text{ AR} < 1.0$) or more remineralization contribution of particulate ^{210}Po relative to ^{210}Pb , leading to $(^{210}\text{Po}/^{210}\text{Pb})_{\text{T}} \text{ AR} > 1.0$); this study evaluates how $(^{210}\text{Po}/^{210}\text{Pb})_{\text{T}}$ and $^{210}\text{Pb}_{\text{T}}/^{226}\text{Ra}$ AR vary in each of the 500 m layer in the water column. As discussed before, the penetration depth of atmospherically-delivered ^{210}Pb is ~ 500 m (Bacon et al., 1976) and hence we have chosen 500 m intervals. Furthermore, it is widely accepted that the biological activity below 500 m from ocean surface is negligibly small.

The ratio of the inventory of $^{210}\text{Po}_{\text{T}}$ and $^{210}\text{Pb}_{\text{T}}$ in each of the 500 m layer is given in Table 4.4 and the corresponding values for $^{210}\text{Pb}_{\text{T}}/^{226}\text{Ra}$ are given in Table 4.5. In 27 of the total 42 layers, the $^{210}\text{Po}/^{210}\text{Pb}$ ratios are either > 1.05 ($n=17$, excluding the upper 500 m, $n=14$) or less than 0.95 ($n=10$, excluding the upper 500 m, $n=8$) leaving 36 % of the total ($n = 15$) with ratios ranging between 0.95 and 1.05 (Table 4.4). The largest disequilibrium (35% excess ^{210}Po over ^{210}Pb) is found in the 1000-1500 m layer of the EPR site (ST 18) this is attributed to higher concentrations of dissolved Mn or colloidal particles of MnO_2 which could preferentially scavenge ^{210}Po from the water column (Kadko, 1987) which is also supported by the highest particulate Fe and Mn inventory at ST 18 as seen in Table 3.7 (Fitzsimmons et al., 2014). The particulate Mn inventory in the upper 300 m is the highest in ST 18 compared to other stations and hence the particulate Mn and scavenging of ^{210}Po at ST 18 is likely related. Note that there is only 9% excess ^{210}Po over ^{210}Pb for the whole water column at the EPR site (Table 3.9). The largest deficiency of ^{210}Po (21%) over ^{210}Pb was found at 3,000-3,500 m in ST 26, but the deficiency is only 3% for the whole water column (Table 3.9).

Table 4.4
 $^{210}\text{Po}_T/^{210}\text{Pb}_T$ activity ratios of inventories in 500m intervals of the GEOTRACES EPZT

Depth (m)	$^{210}\text{Po}_T/^{210}\text{Pb}_T$ AR					
	ST 4	ST 1	ST 11	ST 18	ST 26	ST 36
0-500	1.07 ± 0.29	1.11 ± 0.16	1.10 ± 0.03	0.89 ± 0.03	0.93 ± 0.03	0.96 ± 0.03
500-1000		0.98 ± 0.06	1.32 ± 0.05	1.18 ± 0.06	1.05 ± 0.07	0.95 ± 0.05
1000-1500		1.03 ± 0.06	0.99 ± 0.05	1.35 ± 0.04	1.02 ± 0.04	0.94 ± 0.04
1500-2000		1.10 ± 0.06	1.00 ± 0.04	1.15 ± 0.04	1.17 ± 0.04	0.87 ± 0.03
2000-2500		1.08 ± 0.06	1.02 ± 0.04	0.91 ± 0.03	1.04 ± 0.05	0.88 ± 0.04
2500-3000		1.03 ± 0.06	1.11 ± 0.04		0.97 ± 0.03	0.97 ± 0.03
3000-3500		1.18 ± 0.06	1.08 ± 0.07		0.79 ± 0.04	0.94 ± 0.05
3500-4000		1.00 ± 0.06			0.84 ± 0.06	0.99 ± 0.06
4000-4500		0.94 ± 0.05				1.06 ± 0.06
4500-5000		1.07 ± 0.06				1.06 ± 0.08
5000-5500		1.17 ± 0.05				

Table 4.5
 $^{210}\text{Pb}_T/^{226}\text{Ra}$ activity ratios (AR) of inventories and residence times (RT) of ^{210}Pb in 500m intervals at all 6 super stations at EPZT GEOTRACES cruise transect

Depth (m)	$^{210}\text{Pb}_T/^{226}\text{Ra}$ AR									
	ST 1		ST 11		ST 18		ST 26		ST 36	
	AR	RT(y)	AR	RT(y)	AR	RT(y)	AR	RT(y)	AR	RT(y)
500-1000*	0.87 ± 0.03	223 ± 77	0.83 ± 0.02	153 ± 24	0.92 ± 0.03	385 ± 243	1.05 ± 0.03	< 0	0.98 ± 0.02	>600
1000-1500	0.77 ± 0.02	106 ± 15	0.92 ± 0.02	367 ± 146	0.84 ± 0.02	173 ± 28	0.96 ± 0.02	>600	0.93 ± 0.02	447 ± 209
1500-2000	0.72 ± 0.02	82 ± 8	0.93 ± 0.02	403 ± 186	0.89 ± 0.02	264 ± 74	0.96 ± 0.02	>600	0.87 ± 0.02	213 ± 42
2000-2500	0.73 ± 0.02	87 ± 10	0.89 ± 0.02	252 ± 72	0.62 ± 0.01	54 ± 2	0.50 ± 0.01	32 ± 2	0.81 ± 0.02	137 ± 22
2500-3000	0.76 ± 0.03	100 ± 17	0.65 ± 0.02	59 ± 5			0.30 ± 0.01	14 ± 0	0.69 ± 0.01	71 ± 4
3000-3500	0.59 ± 0.02	46 ± 4	0.57 ± 0.02	43 ± 5			0.54 ± 0.02	38 ± 3	0.78 ± 0.02	116 ± 19
3500-4000	0.45 ± 0.02	26 ± 2					0.56 ± 0.01	41 ± 2	0.82 ± 0.02	150 ± 26
4000-4500	0.41 ± 0.01	22 ± 1							0.85 ± 0.02	179 ± 40
4500-5000	0.29 ± 0.01	13 ± 1							0.87 ± 0.04	214 ± 97
5000-5500	0.33 ± 0.01	16 ± 1								

* 0-500 (m) not shown for all stations - activity ratio (AR) > 1.0, therefore residence time (RT) would be negative value.

The $^{210}\text{Po}/^{210}\text{Pb}$ AR of < 0.95 infers preferential removal of ^{210}Po from the water column, which occurs throughout the water column and a ratio of >1.05 leads to addition of ^{210}Po from the remineralization of particulate ^{210}Po . More in-depth analysis of biogenic trace metals (both in particulate and dissolved phases) at different layers will aid in obtaining insights on the effect of remineralization and active removal of biogenic elements in the water column.

Unlike the $^{210}\text{Po}/^{210}\text{Pb}$ activity ratio, there is ubiquitous disequilibrium between ^{210}Pb and ^{226}Ra in 500 m layers of the whole water column, with values ranging between 0.29 at 4500-5000 m in ST 1 to 0.98 at 500-1000 m at ST 36 (except 1.05 at 500-1000 m in ST 26 as seen in Table 4.5). In 35 out of 36 of the 500 m thick layers below 500 m depth, the $^{210}\text{Pb}/^{226}\text{Ra}$ AR is < 1.0 (Table 4.5). The residence time of ^{210}Pb varies at different layers in a vertical profile. For example, the residence time generally decreases with depth in ST 1. In the upper 2500 m in ST 11, the residence time of ^{210}Pb varied between 153 to 403 years while the residence time is lower below 2500 m. In ST 26, the residence time in the upper 2000 m is > 600 years, much longer than the residence time below 2000 m as well as for the whole water column. Overall, the residence time of ^{210}Pb at each layer is larger in ST 36, as expected, due to lower particle production rate and fluxes resulting in slower scavenging rates.

4.6 Vertical Variations of Fractionation Factor for ^{210}Po and ^{210}Pb

The fractionation factor ($F_{\text{Po/Pb}}$) could be an important parameter to characterize biotic versus abiotic oceanic particles (Hong et al., 1999). The fractionation factor is defined as the ratio of the distribution coefficient (K_d) of ^{210}Po (K_d^{Po}) to that of ^{210}Pb (K_d^{Pb}).

$$K_d^{\text{Po}} = [\text{Po}_p/\text{Po}_d]/C_p$$

$$K_d^{\text{Pb}} = [\text{Pb}_p/\text{Pb}_d]/C_p$$

$$F_{\text{Po/Pb}} = K_d^{\text{Po}}/K_d^{\text{Pb}}$$

where C_p is the suspended particulate matter concentration, Po_d and Pb_d are the concentrations of dissolved ^{210}Po and ^{210}Pb , respectively and Po_p and Pb_p are the concentrations of particulate ^{210}Po and ^{210}Pb , respectively. The calculated values of $F_{Po/Pb}$ are listed and are plotted in Figure 4.9. The fractionation factors in the upper 60 m varied between 2.0 and 2.7, 3.1 and 4.1, 5.0 and 11.8, and 3.6 and 4.8 in ST 1, 18, 26 and 36, respectively with the highest value of 11.8 in ST 26 followed by 9.7 in ST 11. The large variation is likely due to differences in concentrations and composition of the suspended particulate matter (SPM). High fractionation factors, $F_{Po/Pb} \gg 1$ indicate the preferential uptake of ^{210}Po by phytoplankton relative to ^{210}Pb which are removed by inorganic particles (Shannon et al., 1970). Lowest $F_{Po/Pb}$ values are generally found near sediment-water interface zone where most of the particles are inorganic/lithogenic since most of the biogenic particles are likely regenerated before reaching the sediment-water interface (Figure 4.9). The K_d^{Po} values in the euphotic zone in each station is much higher due to more efficient recycling compared to ^{210}Pb (Wei and Murray, 1994; Su et al, 2017). Overall, this range of values is comparable to the fractionation factor calculated based on the inventories of ^{210}Po and ^{210}Pb over a depth of 600 m of 1.5 and 10.5 at the Bermuda time-series study sites (BATS, Hong et al., 2013) in the Atlantic.

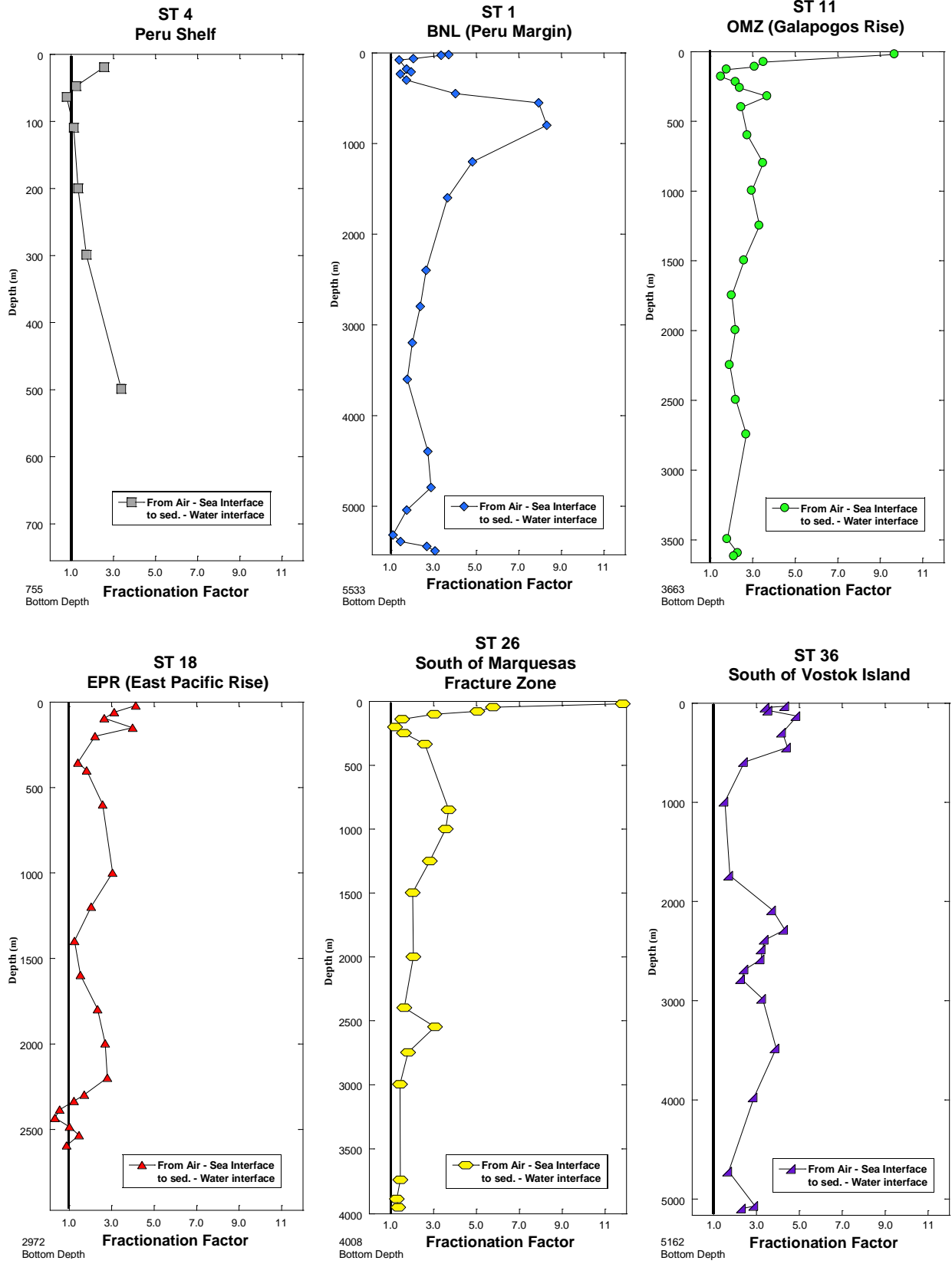


Figure 4.9. Fractionation Factor for all 6 stations to bottom depth.

4.7 Export Fluxes Macro- and Micro-nutrient Elements

If the residence time of ^{210}Po and ^{210}Pb is longer than two years in the upper or surface waters (mixed layer and euphotic zone), then, the $^{210}\text{Po}_T/^{210}\text{Pb}_T$ AR in the upper or surface waters is expected to be ~ 1.0 . However, the shorter residence time and differences in affinity of Po and Pb onto biogenic particulate matter in the upper water results in deficiency of ^{210}Po in the water column. Using the disequilibrium between ^{210}Po and ^{210}Pb one can estimate removal flux of ^{210}Po (F_{Po}) from the measured metal / ^{210}Po ratio in the particulate matter (ideally sinking particulate matter); although the concentrations of ^{210}Po and most metals in large particulate matter is very low, mostly $< 5\%$ in the suspended particulate matter (1-51 μm). Under steady-state conditions, ignoring the atmospheric deposition of ^{210}Po and advective and diffusive processes, export flux of ^{210}Po (F_{Po}) with a depth of 'h' from the surface ocean can be calculated by:

$$\begin{aligned} F_{Po} &= \int_{z=0}^{z=h} P_{Po} dz \\ &= \int_{z=0}^{z=h} \lambda_{Po} (A_{Pb}^t - A_{Po}^d - A_{Po}^p) dz \\ &= \lambda_{Po} \int_{z=0}^{z=h} (A_{Pb}^t - A_{Po}^d - A_{Po}^p) dz \end{aligned}$$

The export fluxes of metal 'M' can be calculated as follows:

$$F_M = F_{Po} \left(\frac{M_i^p}{A_{Po}^p} \right)$$

where A_{Po}^d and A_{Po}^p are the activities of dissolved, particulate ^{210}Po , respectively; A_{Pb}^t is total (particulate + dissolved) ^{210}Pb ; λ_{Po} is decay constant of ^{210}Po (1.83 a^{-1}); P_{Po} represents export flux of particulate ^{210}Po . Using ^{210}Pb as a tracer, one can calculate export fluxes of particulate ^{210}Pb and metal can be calculated as follows:

$$\begin{aligned}
F_{Pb} &= \int_{z=0}^{z=h} P_{Pb} dz \\
&= \int_{z=0}^{z=h} \lambda_{Pb} (I_{Pb}^t + A_{Ra}^t - A_{Pb}^d - A_{Pb}^p) dz \\
&= \lambda_{Pb} \int_{z=0}^{z=h} (A_{Pb}^t - A_{Po}^d - A_{Po}^p) dz \\
F_M &= F_{Pb} \left(\frac{M_i^p}{A_{Po}^p} \right)
\end{aligned}$$

where M_{pi} is concentration of metal 'i' in particulate phase, F_{Pb} is export flux of ^{210}Pb , A_{Ra}^t is total ^{226}Ra activity (particulate ^{226}Ra is assumed to be negligible and hence dissolved ^{226}Ra used in all calculations); A_{Pb}^d and A_{Pb}^p are the activities of dissolved, particulate ^{210}Pb , respectively; λ_{Pb} is decay constant of ^{210}Pb . Trace metal data was obtained from the GEOTRACES database. In principle, one can calculate the export fluxes of biogenic (P, N, Si, Fe, Ba, Sr, Cu, Zn, etc) as well as lithogenic elements (Al, Ti, Th) elements and these results can be compared to other radionuclides, such ^{234}Th in place of ^{210}Po or ^{210}Pb . Export flux values for a suite of elements from the mixed layer, upper 100 m and 500 m are shown in Table 4.6 (flux values are positive values highlighted in blue color) . Future studies with ^{234}Th and results compared from sediment traps can be compared to the values using the ^{210}Po .

Table 4.6
Export Fluxes at 100 and 500 meter for all 6 EPZT Stations

	ST 4	ST 1	ST 11	ST 18	ST 26	ST 36
²¹⁰ Po	<i>Upper 100</i>					
^F Po	-13890.6 ± 761.9	-390.6 ± 357.1	13920.7 ± 427.6	9084.8 ± 423.1	18892.3 ± 614.6	11667.2 ± 521.0
<i>TM</i>						
Al	-9183.0 ± 3096.3	-200.7 ± 198.8	974.5 ± 605.6	579.5 ± 275.3	nd ± nd	nd ± nd
Ba	-411.8 ± 138.5	-20.8 ± 20.6	692.5 ± 392.1	93.0 ± 40.2	nd ± nd	103.3 ± 22.6
Cd	-16.9 ± 5.7	-0.4 ± 0.4	25.2 ± 14.3	0.9 ± 0.4	nd ± nd	1.6 ± 0.4
Co	-6.2 ± 2.1	-0.1 ± 0.1	10.4 ± 5.9	0.7 ± 0.3	nd ± nd	0.5 ± 0.2
Cr	nd ± nd	nd ± nd	nd ± nd	nd ± nd	nd ± nd	nd ± nd
Cu	-179.0 ± 60.6	-7.1 ± 7.0	69.6 ± 40.1	20.2 ± 9.4	nd ± nd	8.5 ± 2.6
Fe	-16551.0 ± 5575.2	-249.8 ± 247.3	542.1 ± 309.8	293.1 ± 127.5	nd ± nd	68.7 ± 17.9
Mn	-46.7 ± 15.9	-1.2 ± 1.2	1063.7 ± 601.8	245.8 ± 106.2	nd ± nd	24.2 ± 5.4
Nd	nd ± nd	nd ± nd	nd ± nd	nd ± nd	nd ± nd	nd ± nd
Ni	-188.2 ± 63.4	-6.2 ± 6.1	93.8 ± 53.4	28.1 ± 12.3	nd ± nd	14.2 ± 3.4
P	-53405.8 ± 18030.1	-931.7 ± 923.2	28360.9 ± 16086.7	10420.5 ± 4522.9	nd ± nd	8650.4 ± 1938.9
Pb	-41.91 ± 14.09	-0.18 ± 0.17	2.12 ± 1.20	31.48 ± 13.57	nd ± nd	0.20 ± 0.04
Th	-0.225 ± 0.076	-0.005 ± 0.005	0.016 ± 0.010	0.009 ± 0.004	0.009 ± 0.003	0.002 ± 0.001
Ti	-224.28 ± 75.90	-5.55 ± 5.51	44.78 ± 26.68	112.32 ± 48.43	nd ± nd	5.87 ± 1.72
Y	-4.35 ± 1.46	-0.14 ± 0.14	1.50 ± 0.86	0.31 ± 0.14	nd ± nd	0.13 ± 0.03

Table 4.6 (continued)

	STN 4	STN 1	STN 11	STN 18	STN 26	STN 36
²¹⁰ Po	<i>Upper 500</i>					
^F po	-17906.8 ± 3350.5	-18397.4 ± 1868.6	-18626.9 ± 1719.1	25905.8 ± 2445.2	18975.8 ± 2304.9	21788.3 ± 2597.6
<i>TM</i>						
Al	-59085.0 ± 22488.9	-3347.9 ± 951.0	-601.8 ± 186.2	10382.9 ± 3241.9	2697.8 ± 936.9	4914.4 ± 2061.1
Ba	-344.1 ± 130.9	-585.7 ± 164.8	-817.0 ± 238.1	821.3 ± 255.1	823.6 ± 275.4	1380.2 ± 572.5
Cd	-4.3 ± 1.6	-2.3 ± 0.7	-2.4 ± 0.7	1.7 ± 0.5	2.1 ± 0.8	3.8 ± 1.7
Co	-4.0 ± 1.6	-1.1 ± 0.3	-4.0 ± 1.3	4.3 ± 1.4	3.4 ± 1.3	5.0 ± 2.2
Cr	nd ± nd	-45.3 ± 13.1	-41.3 ± 12.3	20.9 ± 6.9	nd ± nd	nd ± nd
Cu	-71.0 ± 27.3	-69.7 ± 21.0	-66.3 ± 20.7	35.7 ± 12.7	37.8 ± 14.0	58.2 ± 25.2
Fe	-14438.4 ± 5514.3	-3130.4 ± 899.3	-406.3 ± 129.5	1322.5 ± 418.0	271.7 ± 97.0	2535.5 ± 1054.5
Mn	-173.2 ± 65.9	-28.1 ± 8.2	-204.2 ± 61.0	390.3 ± 122.0	295.7 ± 99.0	403.7 ± 167.5
Nd	nd ± nd	-0.3 ± 0.1	-0.3 ± 0.1	nd ± nd	nd ± nd	nd ± nd
Ni	-73.1 ± 28.1	-48.7 ± 13.9	-42.1 ± 12.6	35.5 ± 11.2	32.2 ± 11.3	77.3 ± 32.9
P	-8363.5 ± 3205.5	-6320.9 ± 1793.1	-4564.0 ± 1354.7	3552.9 ± 1124.8	4224.2 ± 1671.0	6499.0 ± 2912.8
Pb	-2.2 ± 0.8	-2.1 ± 1.1	-5.2 ± 1.5	0.7 ± 0.2	0.5 ± 0.2	2.2 ± 0.9
Th	-0.9 ± 0.3	-0.1 ± 0.02	-0.02 ± 0.01	0.01 ± 0.01	0.01 ± 0.00	0.01 ± 0.01
Ti	-1288.9 ± 490.7	-115.6 ± 32.8	-39.1 ± 11.9	23.9 ± 7.5	31.5 ± 11.4	195.7 ± 81.6
Y	-6.0 ± 2.3	-1.6 ± 0.5	-1.5 ± 0.5	1.3 ± 0.4	1.1 ± 0.4	1.9 ± 0.8

CHAPTER 5

CONCLUSION

For this study, 135 water samples were collected, processed and analyzed from the GEOTRACES EPZT cruise to determine the scavenging intensities, remineralization and residence time of ^{210}Po and ^{210}Pb at key interfaces (biotic, sediment-water and hydrothermal). Based on the data presented in this thesis, the following significant conclusions were drawn:

1) Initially, it was hypothesized (Hypothesis 1) that there should be a decrease in the ^{210}Pb flux (estimated from mixed layer inventories) from east to west along the transect due to the trade wind direction in the southern hemisphere (southeast Pacific Ocean). The results of this study show that the calculated atmospheric depositional flux, using ^{210}Pb concentration in aerosols, decreases from the station off of Peru (ST 4 and 1) to the farthest oceanic station (ST 36), indicating the differences in the sources of air masses as a source of atmospheric ^{210}Pb to the study sites; this supported the hypothesis. However, this hypothesis was incorrect. The total ^{210}Pb inventory in the upper 60 m mixed layer increases from east to west (Figure 3.10) due to the scavenging intensity that decreases from east (off the Peru margin) to the west. $^{210}\text{Pb}_d / ^{226}\text{Ra}$ AR increases (more ^{210}Pb than ^{226}Ra) from east to west, also indicating the scavenging intensity decreases from Peru Margin to west. Furthermore, there are low ^{210}Pb activities in the Peru margin attributed to higher upwelling of ^{210}Pb -deficient deeper water into the upper mixed layer of the Peru margin;

2) This thesis presents a new approach to address the differences in the scavenging intensities and residence times by integrating the activities of ^{210}Po and ^{210}Pb at key interfaces (as proposed in Hypothesis 2) as well as in the whole column. For the first time, the direct evidence for the linkage between the biological activity remineralization of ^{210}Po in the mixed layer is

shown in the continental shelf waters off of Peru. There is a strong coupling between the upper and bottom 300 m in terms of scavenging intensities, as observed both in the EPR (ST 18) and most oligotrophic stations (ST 26 and 36). There is active scavenging in EPR site, whereas there is poor scavenging in the upper and bottom 300 m in the oligotrophic stations;

3) Interfaces between intermediate lithogenic nepheloid layers (INL) or hydrothermal plumes in the East Pacific Rise (EPR) and surrounding seawater is expected to be zones of enhanced TEI scavenging, including the scavenging of ^{210}Po and ^{210}Pb (Hypothesis 3). Lateral advection of these plumes will potentially lead to adsorption of particle-reactive TEIs from even larger areas. Simultaneous measurements of ^{210}Po and ^{210}Pb with other stable TEIs (e.g. key parameters Fe, Mn, Pb) will allow quantification of the fluxes across the sediment-water interface at the benthic boundary layer (BNL). Furthermore, redox mobilization of TEIs associated with Fe/Mn-oxyhydroxides from the intersection of coastal sediments with the OMZ could affect the release of ^{210}Pb and ^{210}Po differently due to the stronger affinity of Pb for hydroxides. There is an intense scavenging of ^{210}Po in the hydrothermal vent waters compared to the most oligotrophic waters, resulting in the lowest residence time of ^{210}Po in the water column. A 35% excess of ^{210}Po over ^{210}Pb at 1,000-1,500 m at EPR station indicates much active remineralization in that layer. The whole water column scavenging of ^{210}Po and ^{210}Pb in the EPR site is likely affected by the dissolved and colloidal Fe and Mn released from the vent which is transported to far away distances, both horizontally and vertically. Deep sea hydrothermal systems may significantly impact global ocean chemistry;

4) The $^{210}\text{Po}/^{210}\text{Pb}$ and $^{210}\text{Pb}/^{226}\text{Ra}$ activity ratios vary at different depth intervals and there are disequilibria between ^{210}Po and ^{210}Pb in the water column as proposed in Hypothesis 4 was confirmed. This study conducted an in-depth analysis of the disequilibrium between ^{210}Po

and ^{210}Pb as well as between ^{210}Pb and ^{226}Ra using integrated activities of ^{210}Po , ^{210}Pb and ^{226}Ra at three key interfaces, namely the biotic (upper 300 m), sediment-water (bottom 300 m) and hydrothermal (bottom 300 m at ST 18). In addition, integrated depth layers at every 500 m and the whole water column were analyzed. Based on the data and analysis, there is wide-spread (64 % of all 500-m integrated layers) disequilibrium between ^{210}Po and ^{210}Pb in the whole water column. While radioactive disequilibria between these two nuclides were not uncommon (from earlier published results) in discrete layers, disequilibrium at 500 m integrated layers indicate varying extents of preferential removal of ^{210}Po and remineralization of ^{210}Po -enriched biogenic particulate matter affecting the $^{210}\text{Po}_T/^{210}\text{Pb}_T$ activity ratio. However, $^{210}\text{Po}_T/^{210}\text{Pb}_T$ ratio over the whole water column varied between 0.97 and 1.09 (3% deficiency to 9% excess of ^{210}Po). From a comparison of the inventories of ^{210}Po and ^{210}Pb and the nutrients in the upper and bottom 300 m of the biologically most productive (ST 1) and least productive waters, it is speculated that the whole water column $(^{210}\text{Po}/^{210}\text{Pb})_T$ AR can be used as a metric for the quantification of biological productivity of a given station;

5) The residence time of ^{210}Pb varies at different layers in the vertical profile, confirming Hypothesis 5, as seen in the 500 m layers. Overall, the residence time of ^{210}Pb is much longer (71 years to >600 years) in the most oligotrophic station (ST 36) compared to other stations, but the residence time of ^{210}Pb at 2,500-3,000 m at ST 26 is the lowest, 14 years. There is an overall decrease in residence time from 1000 m to the sediment-water interface in the most productive margin waters off of Peru;

6) There is disequilibrium between ^{210}Pb and ^{226}Ra throughout the water column, as shown in other major ocean basins;

7) There is a strong correlation between nutrients and ^{210}Po activity confirming the strong linkage between nutrient inventory, biological productivity and remineralization of ^{210}Po -laden biogenic particulate matter in the mixed layer;

8) There is a strong correlation between the inventory of total ^{210}Pb and particulate Al, but there is no correlation between ^{210}Po and particulate Al, suggesting much less removal of ^{210}Po by lithogenic material compared to ^{210}Pb ; and

9) There are large variations on the fractionation factor between Po and Pb, suggesting the particle flux, particle composition and biological activity play key roles on the differential scavenging of ^{210}Po and ^{210}Pb in the water column.

REFERENCES

- Bacon, M. P., Belostock, R. A., Tecotzky, M., Turekian, K. K., and Spencer, D. W., 1988, Lead-210 and polonium-210 in ocean water profiles of the continental shelf and slope south of New England: *Continental Shelf Research*, v. 8, no. 5-7, p. 841-853.
- Bacon, M. P., Brewer, P. G., Spencer, D. W., Murray, J. W., and Goddard, J., 1980, Lead-210, polonium-210, manganese and iron in the Cariaco Trench: *Deep Sea Research Part A. Oceanographic Research Papers*, v. 27, no. 2, p. 119-135.
- Bacon, M. P., Spencer, D. W., and Brewer, P. G., 1976, $^{210}\text{Pb}/^{226}\text{Ra}$ and $^{210}\text{Po}/^{210}\text{Pb}$ disequilibria in seawater and suspended particulate matter: *Earth and Planetary Science Letters*, v. 32, no. 2, p. 277-296.
- Baskaran, M., 2011, *Handbook of environmental isotope geochemistry*, Heidelberg [Germany]; New York, Springer.
- Baskaran, M., 2012. "Environmental Isotope Geochemistry": Past, Present and Future. In *Handbook of Environmental Isotope Geochemistry* (pp. 3-10). Springer Berlin Heidelberg.
- Baskaran, M., Church, T., Hong, G., Kumar, A., Qiang, M., Choi, H., Rigaud, S., and Maiti, K., 2013, Effects of flow rates and composition of the filter, and decay/ingrowth correction factors involved with the determination of in situ particulate ^{210}Po and ^{210}Pb in seawater: *Limnology and Oceanography: Methods*, v. 11, no. 3, p. 126-138.
- Baskaran, M., Hong, G.-H., and Santschi, P. H., 2009, *13 Radionuclide Analysis in Seawater: Practical Guidelines for the Analysis of Seawater*, p. 259.

- Baskaran, M., and Santschi, P. H., 1993, The role of particles and colloids in the transport of radionuclides in coastal environments of Texas: *Marine Chemistry*, v. 43, no. 1, p. 95-114.
- Baskaran, M., and Santschi, P. H., 2002, Particulate and dissolved ^{210}Pb activities in the shelf and slope regions of the Gulf of Mexico waters: *Continental Shelf Research*, v. 22, no. 10, p. 1493-1510.
- Benoit, G., and Hemond, H. F., 1988, Improved methods for the measurement of ^{210}Po , ^{210}Pb , and ^{226}Ra : *Limnology and Oceanography*, v. 33, no. 6part2, p. 1618-1622.
- Carpenter, R., Bennett, J. T., and Peterson, M. L., 1981, ^{210}Pb activities in and fluxes to sediments of the Washington continental slope and shelf: *Geochimica et Cosmochimica Acta*, v. 45, no. 7, p. 1155-1172.
- Cherrier, J., Burnett, W. C., and LaRock, P. A., 1995, Uptake of polonium and sulfur by bacteria: *Geomicrobiology Journal*, v. 13, no. 2, p. 103-115.
- Chung, Y.-c., and Craig, H., 1973, Radium-226 in the eastern equatorial Pacific: *Earth and Planetary Science Letters*, v. 17, no. 2, p. 306-318.
- Chung, Y., 1981, ^{210}Pb and ^{226}Ra distributions in the Circumpolar waters: *Earth and Planetary Science Letters*, v. 55, no. 2, p. 205-216.
- Chung, Y., and Craig, H., 1983, ^{210}Pb in the Pacific: the GEOSECS measurements of particulate and dissolved concentrations: *Earth and Planetary Science Letters*, v. 65, no. 2, p. 406-432.
- Chung, Y., and Finkel, R., 1988, ^{210}Po in the western Indian Ocean: distributions, disequilibria and partitioning between the dissolved and particulate phases: *Earth and Planetary Science Letters*, v. 88, no. 3, p. 232-240.

- Chung, Y., and Wu, T., 2005, Large ^{210}Po deficiency in the northern South China Sea: *Continental Shelf Research*, v. 25, no. 10, p. 1209-1224.
- Church, T., Rigaud, S., Baskaran, M., Kumar, A., Friedrich, J., Masque, P., Puigcorb , V., Kim, G., Radakovitch, O., Hong, G., Choi, H., and Stewart, G., 2012, Intercalibration studies of ^{210}Po and ^{210}Pb in dissolved and particulate seawater samples: *Limnology and Oceanography: Methods*, v. 10, no. 10, p. 776-789.
- Church, T. M., Hussain, N., Ferdelman, T. G., and Fowler, S. W., 1994, An efficient quantitative technique for the simultaneous analyses of radon daughters ^{210}Pb , ^{210}Bi and ^{210}Po : *Talanta*, v. 41, no. 2, p. 243-249.
- Cochran, J., 1992, The oceanic chemistry of the uranium-and thorium-series nuclides, *Uranium-series disequilibrium: applications to earth, marine, and environmental sciences*. 2. ed.
- Cochran, J., and Masqu , P., 2003, Short-lived U/Th series radionuclides in the ocean: tracers for scavenging rates, export fluxes and particle dynamics: *Reviews in Mineralogy and geochemistry*, v. 52, no. 1, p. 461-492.
- Cochran, J. K., Bacon, M. P., Krishnaswami, S., and Turekian, K. K., 1983, ^{210}Po and ^{210}Pb distributions in the central and eastern Indian Ocean: *Earth and Planetary Science Letters*, v. 65, no. 2, p. 433-452.
- Cochran, J. K., Carey, A. E., Sholkovitz, E. R., and Surprenant, L. D., 1986, The geochemistry of uranium and thorium in coastal marine sediments and sediment pore waters: *Geochimica et Cosmochimica Acta*, v. 50, no. 5, p. 663-680.
- Cochran, J. K., McKibbin-Vaughan, T., Dornblaser, M. M., Hirschberg, D., Livingston, H. D., and Buesseler, K. O., 1990, ^{210}Pb scavenging in the North Atlantic and North Pacific Oceans: *Earth and Planetary Science Letters*, v. 97, no. 3, p. 332-352.

- Collé, R., Fitzgerald, R., and Laureano–Perez, L., 2014, A new determination of the ^{209}Po half-life: *Journal of Physics G: Nuclear and Particle Physics*, v. 41, no. 10, p. 105103.
- Cookbook, G., 2014, *Geotraces Cookbook*,
<http://www.geotraces.org/images/stories/documents/intercalibration/Cookbook.pdf>
- Craig, H., Krishnaswami, S., and Somayajulu, B. L. K., 1973, ^{210}Pb ^{226}Ra : Radioactive disequilibrium in the deep sea: *Earth and Planetary Science Letters*, v. 17, no. 2, p. 295-305.
- Fisher, N. S., Bjerregaard, P., and Fowler, S. W., 1983, Interactions of marine plankton with transuranic elements. 1. Biokinetics of neptunium, plutonium, americium, and californium in phytoplankton: *Limnology and Oceanography*, v. 28, no. 3, p. 432-447.
- Fisher, T. R., Harding, L. W., Stanley, D. W., and Ward, L. G., 1988, Phytoplankton, nutrients, and turbidity in the Chesapeake, Delaware, and Hudson estuaries: *Estuarine, Coastal and Shelf Science*, v. 27, no. 1, p. 61-93.
- Fitzsimmons, J. N., Boyle, E. A., and Jenkins, W. J., 2014, Distal transport of dissolved hydrothermal iron in the deep South Pacific Ocean: *Proceedings of the National Academy of Sciences*, v. 111, no. 47, p. 16654-16661.
- Fitzsimmons, J. N., John, S. G., Marsay, C. M., Hoffman, C. L., Nicholas, S. L., Toner, B. M., German, C. R., and Sherrell, R. M., 2017, Iron persistence in a distal hydrothermal plume supported by dissolved-particulate exchange: *Nature Geoscience*, v. 10, no. 3, p. 195-201.
- Flynn, W. W., 1968, The determination of low levels of polonium-210 in environmental materials: *Analytica Chimica Acta*, v. 43, no. 0, p. 221-227.

- Friedrich, J., and Rutgers van der Loeff, M. M., 2002, A two-tracer (^{210}Po – ^{234}Th) approach to distinguish organic carbon and biogenic silica export flux in the Antarctic Circumpolar Current: *Deep Sea Research Part I: Oceanographic Research Papers*, v. 49, no. 1, p. 101-120.
- Fuller, C., and Hammond, D. E., 1983, The fallout rate of PB-210 on the western coast of the United States: *Geophysical Research Letters*, v. 10, no. 12, p. 1164-1167.
- GEOTRACES, 2006, GEOTRACES Science Plan,
http://www.geotraces.org/libraries/documents/Science_plan.pdf.
- Hayes, C. T., Anderson, R. F., Fleisher, M. Q., Vivancos, S. M., Lam, P. J., Ohnemus, D. C., Huang, K.-F., Robinson, L. F., Lu, Y., Cheng, H., Edwards, R. L., and Moran, S. B., 2015, Intensity of Th and Pa scavenging partitioned by particle chemistry in the North Atlantic Ocean: *Marine Chemistry*, v. 170, p. 49-60.
- Henderson, G. M., and Maier-Reimer, E., 2002, Advection and removal of ^{210}Pb and stable Pb isotopes in the oceans: a general circulation model study: *Geochimica et Cosmochimica Acta*, v. 66, no. 2, p. 257-272.
- Heyraud, M., and Cherry, R. D., 1979, Polonium-210 and lead-210 in marine food chains: *Marine Biology*, v. 52, no. 3, p. 227-236.
- Hong, G.-H., Park, S.-K., Baskaran, M., Kim, S.-H., Chung, C.-S., and Lee, S.-H., 1999, Lead-210 and polonium-210 in the winter well-mixed turbid waters in the mouth of the Yellow Sea: *Continental Shelf Research*, v. 19, no. 8, p. 1049-1064.
- Hong, G. H., Baskaran, M., Church, T. M., and Conte, M., 2013, Scavenging, cycling and removal fluxes of ^{210}Po and ^{210}Pb at the Bermuda time-series study site: *Deep Sea Research Part II: Topical Studies in Oceanography*, v. 93, p. 108-118.

- Hong, G.-H., Hamilton, T.F., Baskaran, M. and Kenna, T.C. 2011. Applications of anthropogenic radionuclides as tracers to investigate marine environmental processes. *In: Handbook of Environmental Isotope Geochemistry*, (Ed. M. Baskaran), p. 367-394, Springer (ISBN: 978-3-642-10636-1).
- Kadko, D., Bacon, M. P., and Hudson, A., 1987, Enhanced Scavenging of Pb-210 and Po-210 by Processes Associated with the East Pacific Rise near 8-Degrees-45'n: *Earth and Planetary Science Letters*, v. 81, no. 4, p. 349-357.
- Key, R. M., Stallard, R. F., Moore, W. S., and Sarmiento, J. L., 1985, Distribution and flux of ^{226}Ra and ^{228}Ra in the Amazon River estuary: *Journal of Geophysical Research: Oceans*, v. 90, no. C4, p. 6995-7004.
- Kharkar, D., Thomson, J., Turekian, K., and Forster, W., 1976, Uranium and thorium decay series nuclides in plankton from the Caribbean: *Limnology and Oceanography*, v. 21, no. 2, p. 294-299.
- Kim, G., 2001, Large deficiency of polonium in the oligotrophic ocean's interior: *Earth and Planetary Science Letters*, v. 192, no. 1, p. 15-21.
- Kim, G., Alleman, L. Y., and Church, T. M., 1999, Atmospheric depositional fluxes of trace elements, ^{210}Pb , and ^7Be to the Sargasso Sea: *Global Biogeochemical Cycles*, v. 13, no. 4, p. 1183-1192.
- Kim, G., and Church, T. M., 2001, Seasonal biogeochemical fluxes of ^{234}Th and ^{210}Po in the Upper Sargasso Sea: Influence from atmospheric iron deposition: *Global Biogeochemical Cycles*, v. 15, no. 3, p. 651-661.

- Lam, P. J., Ohnemus, D. C., and Auro, M. E., 2015, Size-fractionated major particle composition and concentrations from the US GEOTRACES North Atlantic Zonal Transect: Deep Sea Research Part II: Topical Studies in Oceanography, v. 116, p. 303-320.
- Lee, H. M., Hong, G. H., Baskaran, M., Kim, S. H., and Kim, Y. I. L. L., 2014, Evaluation of plating conditions for the recovery of ^{210}Po on a Ag planchet: Applied Radiation and Isotopes, v. 90, p. 170-176.
- Moore, W. S., 1999, The subterranean estuary: a reaction zone of ground water and sea water: Marine Chemistry, v. 65, no. 1, p. 111-125.
- Moore, W. S., Bruland, K. W., and Michel, J., 1981, Fluxes of uranium and thorium series isotopes in the Santa Barbara Basin: Earth and Planetary Science Letters, v. 53, no. 3, p. 391-399.
- Moore, W. S., and Dymond, J., 1988, Correlation of ^{210}Pb removal with organic carbon fluxes in the Pacific Ocean: Nature, v. 331, no. 6154, p. 339-341.
- Murray, J. W., Paul, B., Dunne, J. P., and Chapin, T., 2005, ^{234}Th , ^{210}Pb , ^{210}Po and stable Pb in the central equatorial Pacific: Tracers for particle cycling: Deep Sea Research Part I: Oceanographic Research Papers, v. 52, no. 11, p. 2109-2139.
- Nozaki, Y., Dobashi, F., Kato, Y., and Yamamoto, Y., 1998, Distribution of Ra isotopes and the ^{210}Pb and ^{210}Po balance in surface seawaters of the mid Northern Hemisphere: Deep Sea Research Part I: Oceanographic Research Papers, v. 45, no. 8, p. 1263-1284.
- Nozaki, Y., Ikuta, N., and Yashima, M., 1990, Unusually large ^{210}Po deficiencies relative to ^{210}Pb in the Kuroshio Current of the East China and Philippine seas: Journal of Geophysical Research: Oceans, v. 95, no. C4, p. 5321-5329.

- Nozaki, Y., Thomson, J., and Turekian, K. K., 1976, The distribution of ^{210}Pb and ^{210}Po in the surface waters of the Pacific Ocean: *Earth and Planetary Science Letters*, v. 32, no. 2, p. 304-312.
- Nozaki, Y., Tsubota, H., Kasemsupaya, V., Yashima, M., and Naoko, I., 1991, Residence times of surface water and particle-reactive ^{210}Pb and ^{210}Po in the East China and Yellow seas: *Geochimica et Cosmochimica Acta*, v. 55, no. 5, p. 1265-1272.
- Nozaki, Y., and Tsunogai, S., 1973, A simultaneous determination of lead-210 and polonium-210 in sea water: *Analytica Chimica Acta*, v. 64, no. 2, p. 209-216.
- Nozaki, Y., and Tsunogai, S., 1976, ^{226}Ra , ^{210}Pb and ^{210}Po disequilibria in the Western North Pacific: *Earth and Planetary Science Letters*, v. 32, no. 2, p. 313-321.
- Nozaki, Y., Turekian, K. K., and Von Damm, K., 1980, ^{210}Pb in GEOSECS water profiles from the North Pacific: *Earth and Planetary Science Letters*, v. 49, no. 2, p. 393-400.
- Nozaki, Y., Zhang, J., and Takeda, A., 1997, ^{210}Pb and ^{210}Po in the equatorial Pacific and the Bering Sea: the effects of biological productivity and boundary scavenging: *Deep Sea Research Part II: Topical Studies in Oceanography*, v. 44, no. 9–10, p. 2203-2220.
- Ohnemus, D. C., Rauschenberg, S., Cutter, G. A., Fitzsimmons, J. N., Sherrell, R. M., and Twining, B. S., 2016, Elevated trace metal content of prokaryotic communities associated with marine oxygen deficient zones: *Limnology and Oceanography*, p. n/a-n/a.
- Radakovitch, O., Cherry, R. D., Heyraud, M., and Heussner, S., 1998, Unusual $^{210}\text{Po}/^{210}\text{Pb}$ ratios in the surface water of the Gulf of Lions: *Oceanologica Acta*, v. 21, no. 3, p. 459-468.
- Rama, M., and Honda, M., 1961, Natural radioactivity in the atmosphere: *Journal of Geophysical Research*, v. 66, no. 10, p. 3227-3231.

- Resing, J. A., Sedwick, P. N., German, C. R., Jenkins, W. J., Moffett, J. W., Sohst, B. M., and Tagliabue, A., 2015, Basin-scale transport of hydrothermal dissolved metals across the South Pacific Ocean: *Nature*, v. 523, no. 7559, p. 200.
- Rigaud, S., Stewart, G., Baskaran, M., Marsan, D., and Church, T., 2015, ^{210}Po and ^{210}Pb distribution, dissolved-particulate exchange rates, and particulate export along the North Atlantic US GEOTRACES GA03 section: *Deep Sea Research Part II: Topical Studies in Oceanography*, v. 116, p. 60-78.
- Rutgers van der Loeff, M. M., and Geibert, W., 2008, Chapter 7 U- and Th-Series Nuclides as Tracers of Particle Dynamics, Scavenging and Biogeochemical Cycles in the Oceans, *in* Krishnaswami, S., and Cochran, J. K., eds., *Radioactivity in the Environment*, Volume Volume 13, Elsevier, p. 227-268.
- Sanial, V., Kipp, L., Henderson, P., van Beek, P., Reyss, J.-L., Hammond, D., Hawco, N., Saito, M., Resing, J., and Sedwick, P., 2017, Radium-228 as a tracer of dissolved trace element inputs from the Peruvian continental margin: *Marine Chemistry*.
- Sarin, M., Bhushan, R., Rengarajan, R., and Yadav, D., 1992, Simultaneous determination of ^{238}U series nuclides in waters of Arabian Sea and Bay of Bengal: *Indian J. Mar. Sci.*, v. 21, p. 121-127.
- Sarin, M. M., Rengarajan, R., and Krishnaswami, S., 1999, Aerosol NO_3^- and ^{210}Pb distribution over the central-eastern Arabian Sea and their air-sea deposition fluxes: *Tellus B*, v. 51, no. 4, p. 749-758.
- Schlitzer, R., 2016, *Ocean Data View*.
- Shannon, L. V., Cherry, R. D., and Orren, M. J., 1970, Polonium-210 and lead-210 in the marine environment: *Geochimica et Cosmochimica Acta*, v. 34, no. 6, p. 701-711.

- Somayajulu, B. L. K., and Craig, H., 1976, Particulate and soluble ^{210}Pb activities in the deep sea: *Earth and Planetary Science Letters*, v. 32, no. 2, p. 268-276.
- Stewart, G., Cochran, J. K., Miquel, J. C., Masqué, P., Szlosek, J., Rodriguez y Baena, A. M., Fowler, S. W., Gasser, B., and Hirschberg, D. J., 2007, Comparing POC export from $^{234}\text{Th}/^{238}\text{U}$ and $^{210}\text{Po}/^{210}\text{Pb}$ disequilibria with estimates from sediment traps in the northwest Mediterranean: *Deep Sea Research Part I: Oceanographic Research Papers*, v. 54, no. 9, p. 1549-1570.
- Stewart, G. M., and Fisher, N. S., 2003, Bioaccumulation of polonium-210 in marine copepods: *Limnology and Oceanography*, v. 48, no. 5, p. 2011-2019.
- Su, K., Du, J., Baskaran, M., and Zhang, J., 2017, ^{210}Po and ^{210}Pb disequilibrium at the PN section in the East China Sea: *Journal of Environmental Radioactivity*, v. 174, p. 54-65.
- Swarzenski, P. W., McKee, B. A., Sørensen, K., and Todd, J. F., 1999, ^{210}Pb and ^{210}Po , manganese and iron cycling across the $\text{O}_2/\text{H}_2\text{S}$ interface of a permanently anoxic fjord: Framvaren, Norway: *Marine Chemistry*, v. 67, no. 3-4, p. 199-217.
- Thomson, J., and Turekian, K. K., 1976, ^{210}Po and ^{210}Pb distributions in ocean water profiles from the Eastern South Pacific: *Earth and Planetary Science Letters*, v. 32, no. 2, p. 297-303.
- Todd, J. F., Wong, G. T. F., and Reid, D. F., 1986, The geochemistries of ^{210}Po and ^{210}Pb in waters overlying and within the Orca Basin, Gulf of Mexico: *Deep Sea Research Part A. Oceanographic Research Papers*, v. 33, no. 10, p. 1293-1306.
- Toole, J. M., 1996, New data on deep sea turbulence shed light on vertical mixing: *Oceanus*, v. 39, no. 2, p. 33.

- Turekian, K., and Nozaki, Y., 1980, ^{210}Po and ^{210}Pb in the Eastern South Pacific—the role of upwelling on their distributions in the water column: *Isotope Marine Chemistry*. Uchida Rokakuho Publ. Co., Tokyo, p. 157-164.
- Turekian, K. K., Benninger, L. K., and Dion, E. P., 1983, ^7Be and ^{210}Pb total deposition fluxes at New Haven, Connecticut and at Bermuda: *Journal of Geophysical Research: Oceans*, v. 88, no. C9, p. 5411-5415.
- Turekian, K. K., Graustein, W. C., and Cochran, J. K., 1989, Lead-210 in the SEAREX program: An aerosol tracer across the Pacific: *Chemical oceanography*, v. 10, p. 51-81.
- Turekian, K. Y., Nozaki, Y., and Benninger, L. K., 1977, Geochemistry of atmospheric radon and radon products: *Annual Review of Earth and Planetary Sciences*, v. 5, p. 227.
- USGS, 2004, U-238-Decay-Chain.gif, *in* Interior, U. S. D. o. t., ed.
- Verdeny, E., Masqué, P., Garcia-Orellana, J., Hanfland, C., Kirk Cochran, J., and Stewart, G. M., 2009, POC export from ocean surface waters by means of $^{234}\text{Th}/^{238}\text{U}$ and $^{210}\text{Po}/^{210}\text{Pb}$ disequilibria: A review of the use of two radiotracer pairs: *Deep Sea Research Part II: Topical Studies in Oceanography*, v. 56, no. 18, p. 1502-1518.
- Verdeny, E., Masqué, P., Maiti, K., Garcia-Orellana, J., Bruach, J. M., Mahaffey, C., and Benitez-Nelson, C. R., 2008, Particle export within cyclonic Hawaiian lee eddies derived from ^{210}Pb – ^{210}Po disequilibrium: *Deep Sea Research Part II: Topical Studies in Oceanography*, v. 55, no. 10–13, p. 1461-1472.
- Wei, C.-L., and Murray, J. W., 1994, The behavior of scavenged isotopes in marine anoxic environments: ^{210}Pb and ^{210}Po in the water column of the Black Sea: *Geochimica et Cosmochimica Acta*, v. 58, no. 7, p. 1795-1811.

ABSTRACT**COMPARISON OF THE SCAVENGING INTENSITY, REMINERALIZATION
AND RESIDENCE TIME OF ^{210}Po AND ^{210}Pb AT KEY INTERFACES
(BIOTIC, SEDIMENT-WATER AND HYDROTHERMAL)
ALONG THE GEOTRACES EAST PACIFIC ZONAL TRANSECT**

by

JOHN NIEDERMILLER**August 2017****Advisor:** Professor Mark Baskaran**Major:** Geology**Degree:** Master of Science

The contrasting geochemical behavior of two long-lived progeny of ^{222}Rn , namely ^{210}Po and ^{210}Pb , provide valuable insights on the extent of recycling of biogenic particulate matter and their preferential removal from the water column. A total of 135 water samples were collected and analyzed from six vertical profiles for ^{210}Po and ^{210}Pb along the US GEOTRACES East Pacific Zonal Transect. This study shows decreasing atmospheric ^{210}Pb flux calculated from the measured ^{210}Pb activity in aerosols indicating an overall decrease from east to west along the cruise transect. Differences in scavenging intensities, inventories, and residence times of ^{210}Po and ^{210}Pb at key interfaces that include biotic (upper 60 and 300 m), sediment-water (bottom 300 m) and hydrothermal (bottom 300 m at the East Pacific Rise, EPR) stations were calculated and compared. This thesis presents a new approach to address the differences in the scavenging intensities and residence times by integrating the activities of ^{210}Po and ^{210}Pb at key interfaces as well as in the whole column, showing direct evidence for the linkage between the biological activity and remineralization of ^{210}Po in the mixed layer in the continental shelf waters off of Peru. $^{210}\text{Po} / ^{210}\text{Pb}$ and $^{210}\text{Pb} / ^{226}\text{Ra}$ activity ratios vary at different depth intervals establishing

disequilibria between ^{210}Po and ^{210}Pb in the water column; disequilibria are also observed between ^{210}Pb and ^{226}Ra throughout the water column, as shown in other major ocean basins. Lastly, intense scavenging of ^{210}Po and ^{210}Pb in the upper 300 m of the EPR site was observed due to high amounts of dissolved and colloidal Fe and Mn, whereas, lower scavenging was noted in the upper and bottom 300 m at the most oligotrophic station. Overall, radionuclides of ^{210}Po , ^{210}Pb and ^{226}Ra serve as geochemical tracers to investigate and understand the biogeochemical processes in the marine environment.

AUTOBIOGRAPHICAL STATEMENT

My first love was aviation and airplanes and at age 14, I started working at Detroit City Airport. Upon graduating from South Lake High School in St. Clair Shores, Michigan, I attended Benjamin Oliver Davis, Jr., Aerospace Technical School and Macomb Community College where I earned my Airframe and Powerplant (A & P) Mechanics license (issued by the Federal Aviation Administration) and an Associate's Degree in Applied Sciences, respectively. I worked as a federally licensed aircraft mechanic until I changed career paths and became a licensed builder. While working primarily in new home construction for over a decade, I met my wife Dawn who was attending Wayne State University pursuing an education in geology. I have always enjoyed the outdoors and after helping Dawn and the Department of Geology for nearly five years with various geology field trips and working as a research technician for the department, I decided to go back to school and earn a degree in geology. As a first generation college student, I was proud to serve as President of the WSU Geology Club and graduate magna cum laude with a Bachelor Degree in Geology in 2013.

As an undergraduate I was active in field work and research that included air and water sampling, measuring ash tree seedlings related to the Emerald Ash Borer and I worked two summers in the Grand Tetons and Yellowstone National Park area studying the mountain pine beetle and carbon sequestering. After working as a field assistant geologically mapping a diamond exploration project in Wawa, Ontario and then the following summer completing my six-week field camp at the University of Minnesota Duluth studying the Precambrian Canadian Shield and completing the capstone mapping project at Paulsen Lake in the northern boundary waters; I realized that geology was a field of study that well suited me and my many interests.

I decided to pursue a Master Degree in Geology, also at Wayne State University to further and broaden my understanding of geology and to also position myself for a meaningful career as a professional geologist. Although I had much experience in the field and in areas of environmental science and hard rock geology, I was excited about the opportunity to work with Professor Mark Baskaran and I welcomed the challenge to learn and study geochemistry and radionuclides as tracers, specifically ^{210}Po and ^{210}Pb ; a new area of study for me. Upon earning my Master's Degree, I look forward to a career as a geoscientist and I plan to continue K-12 geology outreach to children with my wife. Inspiring a child to learn is one of the greatest gifts that can be given.